Thermal and Electrical Properties of Nanocomposites, Including Material Processing

Thermal and Electrical Properties of Nanocomposites, Including Material Processing

Proefschrift

ter verkrijging van de graad van doctor
aan de Technische Universiteit Delft
op gezag van de Rector Magnificus prof. ir. K.C.A.M. Luyben
voorzitter van het College voor Promoties,
in het openbaar te verdedigen,
op dinsdag 22 mei 2012 om 10:00 uur
door

Roman KOCHETOV

Master of Electrical Engineering,
Lappeenranta University of Technology, Finland
Master of Technique and Technology,
Saint-Petersburg State Electrotechnical University 'LETI', Russia

geboren te Pervosovetsk (Kazachstan, de Sovjet-Unie)

Dit proefschrift is goedgekeurd door de promotor:

Prof.dr. J.J. Smit

Copromotor:

Dr.ir. P.H.F. Morshuis

Samenstelling promotiecommissie:

Rector Magnificus	voorzitter
Prof.dr. J.J. Smit	Technische Universiteit Delft, promotor
Dr.ir. P.H.F. Morshuis	Technische Universiteit Delft, copromotor
Prof.dr. S.J. Picken	Technische Universiteit Delft
Prof.dr. E.F. Steennis	Technische Universiteit Eindhoven
Prof.dr. A.S. Vaughan	University of Southampton
Prof.dr. J.C. Fothergill	University of Leicester
Dr. C.W. Reed	Consultant for DRS Technologies
Prof.dr. M. Zeman	Technische Universiteit Delft, reservelid

This research was financially supported by:
SenterNovem in the framework of IOP-EMVT project

ISBN: 978-94-6203-034-3

Printed by: Wöhrmann Print Service, Zutphen, the Netherlands

This is a thesis about very small things

To my parents,
grandparents and
women, who inspired me

Summary

The research described in this thesis is part of a state-funded IOP-EMVT project in cooperation with industrial companies, aiming at the design, assessment and implementation of new, environmental friendly (e.g. oil and SF_6 - free) solid dielectric materials. A large disadvantage of solid polymer dielectrics is their relatively low thermal conductivity. Therefore, the focus in this thesis is on if and how nanotechnology can improve the thermal conductivity without deteriorating existing electrical properties.
Epoxy resin, which is very common polymer material in the electrical and power industry, has been used as a host to create new insulating materials: nanocomposites. In order to improve the thermal conductivity of epoxy resin, thermally conducting but electrically insulating nanofillers, such as aluminum and magnesium oxides (Al_2O_3 and MgO), silicon dioxide (SiO_2), boron and aluminum nitrides (BN and AlN) were used to dope the polymer matrix. Good compatibility and adhesion was achieved by surface modification of the nanoparticles, using a silane coupling agent.
Proper dispersion of nanoparticles is a vital factor for the final properties of nanocomposites. Good and stable dispersion of nanoparticles in polymer matrices have been achieved by mechanical mixing and ultrasonic vibration. The quality of the dispersion of nanoparticles was satisfactory for most of the nanocomposite samples. The fabricated composites were classified into three types, according to the average particle size and the extent of agglomerates observed inside the polymer matrix.
Dielectric spectroscopy revealed that the relative permittivity of many nanocomposites is lower than that of the pure epoxy. This surprises, since the relative permittivity of the bulk materials of the fillers used is higher than that of the epoxy. The anomalous dielectric behaviour of nanocomposites was explained by the existence of an interface layer between polymer matrix and inorganic filler, and its influence on the macroscopic properties of the composite.
The dielectric spectroscopy investigations demonstrated a reduction of the real and imaginary parts of the complex permittivity for all samples after subjecting the samples to postcuring. The postcuring process leads to evaporation of absorbed water and finalizes the process of epoxy curing.
It was postulated that the interface polymer volume, which is affected by the alignment of polymer chains around surface treated nanoparticles,

conducts the heat much better than an amorphous polymer that is not altered by nanoparticles.
We proposed a three-phase Lewis-Nielsen model to fit the thermal conductivity behaviour of nanocomposites, which have a third phase of aligned polymer layers. The model fits the experimental data very well and takes the thermal resistance of the interface into account. Besides the interfacial layer and its nature, the size of the particles, their aspect ratio, crystal structure and alignment inside the polymer as well as surface modification are important aspects in determining the thermal conductivity of composites.
Several ways are proposed to optimize the nanocomposite processing to enable scaling up to large industrial volumes.
Finally, possible harmful effects of nanoparticles on health and required precautions for the workplace are discussed in the course of this thesis.

Samenvatting

In dit proefschrift wordt onderzoek beschreven dat onderdeel vormt van een door de overheid gefinancierd IOP-EMVT project in samenwerking met de industrie. Dit onderzoek heeft het ontwerpen, vervaardigen en implementeren van nieuwe, milieuvriendelijke (vrij van olie of SF_6) vaste diëlektrische materialen als doel. Een groot nadeel van vaste stof polymeren is hun relatief lage thermische geleidbaarheid. Daarom zal in dit proefschrift de nadruk liggen op de vraag of en hoe nanotechnologie de thermische geleidbaarheid kan verbeteren zonder dat de elektrische eigenschappen negatief worden beïnvloed.
Epoxyhars, een veelgebruikt polymeer in de elektrische energiesector, is gebruikt als basis om nieuwe isolerende materialen te maken, namelijk nanocomposieten. Om de thermische geleidbaarheid van epoxyhars te verbeteren zijn thermisch geleidende doch elektrisch isolerende nanodeeltjes toegevoegd aan de polymeermatrix. Voorbeelden van dit soort nanodeeltjes zijn aluminiumoxide en magnesiumoxide (Al_2O_3 en MgO), siliciumdioxide (SiO_2), boornitride en aluminiumnitride (BN en AlN). Goede compatibiliteit en adhesie werden bereikt door oppervlaktemodificatie van de nanodeeltjes met behulp van een silaan "coupling agent".
Het adequaat dispergeren van nanodeeltjes is een bepalende factor voor de uiteindelijke eigenschappen van nanocomposieten. Een goede en stabiele verspreiding van de nanodeeltjes in de polymeermatrices is bereikt door machinaal mengen en ultrasoon vibreren. De kwaliteit van het dispergeren van de nanodeeltjes was toereikend voor de meerderheid van de nanocomposieten. De vervaardigde composieten zijn onderverdeeld in 3 categorieën, afhankelijk van de gemiddelde deeltjesgrootte en de hoeveelheid geobserveerde agglomeraties in de polymeermatrix.
Uit de resultaten van diëlektrische spectroscopie is gebleken dat de permittiviteit van veel nanocomposieten een lagere waarde heeft dan zuiver epoxyhars. Dit is opmerkelijk, omdat de permittiviteit van nanofillers als bulkmateriaal hoger is dan van zuiver epoxyhars. Dit afwijkende diëlektrische gedrag van nanocomposieten wordt verklaard door de aanwezigheid van een scheidingsvlak tussen de polymeermatrix en de anorganische nanofillers en de invloed van deze laag op de macroscopische eigenschappen van de composieten.
Onderzoek met diëlektrische spectroscopie heeft een verlaging laten zien van het reële en imaginaire deel van de complexe permittiviteit nadat de samples een thermische nabehandeling hadden ondergaan.

Dit ”postcuring” proces leidt tot verdamping van het geabsorbeerde water en completeert het “curing-process” van epoxyhars.
Het volume van de tussenlaag wordt beïnvloed door de uitlijning van de polymeerketens rondom nanodeeltjes, die een oppervlaktebehandeling hebben ondergaan. Er wordt gesteld dat deze tussenlaag warmte veel beter geleidt dan een amorf polymeer dat niet behandeld is met nanodeeltjes.
Wij postuleren een 3-fasen Lewis-Nielsen model voor het gedrag van de thermische geleidbaarheid van nanocomposieten, waarin een 3^{e} fase van uitgelijnde polymeerlagen aanwezig is. Het model komt zeer goed overeen met de experimentele gegevens en houdt rekening met de thermische weerstand. Naast de tussenlaag en de eigenschappen daarvan, zijn ook de grootte van de deeltjes, de geometrische verhoudingen, de kristalstructuur, de uitlijning in het polymeer en de oppervlakteverandering belangrijke aspecten om de thermische geleidbaarheid van composieten te bepalen.
Een aantal manieren om de productie van nanocomposieten te optimaliseren wordt voorgesteld zodat het proces opgeschaald kan worden voor industriële toepassingen.
Afsluitend worden mogelijke schadelijke bijwerkingen van nanodeeltjes op de gezondheid behandeld. Tevens worden enkele voorzorgsmaatregelen voor de werkplek behandeld.

Contents

1

Introduction

1.1 Nanotechnology in history

Nanotechnology is a research field of growing importance. The first remarkable and salient talk concerning nanotechnology was given by Nobel Laureate Richard Feynman at the meeting of the American Physical Society at Caltech in 1959 [1]. In his speech, Feynman foresaw the development of nanomaterials, molecular electronics, nanomanufacturing methods such as nanolithography and manipulation of individual atoms.

The field of nanotechnology is still in its infancy but continues to progress at a much faster rate than any other field. Although the terms 'nanomaterial' and 'nanocomposite' were introduced in the 20th century, such materials have actually been used for centuries and have always existed in nature [2]. Nanoscale materials are all around us, in smoke from fire, volcanic ash, pollen and in the form of spider webs. The size of a typical protein such as hemoglobin, which carries oxygen through the

bloodstream, is about 5 nm, while the thickness of a DNA molecule is only half of that [3].
One of the first examples when humans used nano-objects might be the extraordinary Lycurgus cup. The cup was created in the Roman Empire in the 4th century AD. The opaque green cup turns to a glowing translucent red with illumination. Chemical analysis of the Lycurgus cup indicates that the glass contains approximately 330 ppm of silver and 40 ppm of gold with an average particle size (APS) of approximately 70 nm. However, it is not the presence of these elements that is responsible for the effect, but rather the way how the initial glass composite was produced [4-6]. Another example, where enhanced properties were not obtained from understanding but from empirical experiments is Damascus steel. The swords that were made from Damascus steel were very flexible, sharp and stiff. Many centuries later it was discovered that ancient Muslim smiths were inadvertently using carbon nanotubes within the metallic matrix of the blade in the 17th century [7, 8]. Other primitive nanocomposites were created in the 1860ies. Experiments with vulcanized rubber and carbon black led to significant enhancements of the mechanical properties of rubber tires [9].

1.2 Emergence of nanocomposites

Nanotechnology is now an important interdisciplinary thread in fundamental research. Nanoscience is still in a nascent stage but its impact on the world economy can already be seen since significant potential clearly exists [10, 11]. For the field of electrical power engineering, one of the promising materials that was born by nanotechnology is the *nanocomposite* (NC). Since 1984 when the term 'nanocomposite' was mentioned for the first time [12], it has been generally accepted by the scientific community.
A *nanocomposite* may be defined as a composite system that consists of a polymer matrix and homogeneously dispersed filler particles having at least one dimension below 100 nm. Polymers are the most common materials (thermoplastics, thermosets or elastomers) that are used for nanocomposite fabrication. Over the past decades, *polymer nanocomposites* (PNC) have attracted considerable interest in both academia and industry [13]. The outstanding properties of NC are attributed to the large surface area to volume ratio of the nanoadditives [14]. The size reduction of particles allows tailoring of the physical properties of composites. Every property has a critical length scale, and if a nanoscale item is made smaller than the critical length scale, the fundamental physics of that property change drastically (see Fig. 1.1).

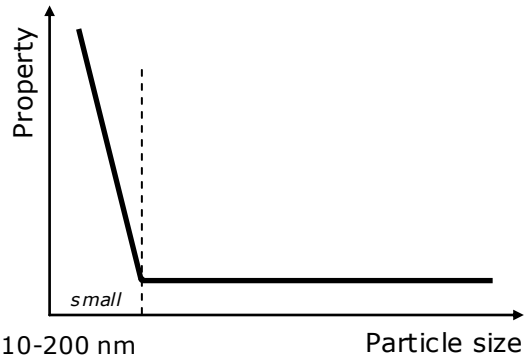

Fig. 1.1: Illustration of the change of a physical property as a function of particle size.

Most material properties may be changed and engineered dramatically through the controlled, size-selective synthesis and assembly of nanoscale building items. The nanoparticles and nanomaterials have unique mechanical, electronic, magnetic, thermal, optical, and chemical properties, thus providing a wide spectrum of new possibilities of engineered nanostructures and nanocomposites for communications, biotechnology and medicine, photonics and electronics [11].
The first nanoclay composite that was produced to reinforce the macroscopic properties of an elastomer, was described in a patent from the National Lead Company in 1950 [15]. Commercial activity started four decades later, when Toyota patented a nanoclay-polyamide system in 1988 [16]. Later on Toyota presented commercial applications of nylon-6 based nanoclay composites for timing belt covers, body panels and bumpers [9, 17, 18].
The discovery of carbon nanotubes (CNT) by Iijima in 1991 [19] and C_{60} fullerene by R.F. Curl, Sir H.W. Kroto and R.E. Smalley in 1995 were the first steps towards a production of single- and multiwalled carbon nanotubes (SWCNT and MWCNT, respectively) and new nanoscale materials and devices based on CNT [20, 21].
A few of the recent commercial applications of nanocomposites include some parts of sport utility vehicles, furniture, and appliances. The fields of application of nanocomposites range from agriculture and food production to space science and medicine [22]. Examples range from improved materials for everyday uses such as toothpaste, scratch and abrasion resistant coatings, self-cleaning paints and bathroom surfaces, water-repellent and anti-microbal nanofilms, deicing surface treatments for aircraft and automobiles in cold climates to new forms of structural materials that might be stronger than steel yet lighter than Styrofoam [3, 23, 24]. Many properties of bulk materials change at nanoscale,

which makes nanotechnology an interesting domain for innovative research [25-28].

1.3 Unique behaviour of nanocomposites

There is no satisfactory explanation for the origin of the improvement of the properties of polymer nanocomposites. It is generally accepted, however, that the large surface-to-volume ratio of the nanoscale inclusions plays a significant role [14, 29]. Smaller particles display a much larger surface area for interaction with the polymer for the same microscopic volume fraction than larger particles [5, 8, 30]. It is currently thought that many of the characteristics of nanocomposites are determined by the interactions that occur at nanoparticle-matrix interfaces. Fig. 1.2 illustrates how the interface area gets more important for smaller particles.

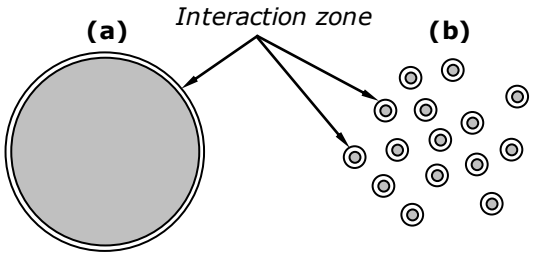

Fig. 1.2: Representation of interaction zones for a microparticle (a) and an assembly of nanoparticles (b) (not in scale) [31].

Major effects on the macroscopic properties can be obtained already at low concentrations, because of the large interfacial area of nanoparticles (see Table 1.1). Therefore, the mechanical, electrical or thermal properties of nanocomposites are strongly affected by the dispersion state and the quality of the interface between nanoparticles and polymer matrices. Agglomerated particles do not lead to the same benefits that dispersed particles do.

Table 1.1: Relation of particle diameters to the number of contained atoms as well as to the fraction of surface atoms [32].

Particle diameter, nm	Number of atoms in a particle	Fraction of surface atoms in a particle, %
20	250.000	10
10	30.000	20
5	4.000	40
2	250	80
1	30	99

The creation of a homogeneous distribution of nanoscaled particles is not an easy task, because particles have a strong tendency to agglomerate. The degree of dispersion can be improved by surface modification of nanoparticles [33]. The formation of chemical bonds between the inorganic and organic components is of great importance to guarantee a homogeneous dispersion of the filler in host polymers. Proper dispersion is the key to the appearance of the desired, and sometimes anomalous, properties [31, 34, 35]. One of the critical aspects of nanotechnology research is how to modify the surface of different nanoparticles to make them compatible with polymer matrices and more useful for different applications [23].
Whereas traditional microcomposites use over 50% by weight of reinforcement material, nanocomposites may show improvements at less than 5% by volume. If the empirical property models are applied for nanocomposites, it often provides estimations which are far from the real values. New behaviour at the nanoscale is not necessarily predictable from what was observed at larger scale structures. The most important changes in properties of NC are caused not by the order of magnitude in size reduction, but by the newly observed phenomena such as size confinement, predominance of interfacial phenomena and quantum mechanisms [10, 36, 37].

The bulk properties of nanocomposites are highly dependent on:

- properties of the filler:
  - ✓ geometry,
  - ✓ size,
  - ✓ filler type,
- host matrix:
  - ✓ crystallinity,
  - ✓ polymer chemistry,
  - ✓ nature (thermoplastic or thermosetting),
- surface treatment,
- interfacial properties,
- fillgrade,
- degree of dispersion and of agglomeration,
- relative arrangements and subsequent synergy between constituents,
- synthesis methods [11, 38].

1.4 Nanodielectrics in high voltage and power engineering

Polymers play an important role in our daily live due to their unique characteristics, such as ease of production, light weight, and often ductile nature. They can be broadly divided into thermosetting resins and thermoplastics, which accounts for 70% of all produced polymers

[39]. Ceramics and inorganic fillers are good insulators and they have relatively high moduli and thermal conductivity. Combining these properties, in polymer-based composites some useful properties can be further improved, while some of the weaknesses can be reduced [22].
In our study we used epoxy resin (ER) as a host polymer. Due to its low viscosity before curing, its excellent processibility, high resistance to chemicals after curing, good adhesive, mechanical and insulating properties, ER is an important material for high performance applications in high voltage and power engineering.
Epoxy nanocomposites have gained much interest in the area of nanotechnology, because of the ease of manufacture and the significant gain in properties [14, 40].
In this thesis we will use the term '*nanodielectric*', which is in our case a synonym for '*nanocomposite*', since both constituents are dielectric materials, where a filler has at least one dimension in the nanoscale range [41-43].
The use of conventional micron-sized particles to improve the thermal or mechanical properties almost always involves a reduction of the electrical properties of the resulting dielectric material. There are promising nanodielectric materials, which can be designed and produced in a manner, so that the electrical strength will not be changed because of the introduction of the nanoscopic filler, while the thermal or mechanical properties are improved [31].
The interfacial region surrounding the particles is dominant for the nanodielectric, while it is insignificant for the composite containing conventional sized filler. The challenge is to design and produce the interfacial zone in a way that provides the desired properties. One of the ways to accomplish that is chemical treatment of the particle surface [31].
Many research groups have made attempts to create a nanocomposite material with extraordinary enhanced properties [44]. Nanotechnology indeed has a potential to be implemented in many branches of electrical engineering, high voltage and power electronics [45, 46].
The improved electrical, mechanical and thermal properties have been observed for various polymers filled with different types of nanoparticles [47-60]. Since this research is focused on the improvement of the properties of epoxy, we give an overview of the research and development that have been done before, particularly on epoxy-based nanocomposites.
One of the electrical properties that have been thoroughly investigated is the resistance to partial discharges (PD). The results show that nanocomposites filled with a few weight percent of aluminum oxide (Al_2O_3), silicon oxide (SiO_2), titanium oxide (TiO_2), silicon carbide (SiC), organically modified layered silicates (OMLS) or clay are more resistant to PD. The erosion depth decreases, compared to the specimens without

nanofillers [61-70]. The damage due to a PD on filled epoxy may be delayed if the filler particles act as thermal shields or heat sinks [62]. Superior resistance can be also attributed to the strong bonding between the ER and incorporated filler [66, 68]. Nanocomposites are even more resistant to PD if the surface of nanoparticles has been modified [64].

The dielectric breakdown (BD) strength might be changed for better or worse, if a nanocomposite is subjected to AC voltage [71]. Nanocomposites filled with nanoclay particles showed an improvement of the AC BD strength [72, 73], while introduction of a small amount of titania, alumina or silica slightly reduce the AC BD [74, 75]. The AC BD strength can also be enhanced by introduction of nanoparticles to a microcomposite [76].

An improvement of the DC BD strength has been obtained for various nanofillers such as clay, magnesium oxide (MgO), aluminum nitride (AlN) boron nitride (BN), alumina and silica [8, 72, 77-79]. One of the potential material candidates for HVDC cables is low density polyethylene filled with MgO nanoparticles [80-83].

The addition of a very small amount of zinc oxide (ZnO) or aluminum oxide nanoparticles in the ER can lead to significant improvements of the long term BD degradation process by increasing the treeing time to breakdown [84-86]. Incorporation of a small amount of OMLS into ER showed that the breakdown time of the nanocomposite under constant AC voltage (10 kV-1kHz) was twice as long as that of the base ER at 20°C and six times at 80°C. In particular, at 145°C, the nanocomposite had a breakdown time of more than 20,000 minutes while the base epoxy resin had a breakdown time of 280 minutes [65].

The incorporation of nanoparticles also appears to reduce the space charge accumulation in some systems. The amount of space charge accumulated by the epoxy-based composites containing TiO_2, ZnO, Al_2O_3, MgO or clay was considerably lower than the one of the neat epoxy [73, 87-90].

A study of the complex permittivity as a function of temperature or frequency is one of the fundamental characterizations of dielectrics. An introduction of a small amount of nanofiller can affect the real and imaginary parts of the complex permittivity. A few percent of nanoparticles can change the relative permittivity of a composite in such a way that it might be higher than any of its constituents [61, 72, 91] or even lower [74, 87, 92-95].

Besides improvement of dielectric properties, the incorporation of nanoparticles leads to the enhancement of thermal and mechanical properties, or to a change of the physical properties of a polymer, such as the glass transition temperature (T_g). The thermal conductivity of filled ER can be improved using thermally conductive but electrically

insulating fillers such as Al_2O_3, BN, SiC, nanodiamond and even cellulose [96-101].
The inclusion of only 0.5 wt.% of surface modified CNT results in significant improvements in the flexural modulus and strength and storage modulus. The drawback of the use of CNT is the higher value of electrical conductivity, which might be negative for the application of ER-CNT as an insulation material [102, 103]. The mechanical properties of polymers change significantly at T_g, therefore it is important to know how nanoparticles influence the viscoelastic behaviour. In case of ER filled with Al_2O_3, ZnO, TiO_2 or CNT a decrease in T_g was reported after adding just 0.5 wt.% of nanofiller [74, 92, 104]. A pronounced increase in T_g was observed with the addition of SiO_2 nanoparticles [105-107]. Negligible changes in T_g with composition have also been reported for ER-Al_2O_3 nanocomposites [61, 108].
A niche where nanodielectrics might find a great potential is cryogenic applications [58, 109-111].

1.5 Current situation. New technology is required

The limits have been reached for current materials and material technologies applied in many components for electrical power systems. Components need to be ever smaller, of less weight (larger application area), more sustainable (oil/SF_6-free), less flammable and more durable. Moreover, an increasing energy density is required, among other things because of the restricted available space.
For many applications we see for this reason a striving towards the application of primarily compact polymeric insulation materials and a gradual disappearance of oil and SF_6 that up to now have been used extensively as insulation media. The quest for compact, polymeric components is not without problems. Due to the high energy density and very low thermal conductivity of most polymeric insulation materials we have arrived at the limit of what is possible using current technology. A further increase of current density, for instance in electrical machines, results in increasing operating temperatures, insufficient heat conduction and adhesion problems at the interface between materials. Further, the electric stress in the insulation will increase and particularly the behaviour of interfaces will become a bottleneck in the realisation of compact and oil-free components. Moreover, in a number of cases also the limits have been reached of what is mechanically possible.
The nanoPOWER project consists of two PhD-studies which run consecutively. Important in the first PhD project is the experimental study and theoretical understanding of the structure-property relations, particularly in relation to the increase of heat conductance. In the second PhD project, the results are validated in industrial prototypes in which the electrical and thermal/mechanical stress factors can be

introduced. The project finishes with the definition of a set of design rules for constructing electrical insulation systems with nanocomposites.

The innovative aspects of this research project are found in the entirely new application of nanotechnology in components used in the electrical power system. Manufacturers of components for the electrical power system such as Prysmian Cables & Systems, Eaton Electric, Hapam, Mekufa as well as TNO Industrie en Techniek are strongly involved in this research project and in the long run we expect them to introduce this technology successfully in their products. Because the presented technology allows the development of environment friendly and less flammable products, a combination of electrical infrastructure seems to be possible with other infrastructures, resulting in a better use of the available space.

The nanoPOWER project is sponsored by a Dutch government IOP-EMVT grant and SenterNovem organization.

1.6 Goals of the research

The goal of the research was to improve the thermal conductivity of epoxy resin insulation without deteriorating electrical insulation properties, by introduction of a low concentration of various nanofillers. The main objectives of the investigation were the synthesis of nanocomposites, analysis and modelling of the heat conduction process, taking into account the features inherent to nanocomposites. The main application of the produced nanocomposite materials is insulating systems, therefore it is also important to determine the influence of nanofiller on the dielectric properties.
The high voltage engineering and especially insulation technology is a conservative business area. Nanotechnology is a rather new field, which is expected to have an impact on many areas of research. In our study we tried to combine these two areas in order to create a material for high voltage applications with less impact on the environment and more durable at the same time.

1.7 Description of the thesis structure

The thesis at hand has been organized in chapters, each handling a different item of study.
Chapter 2 describes how the nanocomposites have been created step by step. It is explained what kind of polymer and filler materials are used for insulation properties and which one have been used for our study. The following questions have been answered: why homogeneous dispersion is a vital factor in the nanocomposite synthesis; how it was obtained by surface functionalization of the particles; what is an

optimum method and solvent to disperse nanoparticles in the polymer; how successful was surface modification.
In the second part of Chapter 2 we present the morphological characterization of as-received particles and fabricated samples.
Chapter 3 deals with the thermal characterization of created specimens. In the beginning of the chapter, the thermal conductivity as a property of a material is presented. Various theoretical models to describe the thermal conductivity of the two-phase systems are given and the difference between them is discussed. The experimental results as well as modelling of the thermal conductivity of composite materials are presented and the influence of filler size, aspect ratio and crystallinity are discussed.
In Chapter 4 we discuss the electrical properties of the nanocomposites. This chapter describes the influence of filler type, concentration, size and impact of water absorption and curing on the dielectric response of nanocomposites.
Chapter 5 gives advice about how to optimize the synthesis of nanocomposites, the ways how the surface modification process can be separated from the rest, which alternative synthesis methods exist and where the new composites can be applied in industry.
Chapter 6 raises issues about health and environmental aspects in using nanoparticles and how to prevent harmful affect on humans.
Chapter 7 provides concluding remarks on the work presented. The chapter summarizes the thesis, outlines its contributions. It also proposes future research directions.

2

Synthesis of epoxy–based nanocomposites

2.1 Introduction

Polymer nanocomposites are a major factor in the design of novel advanced materials suitable for a variety of different applications, such as electrical engineering. Section 2.2 describes thermoplastic and thermosetting polymers, which are currently used as dielectric materials. The properties of polymer materials can be improved by introduction of different types of filler (see Section 2.3). The focus of the present work is epoxy-based nanocomposites. A classification of different types of nanoparticles that can be used to enhance the properties of polymer materials is given in Section 2.3.2.

The companies which produce nanocomposite materials do not willingly share the synthesis procedure. The creation of nanocomposites is a

complex process and many techniques were probed and studied before an optimal processing scheme was found (Section 2.5). The synthesis of nanocomposites, which is explained step by step in this chapter and illustrated in Fig. 2.1, can be used to prepare epoxy-based nanocomposites with well dispersed particles.

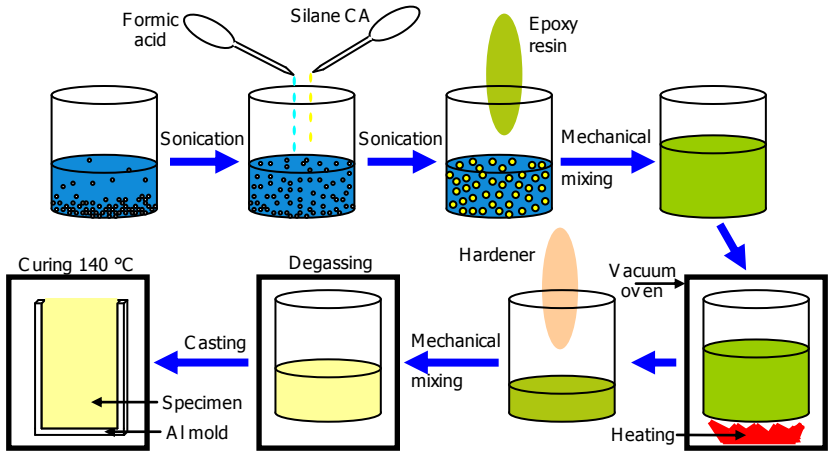

Fig. 2.1: Schematic representation of the synthesis of nanocomposites.

An appropriate solvent for nanoparticles has been chosen. Ethanol as a solvent was compared with water and methanol. The stability and size distribution of nanoparticles have been checked in water and ethanol. It was determined which technique is the most suitable and successful for dispersion of nanoparticles (Section 2.5.1). Pre-treatment of nanoparticles is necessary to make them compatible with the epoxy host (Section 2.5.2).
The successful surface modification of the particles has been proven by thermogravimetric analysis (TGA) and Fourier transformed infrared spectroscope (FTIR). The specimens which have been created are shown in Section 2.8.

Different analyses have been applied to investigate the morphological properties of as-received particles and created composites:

- The Laser Diffraction method has been used to validate the dispersion of nanoparticles in the solvent,
- X-ray diffraction (XRD) was used to identify the crystalline structure of as-received particles (Section 2.9.1),
- All nanoparticles that have been used for composite preparation were investigated with Transmission and Scanning Electron Microscopy (TEM and SEM, respectively). The quality of

dispersion of the filler inside the host material was validated with the help of TEM and SEM as well (2.9.2),
- TGA has been performed to confirm the grafting of silane coupling agent on the surface of nanoparticles and check the sedimentation of particles (2.9.3).

The conclusions are presented in Section 2.10.

2.2 Thermoplastic and thermosetting polymers

Polymers play an important role in our daily life due to their unique characteristics, such as easy production, light weight, and often ductile nature. Polymers can be broadly classified into three basic types, namely thermoplastics, thermosets, and elastomers [39]. Each polymer has its own set of individual chemical characteristics based on the molecular structure.

The transformation process from prepolymer to final product polymer represents the line of demarcation separating the thermosets from the thermoplastic polymers. Thermoplastic materials are polymers, which are capable of being repeatedly softened or melted by increasing the temperature and solidified by decreasing the temperature. These changes are physical rather than chemical. Thermosetting materials are polymers that will undergo, or have undergone, a chemical reaction by the action of heat, a catalyst, ultraviolet light, leading to a relatively infusible state that will not remelt after setting. Elastic rubberlike materials, known as elastomers, are polymers, which are processable under thermoplastic conditions and have a soft structure and low glass transition temperature. The glass transition temperature (T_g) is the temperature at which a plastic changes from a rigid state to a softened state. Both mechanical and electrical properties degrade significantly at this point, which is usually characterized by a narrow temperature range rather than a sharp phase change, such as the freezing or boiling temperature [112].

Thermoplastic polymers such as polyethylene and polyvinyl chloride may be thought of as permanently fusible compounds composed of long linear chains lying together in three dimensions, but not interconnected. In a plane, the system might appear as is illustrated in Fig. 2.2.

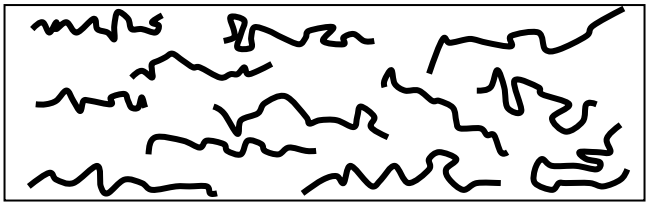

Fig. 2.2: Schematic representation of a thermoplastic polymer.

The movement of a molecule in any direction is not restricted by crosslinking with surrounding molecules.
The thermosetting resins such as epoxy, polyester or phenolic resins become hard when converted by a curing agent. The system may be regarded as a network cross-linked in all three dimensions. In a plane it might appear as is shown in Fig. 2.3.

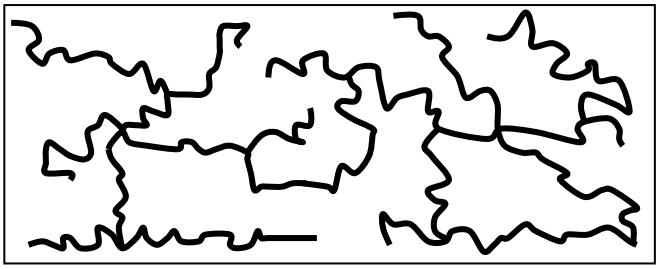

Fig. 2.3: Schematic representation of a thermosetting polymer.

The movement of a molecule in any direction is opposed by the crosslinking arrangement.
In practice, thermoplastic materials will soften with heat or flow with pressure, while thermosetting materials will retain their shape below T_g, while become rubbery above T_g.
Beside the widely used epoxy resin (ER) and polyethylene (PE) in its low density and high density modifications (LDPE and HDPE), such polymers are used in electrical engineering include polypropylene (PP), polyvinyl chloride (PVC), polymethyl methacrylate (PMMA), polycarbonate (PC), polyamide (PA) and polyimide (PI).

2.2.1 Epoxy resins

The first industrially-produced epoxy resins were introduced to the market around 1947. Their commercial debut was in the United States, the first product was made by Devoe-Raynolds Company [113]. The discovery of the epoxy took place much earlier. In 1909, the Russian chemist Prilezhaev discovered the formation reaction of epoxides [114]. In the late 1930s Pierre Castan from Switzerland and Sylvian Greenlee

from United States independently synthesized the first bisphenol-A epichlorohydrin-based resin material [14, 115].
The wide variety of epoxy resin applications include: coatings, electrical, automotive, marine, aerospace and civil infrastructure, sealing liquids, laminates, adhesives as well as tool fabrication and pipes and vessels in the chemical industry, food packing, construction and building material, light weight structural components. Due to their low density and good adhesive and mechanical properties, epoxy resins became a promising material for high performance applications in the transportation industry, usually in the form of composite materials. In the aerospace industry, epoxy-composite materials can be found in various parts of the body and structure of military and civil aircrafts, with the number of applications on the rise. Epoxy resins are widely used in commercial and military applications because of their high mechanical/adhesion characteristics, solvent and chemical resistance combined with the versatility of cure over range of temperatures without by-products.
Epoxy resin systems are thermosets, which are widely used in electrical engineering applications such as rotating machines, bushings, switchgear systems, generator groundwall insulation system, cast resin transformers and insulators [74, 116, 117].
The term "epoxy resin" refers to both the prepolymer and its cured resin/hardener system. Before the curing agent is incorporated, the resins have indefinite shelf life. One of the valuable properties of epoxy resins is their ability to transform from liquid (or thermoplastic) state to hard thermoset solids. The solidification is accomplished by the addition of a chemical reagent known as a curing agent or hardener. Some curing agents promote curing by catalytic action, others participate directly in the reaction and are absorbed into the epoxy chain. The polymerization reaction may be accomplished at room temperature, with heat produced by an exothermic reaction, or may require external heat [115]. A schematic representation of the curing process of a thermoset polymer is shown in Fig. 2.4.
Epoxy resins can be cross-linked through a polymerization reaction with a hardener at elevated temperatures. In general, the higher temperature cured resin systems have improved properties, such as higher glass transition temperatures, strength and stiffness, compared to those cured at room temperature [115].

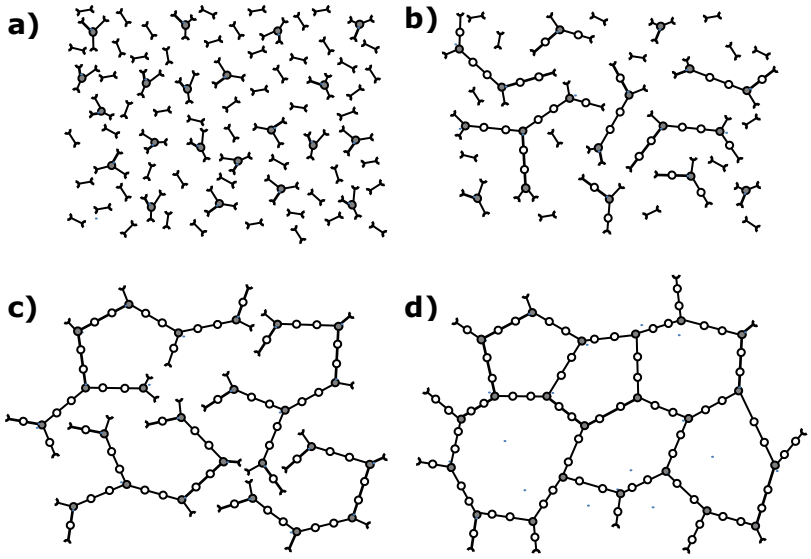

Fig. 2.4: Schematic curing of a thermoset. Cure begins with monomers (a); proceeds via linear growth and branching to a material below gel point (b); continues with formation of gelled but incompletely crosslinked network (c); finishes as fully cured thermoset (d).

2.3 Polymer-based composites

The reinforcement of polymers using different types of organic or inorganic fillers is common practice in the production of systems with improved mechanical, thermal, electrical and other properties [118-121]. Micrometer-sized inorganic particles are currently widely used for the reinforcement of epoxy matrices to lower shrinkage on curing, thermal expansion coefficients, improve thermal conductivity, and meet mechanical requirements. The final properties of the polymer microcomposites (PMC) are affected by several factors, such as the intrinsic characteristics of each component, the contact, the shape and dimension of the fillers, and the nature of their interfaces. To enhance these properties, the use of submicron particles and thus the creation of mesocomposites (PMesC) can lead to a significant improvement of the properties of PMC [122]. In the past decades, a tremendous amount of research has been conducted in the preparation of submicron inorganic particles, leading to the possibility of preparing composites with nanofillers, i.e. nanocomposites (PNC) [23]. ER reinforced with nanoparticles represents one of the most actively studied nanodielectric systems [11].

2.3.1 Nanocomposites

In contrast to traditional polymer composites with high loadings (60 vol.%) of micrometer-sized filler particles, polymer nanocomposites are being developed with low loadings (less than 10 wt.%) of well-dispersed nanofillers [67, 123]. Polymer nanocomposites are defined as an interacting mixture of two phases, a polymer matrix and a solid phase, which is in the nanometer size range in at least one dimension [124]. Nanostructured materials have unusual physical and chemical properties as a result of their extremely small size and large specific area [38].

The properties of polymer composites are affected by

- ✓ nature of the polymer matrix and filler;
- ✓ filler size and shape;
- ✓ dispersion state of the particles;
- ✓ surface modification of the filler;
- ✓ filler-matrix interaction.

2.3.2 Classification and types of fillers

The fillers which are widely used to reinforce a polymer material can be divided in three groups depending on their size.
The first group of filler consists of micron sized particles, which are also called conventional sized filler. The size of these particles can vary in a broad range but typically lies between 1 μm and 100 μm.
The second group can be called submicron sized particles. Their size is between 100 nm and 1 μm.
The first two groups are sometimes combined in one and called "microparticles". We do not agree with this classification, since submicron particles are entitled to be allocated to a separate subgroup.
The third group of particles is the group of nanometer sized particles. The size of these particles should be below 100 nm at least in one dimension. The nanofiller can be one-dimensional (nanotubes, fibers, rods) two-dimensional (clay, plane-like particles) or three-dimensional (spherical particles). Fillers may be classified according to their shape and size or aspect ratio. There is significant diversity in the chemical structures, forms, shapes, sizes, and intrinsic properties of the various compounds used as fillers. Fillers may be classified as inorganic or organic substances, and are further subdivided according to their chemical family [125].
The use of nanostructured fillers in epoxy systems has gained significant importance in the development of thermosetting composites [108].

Table 2.1: Different types of filler.

Chemical family	*Examples*
Inorganics	
Oxides	Al_2O_3, SiO_2, MgO, ZnO, TiO_2, glass
Hydroxides	$Al(OH)_3$, $Mg(OH)_2$
Silicates	Talc, mica, nanoclays, asbestos
Salts, compounds	$CaCO_3$, $BaSO_4$, $CaSO_4$, $BaTiO_3$, $SrTiO_3$
Metals	Al, Ag, Sn, Au, Cu
Nitrides, carbides	AlN, BN, Si_3N_4, SiC
Organics	
Carbon	Carbon fibers, carbon black, graphite fibers and flakes, carbon nanotubes, nanodiamonds
Natural polymers	Cellulose fibers, wood flour, flax, sisal
Synthetic polymers	Polyamide, polyester, aramid

2.3.3 Dispersion

The dispersion of nanoparticles is a crucial factor for the final properties of nanocomposites. Nanoparticles tend to form agglomerates and clusters in a polymer matrix due to their high surface energy [34, 126-128]. The agglomeration may lead to a deterioration of the aimed properties of the final products. In order to obtain good and stable dispersion of nanoparticles in polymer matrices, several methods can be applied to break up the agglomerates [129]. There are two approaches: mechanical dispersion methods, including ultrasonic vibration [130, 131], special sol-gel techniques [132-134], the high shear energy dispersion mixing [135] and surface modification of nanoparticles [136, 137]. The surface modification is a chemical method for improving the compatibility and interaction between polymer and incorporated filler, leading to enhanced dispersion [103].

The filler geometry is a key factor that influences the dispersion of nanoparticles. In general, low-dimensional fillers are more difficult to disperse than three-dimensional. The difference arises from the fact that three-dimensional quasi-spherical particles exhibit only point-to-point contacts, whereas one-dimensional rods or tubes can have contact along the full length of the cylinder, which increases the particle-particle interaction. Two-dimensional sheets have even larger contact area. The increased particle contact area and interaction make a homogeneous dispersion even more difficult. Therefore, spherical particles have been chosen for the research as it is more straightforward to disperse them than either rods or sheets [39].

The surface functionalization of particles can be realized with a surfactant or coupling agent. A surfactant is a chemical that lowers the interfacial tension between a polymer and a solid filler. And even better alternative is the use of coupling agents.

2.3.4 Coupling agent

Stable dispersion of filler in the final composite is necessary to eliminate filler agglomerates that would act as weak points that might induce electrical or mechanical failure.
A coupling agent is a chemical that is applied to the surface of a material that has to be modified to make it compatible with another material of a different nature [138]. The molecular structure enables the coupling agent to work as an intermediary in bonding organic and inorganic materials [139]. The first coupling agents were applied in the early 1940s, when glass fibers saw their first use in enhancing the properties of organic polymers. A variety of coupling agents, such as silanes, zirconates, titanates and zircoaluminates have been introduced to the market since then in order to improve the interface between the polymer and the filler [140].

The major roles of surface functionalization are:

1) to stabilize the nanoparticles inside a polymer matrix (obtain a good dispersion of the particles) via chemical bonding,
2) to obtain thermodynamical and chemical compatibility between polymer matrix and incorporated filler and keep the particles separated from each other;
3) to improve the adhesion at the interfaces between matrix and particles [141].

Among these, silane coupling agents (SCA) form the most widely studied group [142].
In general, the SCA molecule contains two classes of functionality. A common formula for SCA is $R(CH_2)_nSiX_3$. X is a hydrolysable group, typically alkoxy, acyloxy, halogen or amine. The R group is a nonhydrolysable organic radical that may possess functionality that shows the desired characteristics (see Fig. 2.5).

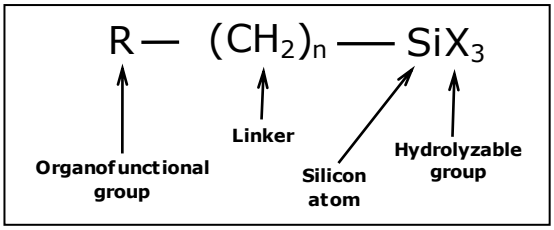

Fig. 2.5: The general formula for a silane coupling agent [143].

Silane coupling agents present three main advantages:

1) they are commercially available at a large scale;
2) at one end, they have alkoxy silane groups capable of reacting with an OH-rich surface, and
3) at the other end they have a large number of functional groups which can be tailored as a function of the matrix to be used [144].

The thermal conductivity of the polymer-filler system can be improved by surface modification of the particles due to a decrease of the thermal contact resistance in the composite. This is done through the improvement of the interface between matrix and particles [145]. Good quality interfaces between matrix and filler are needed to achieve high performance, because the interface is usually the weakest point of the composite.
A coupling agent acts as a "molecular bridge" at the interface of dissimilar polymer matrix and fillers, resulting in the formation of covalent bonds across the interface, which subsequently improves the properties of the composite system. Silane treatments on particular inorganic fillers may provide important improvements in rheology of filled polymers and in protecting the filler against mechanical damage during high-shear operations such as mixing, extruding, and injection molding.

2.4. Materials used

2.4.1 Host material

The base polymer material used in this research is ER. The epoxy consists of a diglycidyl ether of bisphenol-A (DGEBA) type CY231 and preaccelerated methyltetrahydrophthalic acid anhydride (MTPHA) curing agent type HY925 supplied by Huntsman. The chemical structures are indicated in Figs. 2.6 and 2.7. The system was chosen because of low viscosity before curing and the widespread use in the high voltage industry.

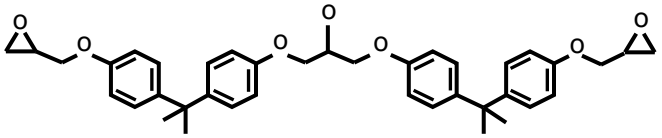

Fig. 2.6: Chemical structure of a bisphenol-A type epoxy resin.

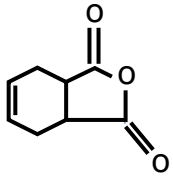

Fig. 2.7: Chemical structure of the curing agent (MTPHA).

2.4.2 Filler material

Conventional alumina (Al_2O_3) is commonly used as filler to improve electrical, mechanical and thermal properties (λ ~ 20-30 W/m·K at room temperature) in insulating composites. Al_2O_3 has a low thermal expansion, it is resistant to most chemicals, and it is a good electrical insulator with high wear resistance [146]. Aluminum oxide in the form of micro- and nano-filler was studied by many research groups and results of experiments have been presented in many papers. Al_2O_3 was therefore chosen for comparison and to have a proof-of-concept to build on.

Aluminum nitride (AlN) was chosen as ceramic filler because of its unique combination of high thermal conductivity (λ ~ 40-200 W/m·K at room temperature), moderate strength and good dielectric properties (ε_r =8.9 at 1 MHz, $\tan\delta$ =10^{-3}-10^{-4}, ρ_R >10^{14} Ohm·cm, dielectric strength 20 kV/mm, bandgap 6.2 eV) [23, 147-149].

Magnesium oxide (MgO) was chosen as a filler material because it has shown to reduce the amount of space charge in the polymer and better withstand tree propagation and partial discharges than neat polymer [80, 81, 150].

Boron nitride (BN) is a high thermal conductivity material with low dielectric permittivity and high dielectric breakdown strength [151-154].

It has been reported in literature that the presence of silicon dioxide (SiO_2) nanoparticles affect the intrinsic properties of neat epoxy in different aspects [155]. Epoxy-silica is one of the most popular composite resins in use, showing improved electrical breakdown strength [64, 65, 77, 156], lowered thermal expansion [156], enhanced PD resistance [63-65, 68, 156], reduced erosion depth [64, 68, 156, 157], higher volume resistivity [65, 105], enhanced mechanical properties [156] and improved thermal conductivity [99].

Nano-Al_2O_3 and AlN particles were obtained from Sigma-Aldrich. Nano-SiO_2 was supplied in the form of Nanopox® from the company Nanoresins. MgO was provided by Strem Chemicals. Micro-Al_2O_3 and micro-SiO_2 were received from Albemarle and Huntsman, respectively.

2.4.3 Silane coupling agent

The particle surface modification was performed with an epoxyde-functionalized SCA, namely γ-glycidoxypropyl-trimethoxysilane (GPS or GLYMO) (see Fig. 2.8). GPS consists of an organofunctional epoxy group, which is compatible with the ring of ER, and 3 alkoxy groups, which transform to hydroxy groups in the presence of water and react with the surface of the particles we use.

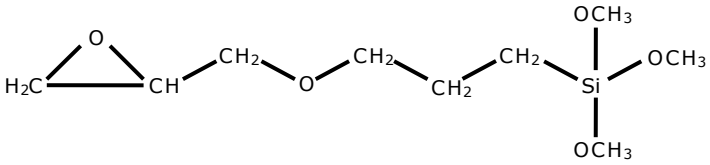

Fig. 2.8: Chemical structure of γ -glycidoxypropyltrimethoxysilane (silane coupling agent).

2.5 Synthesis

A schematic representation of the synthesis procedure that was developed is shown in Fig. 2.9.

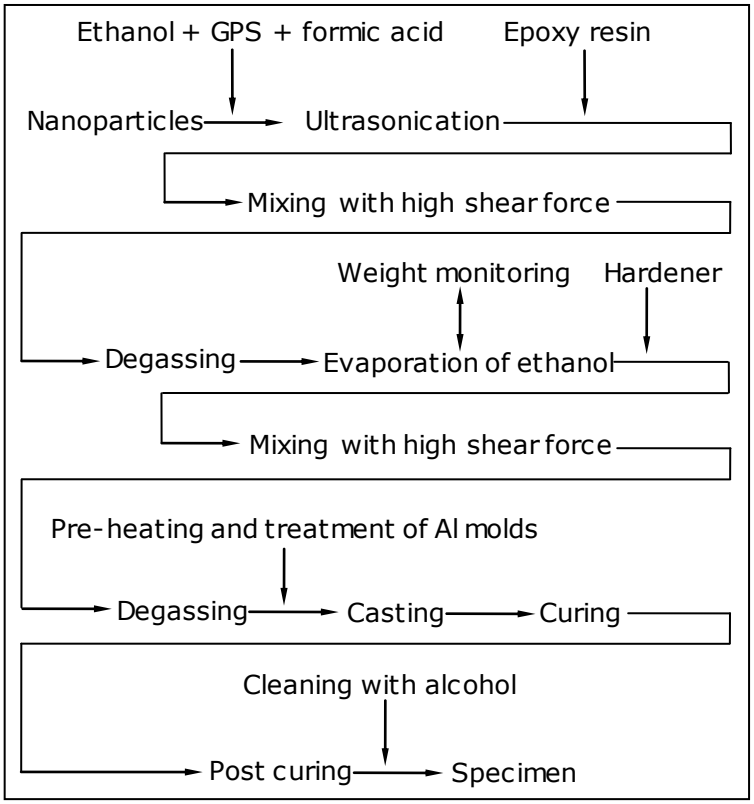

Fig. 2.9: Schematic representation of the nanocomposite preparation.

2.5.1 Dispersion of particles

The as-received nanoparticles were dispersed in ethanol (C_2H_5OH) by means of ultrasonication at room temperature to break up any agglomerates. Formic acid was added to adjust the pH value to about 4 for AlN and Al_2O_3 particles, pH 3 for MgO particles and 2 for BN to reach a higher zeta-potential [158-161]. The zeta potential indicates the degree of repulsion between adjacent, similarly charged particles in a dispersion. GPS was added to the solution for functionalization of the particles and the solution underwent further sonication to allow hydrolysis and silanol formation. The dispersion of nanoparticles was verified using laser diffraction. The objective was to determine the best way of dispersing the nanoparticles.

2.5.1.1 Laser diffraction method

Laser Diffraction is the most widely applied particle sizing technique. It uses angular light scattering to determine the particle size distribution. It is suitable for almost any kind of sample because of its broad measuring range and high resolution (particle diameter range 0.04 - 2000 µm). Dry samples are dispersed in water, ethanol, cyclohexane or air. Suspensions and emulsions can be measured in water. Spray droplets can also be measured in air. The result from the laser diffraction comes in the form of a size distribution of the particles. It is intended for characterization of spherical or almost spherical particles. The instrument used is the Coulter LS 230.

2.5.1.2 Sample preparation procedure

0.5 g of alumina nanoparticles were dispersed in 10 g of demineralized water or ethanol. Sodium-diphosphate ($Na_4P_2O_7$) was added to a solution as a dispersant. It is an anionic dispersant which reduces the surface tension of the particles and keeps the solution stable. The particles in water were manually shaken for some seconds. The dispersion of particles in ethanol was realized in different ways:

- ✓ ultrasonic (US) bath for 30, 60 and 120 minutes,
- ✓ ultrasonic probe for 5 minutes,
- ✓ ultraturrax for 8 minutes,
- ✓ mixing by hand.

2.5.1.3 Dispersion of nanoparticles in a solvent

Fig. 2.10 shows the particle distribution of Al_2O_3 particles in water and ethanol. The particles were mixed only by manual shaking of the suspension. It can be seen that the suspension of nanoparticles inside water is good. Only 5 wt.% of the particles are larger than 350 nm. The average particle size is 141nm. The result for the dispersion inside ethanol is completely different from the suspension in water: only 5 wt.% of the particles are smaller than 1 micron. Most agglomerates of particles have a diameter of approximately 15 µm. The suspension of nanoparticles inside ethanol was subjected to various mechanical methods to disperse nanoparticles evenly inside the solvent. Fig. 2.11 shows the results of dispersion for different methods.
Surprisingly, the least powerful method, the ultrasonic bath shows to be the best method for particle dispersion. After 30 minutes of sonication about 90% of the particles are below 350 nm, with average particle size (APS) of 141 nm, which is similar to the results of water (see Fig. 2.10).

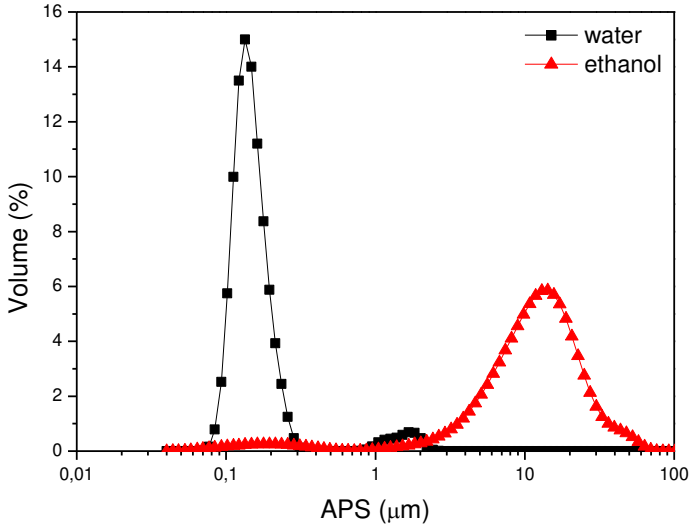

Fig. 2.10: The dispersion of Al_2O_3 nanoparticles in water and ethanol.

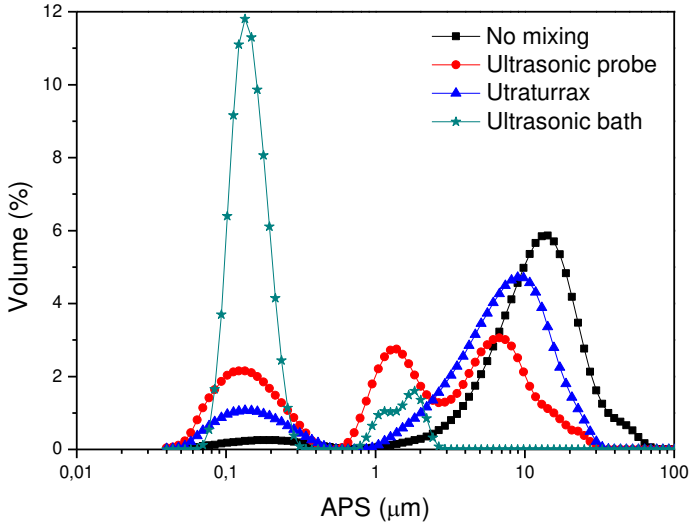

Fig. 2.11: Influence of the mixing method on the dispersion of Al_2O_3 in ethanol.

After 60 minutes all agglomerates above 300 nm are broken down, as can be seen in Fig. 2.12.

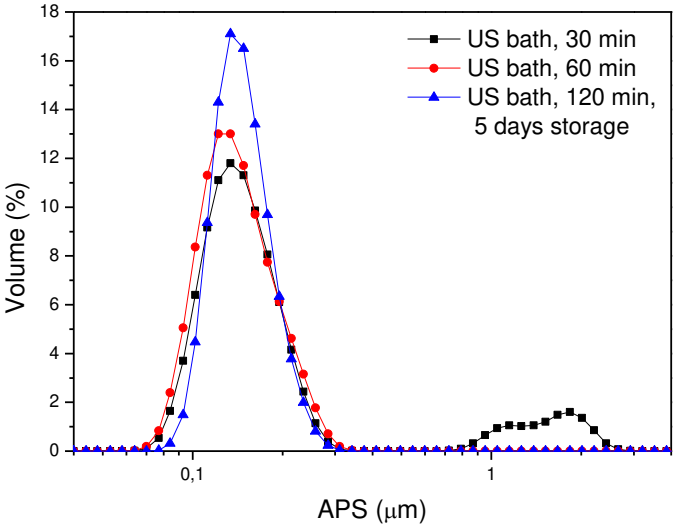

Fig. 2.12: Influence of time duration of an US bath on the Al_2O_3 dispersion in ethanol.

Ultraturrax is a dispersion tool which main part consists of a rotating and a fixed part (stator). Due to the high rotation speed of the rotor, the medium, which is to be processed, is drawn axially into the dispersion head and then forced radially through the slots in the rotor/stator arrangement. The high acceleration of the material produces extremely strong shear and thrust forces. In addition, high turbulence occurs in the shear gap between rotor and stator, which provides optimum mixing of the suspension (see Fig. 2.13).
The ultraturrax gives a particle size distribution which is slightly better than without mixing, but not much. Only 15 wt.% of the particles are below 1 micron.

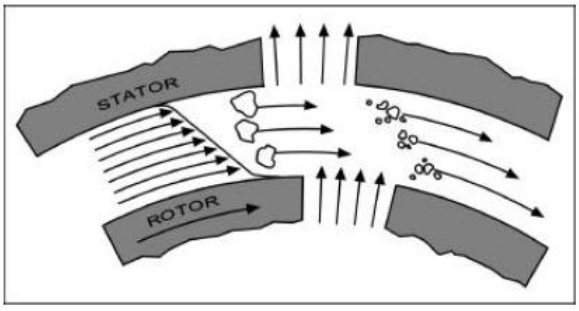

Fig. 2.13: Principle operation of ultraturrax [162].

The ultrasonic probe is the dispersion method with the highest energy density in this series of measurements. Drawback of this method is the relatively short time the probe can be applied. When the probe is applied longer than 10 minutes, the solution starts to boil. The size distribution is better than for ethanol without mixing, but still only 30 wt.% of the particles are below 0.6 µm. Interesting are the two peaks above 0.6 µm, which indicate that the ultrasonic probe does not simply disperse the particles but also encourages agglomerations of specific sizes.

2.5.1.4 Stability of the nanoparticle dispersion in the solvent

Additional tests have been made on Al_2O_3 treated with GPS, in order to check if the ethanol-Al_2O_3 suspension is stable and can be stored for longer periods of time. The suspensions of both treated and untreated particles did not show any reagglomeration of particles even after 5 days of storage (see Fig. 2.14). Therefore, we can draw a conclusion that nanoparticles can be dispersed in ethanol and stored for at least a week.

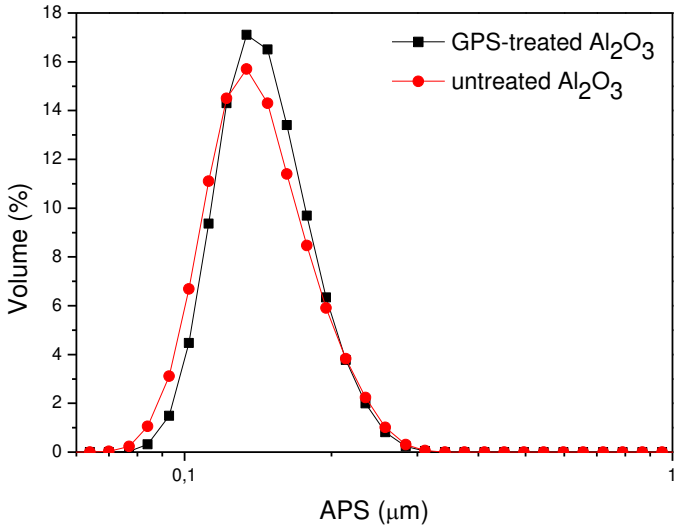

Fig. 2.14: Influence of silane surface treatment on the Al_2O_3 dispersion in ethanol after 5 days of storage.

2.5.1.5 Alternative solvent

Methanol can be used as an alternative solvent instead of ethanol. Methanol has a boiling point (64.7 °C) which is about 15 °C lower compared to ethanol (78.4 °C). This makes it easier for the solvent to evaporate in the next step of synthesis. A good dispersed suspension

was obtained using methanol as a solvent. The use of methanol makes the sample preparation faster. The drawback is that we could not check the dispersion of nanoalumina in methanol, since only the use of water- or ethanol-based solutions is allowed in the Laser Diffraction instrument Coulter LS 230. The second disadvantage of methanol is that it is not environment friendly.

2.5.1.6 Summary

The laser diffraction analysis showed that water would be the best solvent for nanoparticles. However, due to the relatively high boiling point it was not chosen for the synthesis of nanocomposites. Methanol can be an alternative solvent but it is more harmful compared to ethanol. Ethanol is a good solvent in combination with an ultrasonic bath. 60 minutes was found to be sufficient to break down all micron-sized agglomerates. The laser diffraction results of the suspension of ethanol with Al_2O_3 indicated that nanoparticles do not reagglomerate within 5 days and can be stored in these conditions.

2.5.2 Surface functionalization

Pretreated fillers may be much easier to disperse in an organic phase since the water layer, which acts as an adhesive to hold filler agglomerates together, is replaced (or covered) by an organofunctional silane [142].
SCA keeps nanoparticles separated from each other and make them compatible with the ER matrix (see Fig. 2.15).

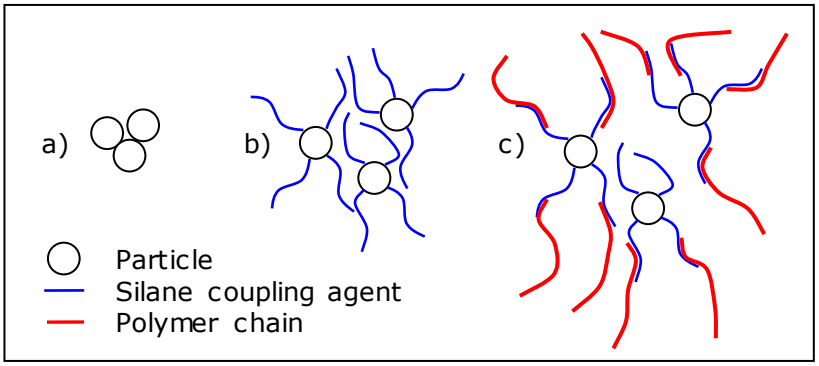

Fig. 2.15: The role of the surfactant: (a) Particles without surfactant tend to stick together; (b) the surfactant connects to the particle and isolates them, in the ideal case it keeps them separated; (c) when introduced into the epoxy resin, the surfactant connects to the polymer chains.

The reaction between inorganic particles and GPS can be shown in two steps.
The first step is the hydrolyzation of alkoxy groups of silane by the water in the solvent, in our case ethanol, to form silanol groups [163]:

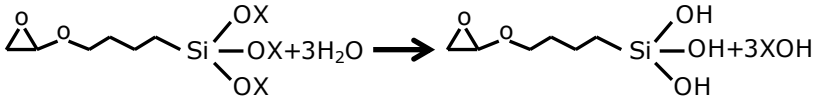

Fig. 2.16: Hydrolysis of SCA.

The second step is the condensation of silanol groups with the hydroxyl groups on the surface of nanoparticles, or with neighboring hydrolyzed silane molecules [164]:

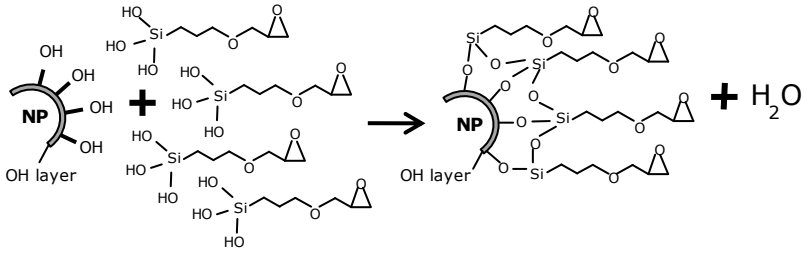

Fig. 2.17: Condensation of silanol on alumina surface.

As it is evident from the hydrolysis reaction, the availability of free OH-groups on the nanoparticle surface is necessary for successful surface modification. The particles we use have a hydroxide layer on their surface, which reacts with the OH-groups of the GPS. In case of oxides like Al_2O_3 and MgO the presence of hydroxyl groups on the surface is known. Oxidation causes the formation of an oxide hydroxide layer around the oxide core. The reactivity of AlN powder with water has been reported by Bowen et al. [165]. A thin aluminum hydroxide shell forms on the surface of the AlN core at room temperature. When AlN nanoparticles are hydrolyzed, initially an amorphous layer composed of AlOOH is formed on the surface of the AlN particles, which then transforms into $Al(OH)_3$. The aluminum hydroxide layer formation is realized according to the following chemical reactions:

$$AlN(s) + 2H_2O(l) \rightarrow AlOOH(amorph) + NH_3(g)\,, \tag{2.1}$$

$$NH_3(g) + H_2O(l) \rightarrow NH_4^+(aq) + OH^-(aq)\,, \tag{2.2}$$

$$AlOOH(amorph) + H_2O(l) \rightarrow Al(OH)_3\,. \tag{2.3}$$

The surface treatment of BN nanoparticles was reported in [145].

2.5.2.1 The optimum amount of coupling agent

The crucial question is how to calculate the exact amount of GPS needed for particle treatment. An excess of GPS can lead to a homoreaction between the molecules of the SCA. This can subsequently lead to a formation of a gel substance in quantities large enough, so that their influence results in the deterioration of the properties of the nanocomposite [144]. For this reason it is important to determine the minimal amount of GPS needed for a successful surface modification of the filler.

The approximate amount of GPS can be calculated with two methods. The first method calculates the amount as:

$$m = \frac{4 \cdot \pi \cdot r^2 \cdot l \cdot \rho_{GPS}}{\left(4/3\right) \cdot \pi \cdot r^3 \cdot \rho_f} = \frac{3 \cdot l \cdot \rho_{GPS}}{r \cdot \rho_f}, \tag{2.4}$$

where r is the average radius of the nanoparticles which are assumed spherical, l is the thickness of the SCA layer, ρ_{GPS} and ρ_f are the density of SCA and the filler material, respectively. In our experiments we assumed that the GPS layer is about 1 nm thick (see Fig. 2.18).

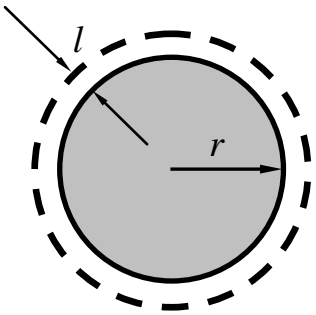

Fig. 2.18: Schematic representation of a nanoparticle with grafted SCA on it.

$$m = \frac{3 \cdot l \cdot \rho_{GPS}}{r \cdot \rho_f} = \frac{3 \cdot 1 \cdot 1}{25 \cdot 4} = 3\%$$

The second method to approximate the amount of SCA needed is via the amount of hydroxyl groups on the particle surfaces, since GPS reacts with those groups on the surface area of the nanoparticles. Since GPS reacts with OH-groups, it is needed to find out how many hydroxy-groups 1 gram of the filler material contains. One of the easiest ways to

find out the amount of OH-groups inside the material is to perform thermogravimetric analysis (TGA) under nitrogen atmosphere. The covalent bonds between the mineral and hydroxy groups are breaking up in the temperature interval between 450 and 600 °C. For a specific example we used alumina nanoparticles. The mass of as-received alumina particles is decreased by 0.312% in the mentioned temperature range (see Fig. 2.19).

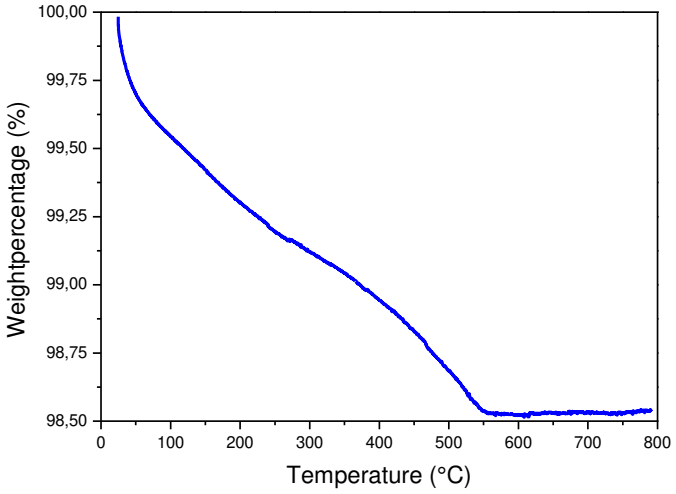

Fig. 2.19: TGA graph of the loss of mass of alumina nanoparticles as a function of temperature.

We can conclude that 1 gram of Al_2O_3 contains 3.12 mg of hydroxyl groups. For our case it is necessary to know the number of OH-molecules. This number can be calculated using the formula:

$$N = N_A \cdot \nu \ , \tag{2.5}$$

where N_A is Avogadro's number and ν is the number of moles. Avogadro's number (or Avogadro constant) is the number of molecules in one mole. The number of moles can be found by simply calculating the ratio of the mass of the material and its molar mass:

$$\nu = \frac{m}{M} \ . \tag{2.6}$$

Formula (2.5) can be rewritten as follows:

$$N = N_A \cdot \frac{m}{M} \ . \tag{2.7}$$

The mass of the material we know, the molar mass is 17 g·mol^{-1}, N_A is 6.022·10^{23} mol^{-1}.

$N = 6.02 \cdot 10^{23} \cdot \frac{3.12 \cdot 10^{-3}}{17} = 1.104 \cdot 10^{20}$ OH molecules in 1 gram of alumina powder.

The density of hydroxy groups per square nanometer can be found using the surface area of nanoparticles. The effective surface area of Sigma-Aldrich alumina particles is 40 m^2/g. In 40·10^{18} nm^2 1.104·10^{20} molecules are contained, in 1 nm^2 only 2.76 molecules. It means that 1 square nanometer of particle surface contains approximately 3 OH groups. The minimum number of GPS molecules that can attach to the surface unit is 1, because GPS has 3 hydrolyzable groups in one molecule. To modify 1 gram of alumina 40·10^{18} molecules of GPS are needed. Since we know the molar mass of GPS, which is equal to 128 g·mol^{-1}, the mass can be calculated, using the following equation:

$$m = \nu \cdot M = \frac{N}{N_A} \cdot M \ , \tag{2.8}$$

$$m = \frac{40 \cdot 10^{18}}{6.02 \cdot 10^{23}} \cdot 128 = 0.0085 \text{ g.}$$

The obtained value should be multiplied by an empirical factor of 5, because we assumed that all three hydrolyzable groups would react at the same time. But the silane can also attach with only one or by two bonds instead of all three.

At the end of this calculation, we can summarize that the amount of GPS that should be used is 3% of the weight of the alumina nanoparticles to be treated.

The main parameters which are needed in this method are the surface area of nanoparticles and the TGA results under a nitrogen atmosphere.

According to both methods the amount of GPS needed for e.g. functionalizing nanosized alumina equals approximately 3% of the weight of the filler used.

The effect of the coupling agent is to alter the adhesion between filler and polymer matrix in the composite, which in turn will change the composite properties. Therefore, if too much coupling agent would be dispersed in the system, the thermal conductivity of the composite could

be affected, since the used silane-based coupling agent is a material with low thermal conductivity similar to the polymer matrix. The excess of coupling agent can cause phonon scattering, hence decreasing the thermal conductivity of the composite. Thus, care should be taken to determine the correct amount of coupling agent.

2.5.2.2 Validation of GPS grafting

The surface chemistry of as-received and GPS-treated nanoparticles was characterized by a Fourier transformed infrared (FTIR) spectroscope and thermogravimetric analysis (TGA). This was done to check whether the GPS was indeed present at the surface of the nanoparticles.

FTIR is a technique that utilizes the vibrational response of molecules when exposed to infrared (IR) radiation. The utility of IR spectroscopy comes from interactions of light with specific molecular vibrations. When molecules are exposed to IR, they absorb energies that correspond to their vibration frequency and transmit the unabsorbed frequencies. These absorbed frequencies are recorded by a detector. The absorbed IR energizes the components of the molecule, which vibrates at greater amplitudes. From the absorption spectrum produced, the molecule in question can be identified by matching the absorption wavelength or frequency to those already known. The infrared spectrum of a material provides a fingerprint unique to that chemical structure [166].

The FTIR spectrum was recorded in the range from 4000 to 450 cm^{-1}. As an example, the FTIR spectra of as-received and GPS treated nanoalumina particles are shown in Fig. 2.20.

It can be noticed that the spectrum of as-received (nonmodified) particles has a broad peak at around 3442 cm^{-1} due to hydroxyl groups on the surface of the nanoparticles that are bound either to absorbed water molecules or to each other, via hydrogen bonding. The small peak at 1634 cm^{-1} indicates the deformation of OH groups or water molecules [167]. After surface treatment the peak corresponding to the OH-groups was reduced. This indicates a reaction of GPS with the functional OH groups on the surface of the Al_2O_3 particle. The FTIR spectrum of functionalized particles shows two peaks at 2929 and 2858 cm^{-1}, which correspond to asymmetrical and symmetrical stretching of CH_3 and CH_2. The GPS contains both groups in its chemical structure. The peak of the nonmodified particles at around 924 cm^{-1} corresponds to stretching vibrations of Al-O bonds.

Due to the very small amount of coupling agent used, the peaks corresponding to epoxyde ring vibration (~1250, 950, 860 cm^{-1}) or silanol (Si-OH, Si-O, Si-O-Al) groups (1050-1250 cm^{-1}) were hardly detected [160, 168].

Summarizing, FTIR analysis indicates a broad OH peak in the region 3000-3700 cm^{-1} for the nonmodified particles and shows that the SCA can react with these hydroxy functional groups, subsequently allowing

chemical and physical bonding between the alumina nanoparticles and the epoxy polymer matrix [169].

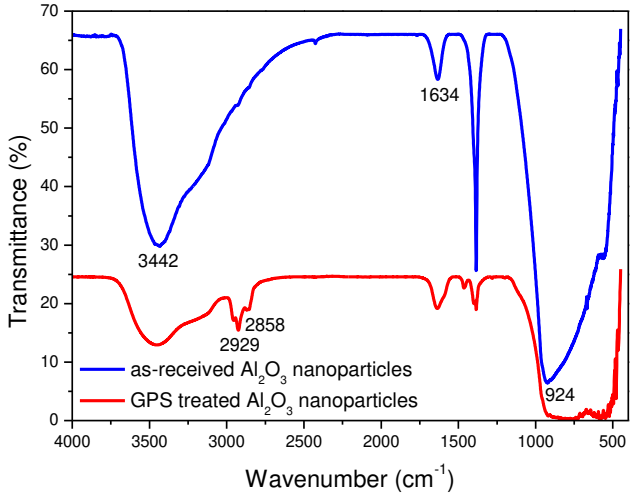

Fig. 2.20: FTIR spectra of untreated and GPS treated nanoalumina particles.

The thermal degradation behaviour of untreated nanoparticles and particles treated with silane coupling agent were characterized using TGA. This was done to check whether the GPS was indeed present at the surface of the alumina particles. The measurement was realized with a TGA 7 Thermogravimetric Analyzer (produced by PerkinElmer) in air atmosphere. The heating rate for the measurement was 10 °C/min.
Figs. 2.21 and 2.22 show the effect of the treatment with SCA on the degradation behaviour of Al_2O_3 and MgO nanoparticles, respectively. Modified particles have higher weight loss than untreated particles. The SCA grafted on the particle surface has an organic chain, which degrades at elevated temperatures, thus a weight loss was observed for treated alumina and MgO particles. TGA analysis confirmed that the SCA was successfully grafted on the nanoparticles surface [170, 171].
Unfortunately, nuclear magnetic resonance (NMR) analysis did not indicate silicon atoms on the surface of nanoparticles. It can be explained by the small amount of silicon. The minimum amount of silicon that can be detected with NMR depends on the state of the atom, such as its symmetry. Silicon is not very sensitive to magnetic fields. Therefore NMR can only identify the active isotope ^{29}Si, which is only 4.7% of the total amount of silicon. The sensitivity of ^{29}Si NMR compared to ^{1}H NMR is $8 \cdot 10^{-3}$.

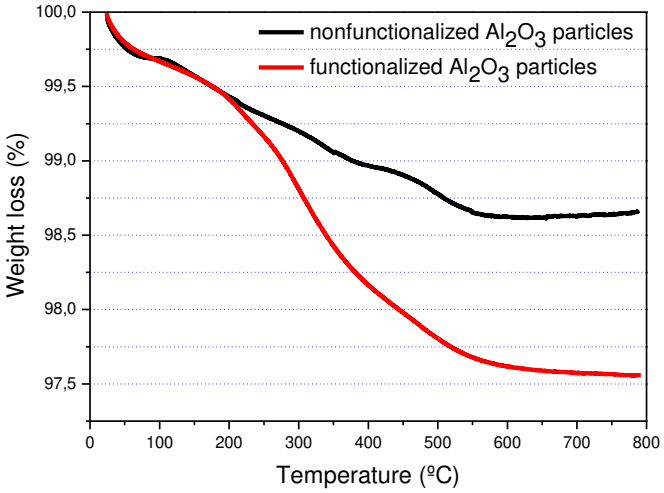

Fig. 2.21: TGA spectra of untreated and GPS treated Al_2O_3 nanoparticles.

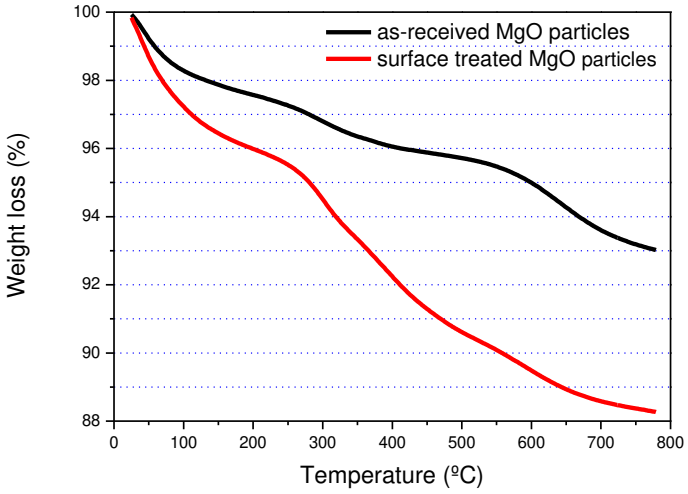

Fig. 2.22: TGA spectra of untreated and GPS treated MgO nanoparticles.

2.5.3 Mixing

The ER was added to the suspension of ethanol and surface modified nanoparticles and mixed with a high shear force mixer in order to disperse the functionalized particles in the resin. It is better to mix nanoparticles with resin instead of hardener, because the hardener is very sensitive to humidity. So mixing nanofillers with hardener would

influence the electrical and dielectric properties of the test specimens [172].
The solution of epoxy resin and functionalized particles together with ethanol was heated in a reflux apparatus for approximately 12 hours to remove the solvent. A magnetic stirrer was used during the evaporation process in order to ensure good dispersion of the nanoparticles inside the epoxy. Subsequently, the hardener was added and the mixture was stirred with a high shear mixer at 5000 rpm for 15 minutes. Afterwards the resin was degassed under vacuum and subjected to ultrasonication for typically one to two hours in order to remove air voids that were trapped during the mixing process.

2.5.4 Casting and curing

The final composite was cast in pre-heated aluminum molds, treated with release agent and cured at 140°C for 3 hours. The samples were post-cured at 140°C for 14 hours.

2.6. Ex-situ and in-situ polymerization processes

The ex-situ process stated above was successfully applied for Al_2O_3, AlN, BN and MgO nanoparticles.
ER-SiO_2 compounds were not created using this ex-situ polymerization process. The silica nanoparticles were synthesized inside the epoxy resin (in-situ). The binary composite system of 31.8 wt.% of silica and the ER was diluted to prepare appropriate concentrations of SiO_2. The rest of the procedure was the same as for the other nanocomposite samples, i.e. mixing with hardener, degassing and curing.
The preparation process of composites containing a combination of two different fillers inside the host polymer was the same as for Al_2O_3 or any other filler, but instead of ER the diluted silica-epoxy system with the required amount of SiO_2 inside was added.

2.7 Microcomposite preparation scheme

The epoxy composites containing Al_2O_3 or SiO_2 microparticles were fabricated in six steps:

1) mixing the epoxy resin, hardener and filler by conventional mechanical high shear stirring;
2) degassing;
3) mixing in an ultrasonic bath;
4) casting into the molds;
5) curing;
6) postcuring.

2.8 Specimens investigated

The specimens, volume fraction of the filler, details about surface modification of the particles, and type of the composite are summarized in Table 2.2.

Table 2.2: Specimens investigated.

Specimen	Vol.%	SCA	Type of composite
Neat ER	0		
ER-Al_2O_3-0.5	0.002	+	PNC
ER-Al_2O_3-2	0.006	+	PNC
ER-Al_2O_3-5	0.016	+	PNC
ER-Al_2O_3-10	0.033	+	PMesC
ER-Al_2O_3-15	0.051	+	PMesC
ER-AlN-0.5	0.002	+	PNC
ER-AlN-2	0.007	+	PNC
ER-AlN-5	0.019	+	PMesC
ER-AlN-10	0.039	+	PMesC
ER-MgO-0.5	0.002	+	PNC
ER-MgO-2	0.007	+	PNC
ER-MgO-5	0.017	+	PNC
ER-MgO-10	0.036	+	PMesC
ER-MgO-30	0.126	-	PMesC
ER-SiO_2-0.5	0.003	-	PNC
ER-SiO_2-2	0.011	-	PNC
ER-SiO_2-5	0.028	-	PNC
ER-SiO_2-10	0.057	-	PNC
ER-SiO_2-15	0.088	-	PNC
ER-70BN-10	0.058	-	PNC
ER-70BN-10*	0.058	+	PNC
ER-0.5BN-10	0.058	-	PMC
ER-0.5BN-10*	0.058	+	PMC
ER-1.5BN-10	0.058	-	PMC
ER-1.5BN-10*	0.058	+	PMC
ER-5BN-10	0.058	-	PMC
ER-5BN-10*	0.058	+	PMC
ER-70BN-20	0.121	-	PMC
ER-0.5BN-20	0.121	-	PMC
ER-1.5BN-20	0.121	-	PMC
ER-5BN-20	0.121	-	PMC
ER-Al_2O_3-5 (m)	0.016	-	PMC
ER-Al_2O_3-10 (m)	0.033	-	PMC
ER-Al_2O_3-20	0.070	-	PMC
ER-Al_2O_3-30	0.115	-	PMC
ER-Al_2O_3-40	0.168	-	PMC
ER-Al_2O_3-50	0.232	-	PMC
ER-Al_2O_3-60	0.312	-	PMC
ER-SiO_2-5 (m)	0.028	-	PMC
ER-SiO_2-10 (m)	0.057	-	PMC
ER-SiO_2-15	0.088	-	PMC
ER-SiO_2-20	0.120	-	PMC
ER-SiO_2-40	0.267	-	PMC
ER-SiO_2-60	0.450	-	PMC

2.9 Morphological characterization of the particles and created composites

2.9.1 XRD technique

Crystalline materials have a higher thermal conductivity compared to amorphous bodies. The distance between neighbouring atoms in a solid crystal is shorter than in an amorphous material and arranged in a regular pattern. Therefore the heat can be transferred much faster (see sections 3.4-3.6). An inorganic material such as alumina crystallizes in different phases, depending on production conditions [173-175]. All these phases have different thermal conductivity [176, 177]. We used X-ray diffraction (XRD) in order to identify the crystalline structure and purity of as-received particles.

2.9.1.1 Theoretical background and measurement principle

XRD is a non-destructive analytical technique which reveals information about the crystallographic structure, chemical composition, and physical properties of materials. The XRD technique is based on observing the scattered intensity of an X-ray beam hitting a sample as a function of incident and scattered angle, polarization, and wavelength or energy.
XRD is used to identify bulk phases, to monitor the kinetics of bulk transformations, and to estimate particle size. An attractive feature is that the technique can be applied in situ.
Fig. 2.23 illustrates how diffraction of X-ray by crystal planes allows one to derive the lattice spacing by using the Bragg relationship:

$$n\vartheta = 2d\sin\theta,\ \ n = 1, 2, \ldots \tag{2.9}$$

where ϑ is the wavelength of the X-rays;
d is the distance between two lattice planes;
θ is the angle between the incoming X-rays and the normal to the reflecting lattice plane;
n is an integer called the order of the reflection [178, 179].
The XRD pattern of a powdered sample is measured with a stationary X-ray source (usually CuK_{α}) and a movable detector, which scans the intensity of the diffracted radiation as a function of the angle 2θ between the incoming and the diffracted beams.

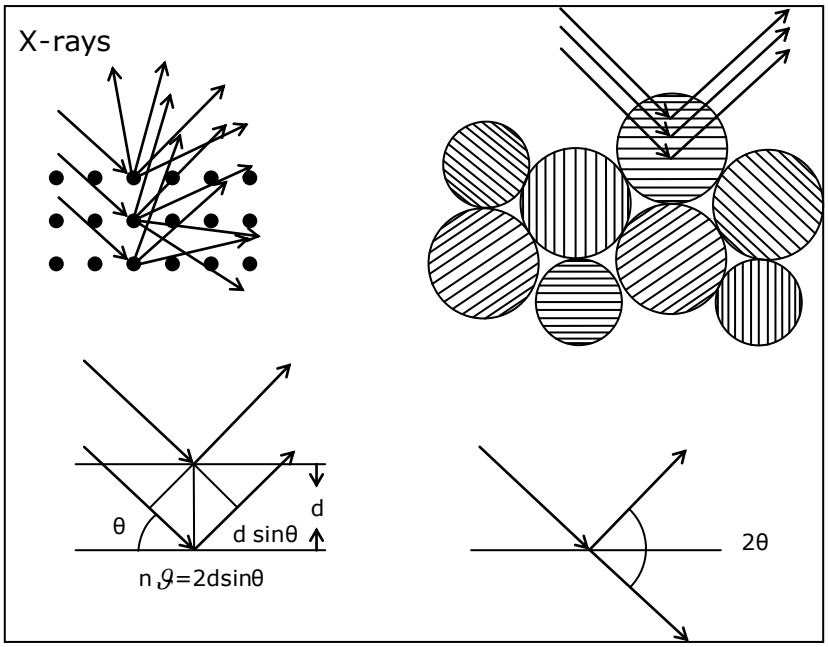

Fig. 2.23: X-ray scattered by atoms in an ordered lattice interface constructively in directions given by Bragg's law. Diffractograms are measured as a function of the angle 2θ. Rotation of the sample during measurement enhances the number of particles that contribute to diffraction [180].

When crystallites are less than approximately 100 nm in size, appreciable broadening in the X-ray diffraction lines will occur. The broadening can be attributed either to the amorphous or semicrystalline nature of the investigated powder or to the small particle size. These regions may in fact correspond to the actual size of the particles. At other times, however, these regions form "domains" in the larger particle and may be a distinguishing and important feature [179].
Fig. 2.24 shows the X-ray diffraction pattern of nanocrystalline silicon which exhibits significant line broadening. Shown for comparison is the diffraction pattern from bulk Si with a particle size greater than 20 nm. It can be noticed that the $K_{\alpha 2}$ line is well resolved in the bulk sample, but indistinguishable in the n-Si case. The extent of broadening is described by *b*, which is the width at 50% of the peak value intensity.

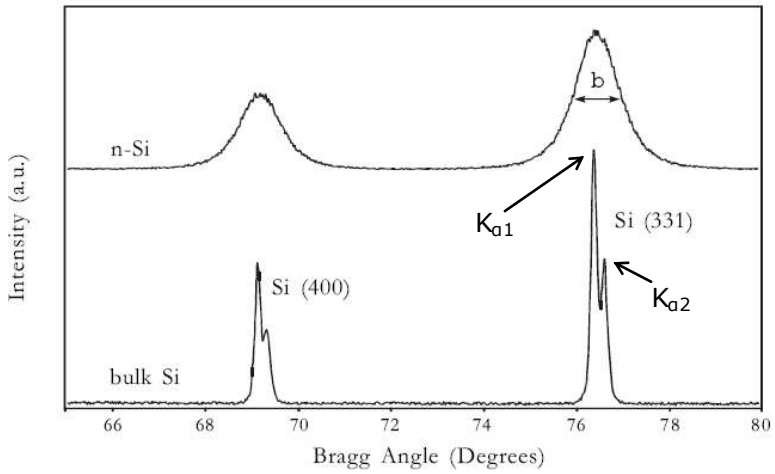

Fig. 2.24. Diffraction patterns of nanocrystalline silicon showing broadening because of particle size [181].

2.9.1.2 Measurement results

X-ray diffraction measurements of as-received particles were performed on a Bruker-AXS D8 Advance diffractometer using a CuK_α wavelength as radiation source. The 2θ ranges of the data were taken from 10° to 90° with an increment of 0.02°. The spectra obtained with XRD can be compared to reference spectra to identify the lattice structure.
The XRD chart of the BN fillers with different average particle size shows that the BN particles have a hexagonal crystal structure (see Fig. 2.25). Diffraction patterns on nano-, meso- and micro-crystalline BN indicate that the particles have exactly the same structure.

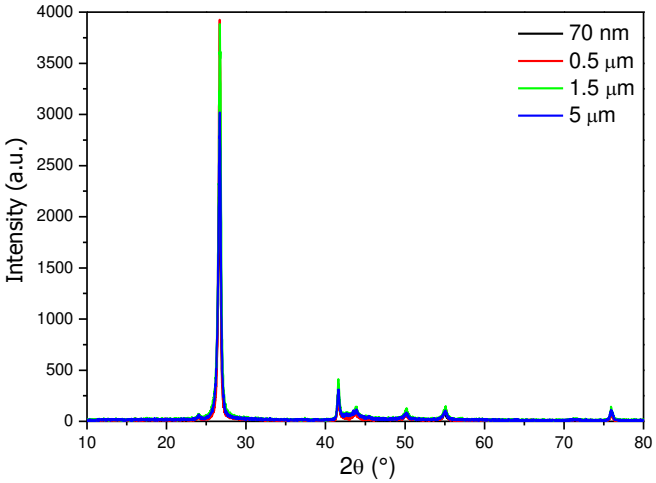

Fig. 2.25: X-ray diffraction patterns of BN particles. The spectra are hard to distinguish from each other because of the similarities of the BN particles.

As it can be seen from Fig. 2.26, AlN particles are present in a cubic and hexagonal crystalline structure. Al_2O_3 particles supplied by Sigma-Aldrich have orthorhombic and cubic crystalline structure (Fig. 2.27).

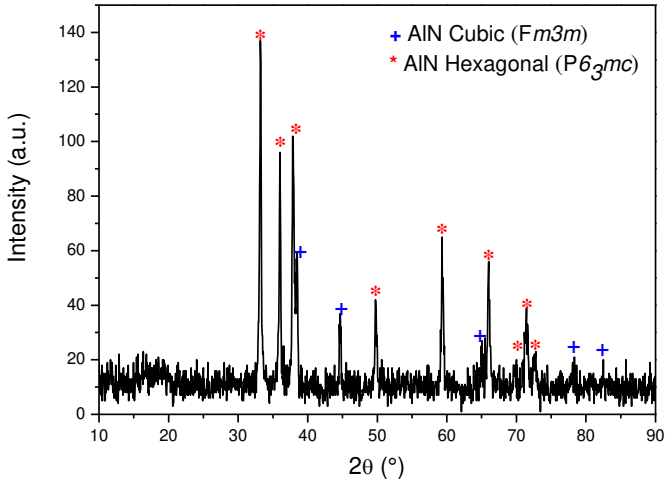

Fig. 2.26: X-ray diffraction pattern of AlN nanoparticles.

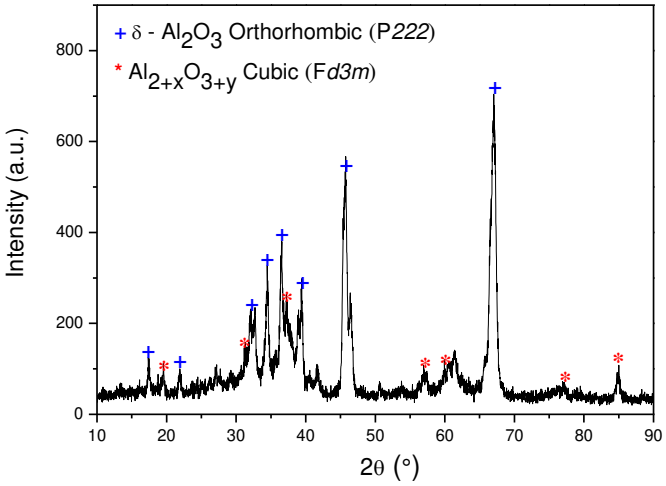

Fig. 2.27: X-ray diffraction pattern of Al_2O_3 nanoparticles.

α-Al_2O_3 nanoparticles supplied by IoLiTech have an orthorhombic crystal structure, while γ-Al_2O_3 have a monoclinic crystal structure (see Figs. 2.28 and 2.29). As it can be seen in Fig. 2.29b, the X-ray diffraction pattern of nanoalumina with an average particle size of 20 nm has a dramatic line broadening. That can be explained by the large amount of the amorphous phase in the sample.

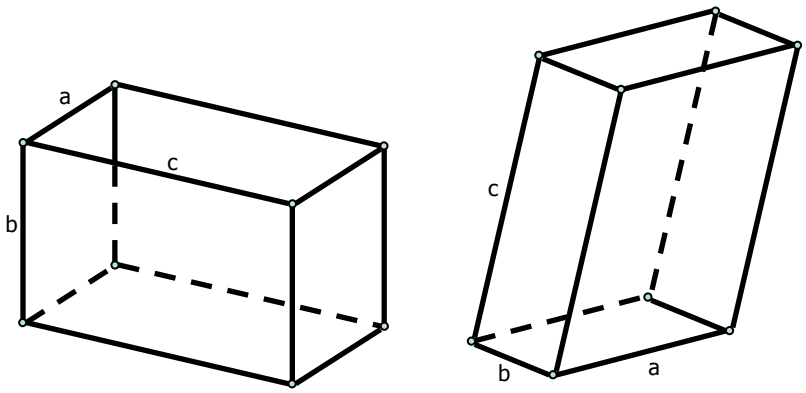

Fig. 2.28: Orthorhombic ($a \neq b \neq c$, $\alpha=\beta=\gamma=90°$) and monoclinic ($a \neq b \neq c$, $\alpha=\gamma=90°$, $\beta \neq 90°$) lattice structures (left and right, respectively).

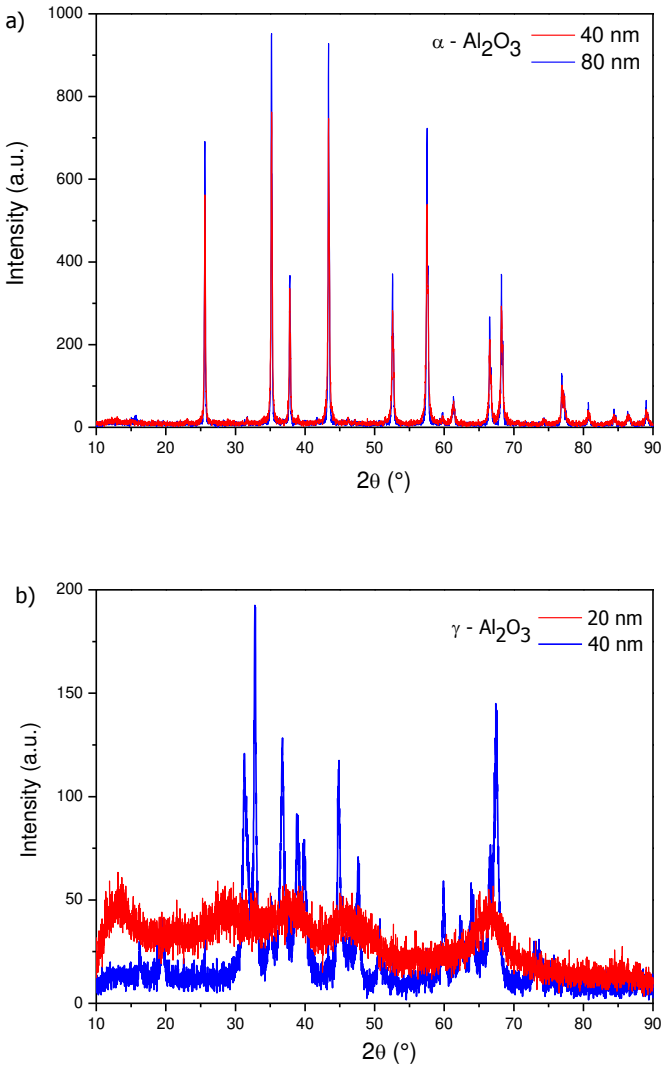

Fig. 2.29: XRD spectra of α-Al_2O_3 (a), γ-Al_2O_3 (b) nanoparticles with different size.

2.9.2 Electron microscopy

Normal visual light has a wavelength between 300 nm and 800 nm. Therefore, investigating an object smaller than 0.4 µm (400 nm) is not possible with a conventional optical microscope (OM). The typical wavelength of an electron beam is about 1 Å. Therefore the smallest detectable object is much smaller compared with OM.

Morphological observations of as-received particles and thin layers of created composites were performed by means of transmission electron microscopy (TEM) and scanning electron microscopy (SEM).
TEM was performed using a Philips CM30T electron microscope with a LaB_6 filament as electron source operated at 300 kV, to investigate the individual as-received nanoparticles, as well as the dispersion of filler inside the host polymer.
TEM is a microscopy technique where a beam of electrons is transmitted through a very thin specimen, interacting with the specimen as it passes through.
The sample preparation for TEM is a complex procedure, because the specimens are required to be less than a hundred nanometers thick and very smooth. High quality samples will have a thickness that is comparable to the mean free path of the electrons that travel through the samples, which may be only a few tens of nanometers.
The most simple and classical way to prepare a sample for TEM is mechanical polishing. Polishing needs to be done to a high quality, to ensure constant sample thickness across the region of interest. In our case mechanical polishing is not an option, because the mechanical influence on the organic material (epoxy) leads to rises in temperature, which in turn causes partial burning and twisting of the sample.
Ultramicrotomy is a method for cutting a specimen into extremely thin slices, which can be viewed in a TEM. For the best resolution, slices should be from 20 to 50 nm thick. Thin slices are cut with a diamond knife using an ultramicrotome and the sections are left floating on water that is held in a boat or trough. The slices are then retrieved from the water surface and mounted on a copper grid. Very often the Quantifoil® carbon polymer microgrid is placed on the top of copper grid, because one cell of the copper grid is relatively big and a specimen of nanometric dimensions can fall through it (see Fig. 2.30).

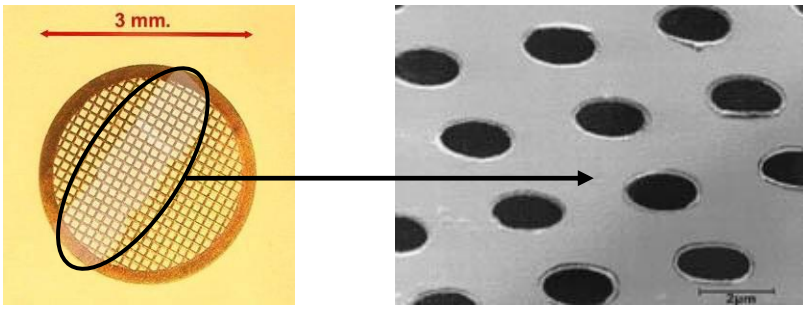

Fig. 2.30: The TEM sample holder – copper mesh with the part of Quantifoil® carbon polymer microgrid on top of it.

The quality of microparticle dispersion in the epoxy matrix has been investigated by means of SEM. A Philips XL20 and Jeol JSM 7500F field emission scanning electron microscopy (FESEM) were used to investigate the dispersion of fillers in the polymer matrix. Samples were broken and the resulting fracture surfaces were sputtered with a thin layer of gold to avoid charge accumulation. A Balzers SCD 040 has been used as coating device. X-ray energy dispersive spectroscopy (EDS) was used to determine the elements in the surface of the samples. The specimens were examined at acceleration voltages of 15 kV.

2.9.2.1 Morphology of the particles

TEM allows viewing individual particles in an ethanol suspension. Particle size distribution analysis revealed that the average particle size was approximately 20 nm for SiO_2, 22 nm for MgO, 30 nm for Al_2O_3 and 60 nm for AlN (see Figs 2.31 and 2.33).

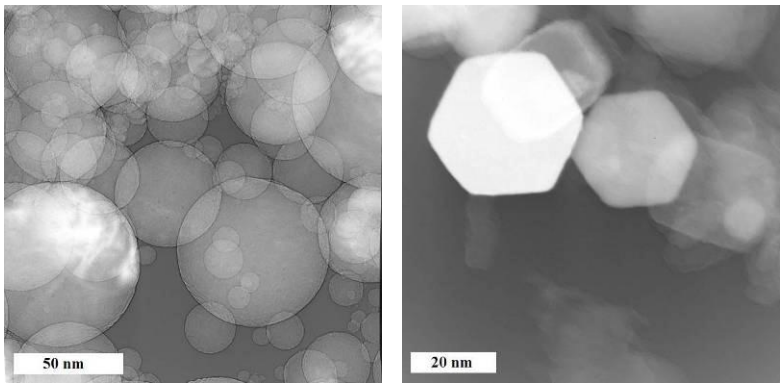

Fig. 2.31: TEM micrographs of Al_2O_3 (left) and AlN (right) nanoparticles.

MgO and SiO_2 particles have a narrow size distribution. The size distribution appeared to be broad for AlN and Al_2O_3. AlN particles ranged in size from 20 to 500 nm, with 70% being smaller than 100 nm. Al_2O_3 particles have a size distribution between 10 and 200 nm. The fraction of particles with diameters larger than 200 nm was negligible.
The micrographs of Al_2O_3 and SiO_2 show the shape of the particles to be spherical. MgO particles have spherical, egg-like and truncated cubic shapes. AlN particles have spherical, hexagonal and cubic structures.
Microscopy revealed the different structure of the Al_2O_3 filler material: alumina particles supplied by IoLiTec have irregular shape (see Fig. 2.32), while Al_2O_3 obtained from Sigma-Aldrich consists of spherical particles.
SEM allows getting an impression of the shape and size distribution of particles. The shape of BN particles with 70 nm, 1.5 µm and 5 µm is

spherical. BN particles with 0.5 µm on the other hand have a platelet-like structure (see Fig. 2.33).

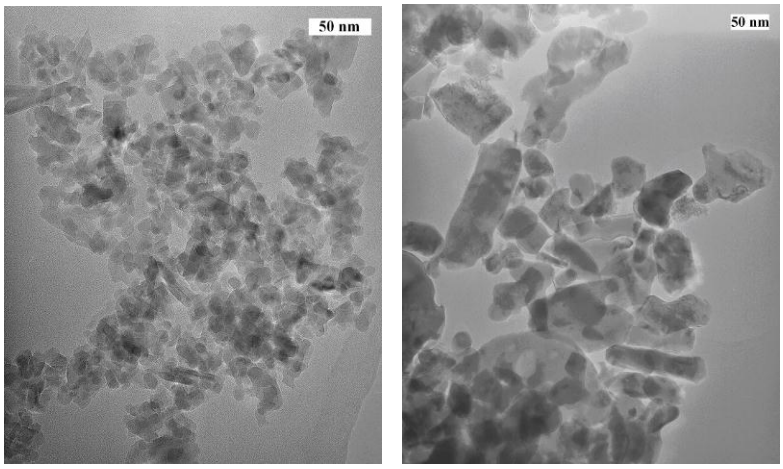

Fig. 2.32: TEM images of γ-Al_2O_3 APS 20nm (left) and α-Al_2O_3 APS 80nm (right).

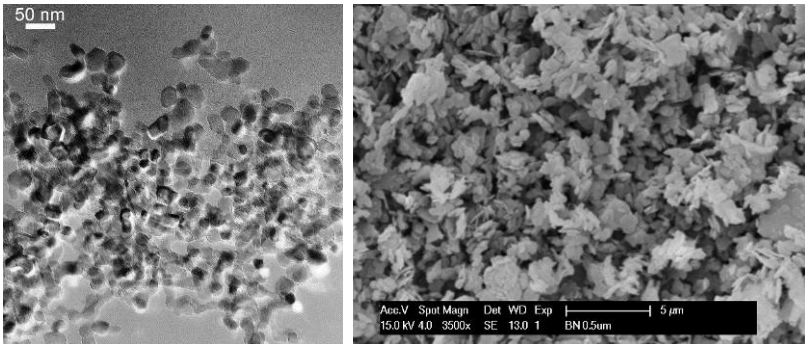

Fig. 2.33: TEM micrograph of MgO nanoparticles (left) and SEM micrograph of BN submicron particles with APS 500 nm (right).

The silica and alumina microparticles are of polycrystalline structure and an irregular shape. Their size distribution is broad. The micro aluminum oxide (Al_2O_3) and silicon dioxide (SiO_2) particles have an average particle size of 4 and 20 µm, respectively.

2.9.2.2 Dispersion of the particles

The quality of the dispersion for some nanofilled specimens is shown in Fig. 2.34. For example Al_2O_3 and SiO_2 particles are fairly well dispersed inside the epoxy matrix.

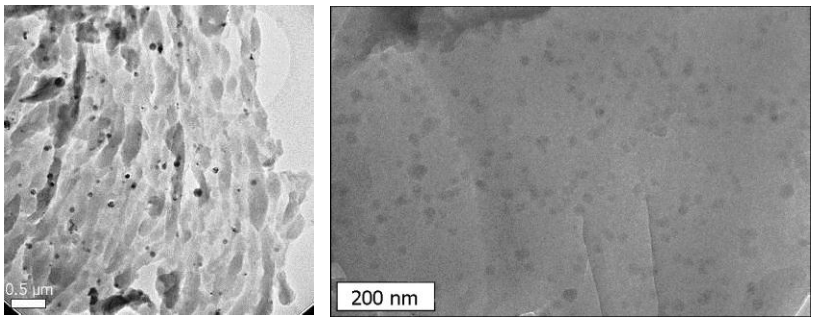

Fig. 2.34: TEM pictures of epoxy resin with 2 wt% of Al_2O_3 (left) and 2 wt% of SiO_2 (right).

As it can be seen from the TEM pictures, agglomeration could not be completely avoided since physical and chemical forces between primary particles are sometimes stronger than the high shear forces that were applied during the mixing process. Despite the preventive measures to avoid agglomeration, the composites have aggregates of particles of up to 400 nm for AlN, and up to 200 nm for Al_2O_3 filler material as it can be seen in Figs. 2.35 and 2.36. These clusters are however well dispersed in the polymer volume.

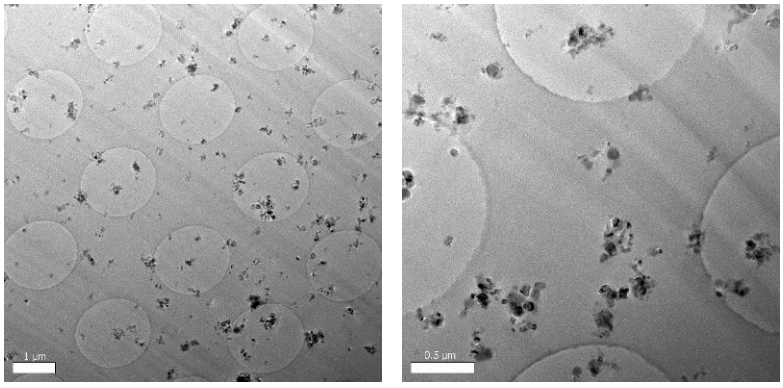

Fig. 2.35: TEM images of thin slices of epoxy resin with 5 wt.% of AlN.

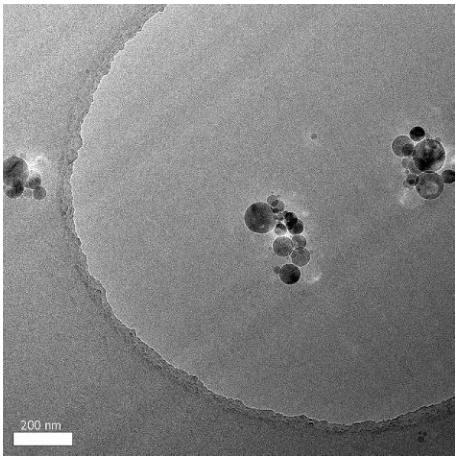

Fig. 2.36: TEM micrograph of 10 wt.% Al_2O_3 particles in an epoxy film.

The fabricated composites are classified in three types:

- nanocomposites (NC) – the dispersion is good and the average size of agglomerations (if they are observed) is not more than 100 nm;
- mesocomposites (MesC) – the average size of clusters of particles are larger than 100 nm but smaller than 500 nm; and
- microcomposites (MC) – the average size of clusters of particles are larger than 500 nm.

The quality of the dispersion allows to conclude that the samples with silica can be labeled as nanocomposites (NC).
ER-AlN-5, ER-AlN-10, ER-Al_2O_3-10, ER-MgO-10 systems are considered mesocomposites; while ER-Al_2O_3-0.5, ER-Al_2O_3-2, ER-Al_2O_3-5, ER-AlN-0.5, ER-AlN-2, ER-MgO-0.5, ER-MgO-2, ER-MgO-5 are all nanocomposites.
The dispersion state of micro- Al_2O_3 and SiO_2 was determined by SEM.
Fig. 2.37 shows the SEM micrographs of the fracture surfaces of Epoxy-Al_2O_3-20, Epoxy-Al_2O_3-30, Epoxy-Al_2O_3-40 and Epoxy-Al_2O_3-60. The results indicate good compatibility and good dispersion of the Al_2O_3 in the epoxy resin matrix. The average size of Al_2O_3 particles is around 4 μm.
Fig. 2.38 shows the dispersion of Al_2O_3 and SiO_2 microparticles in the epoxy. The average particle size of SiO_2 is about 20 μm, but we observed that some of them are bigger than 100 μm in one dimension.

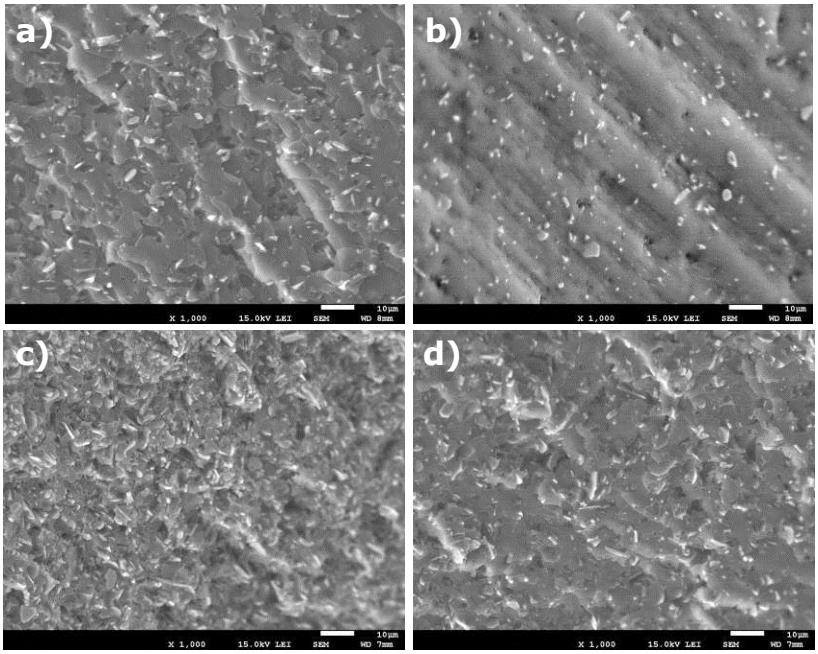

Fig. 2.37: SEM micrographs of the fracture surfaces of the ER filled with 20 wt.%, 30 wt.%, 40 wt.% and 60 wt.% of Al_2O_3 microparticles (a, b, c and d, respectively) with 1000 times magnification.

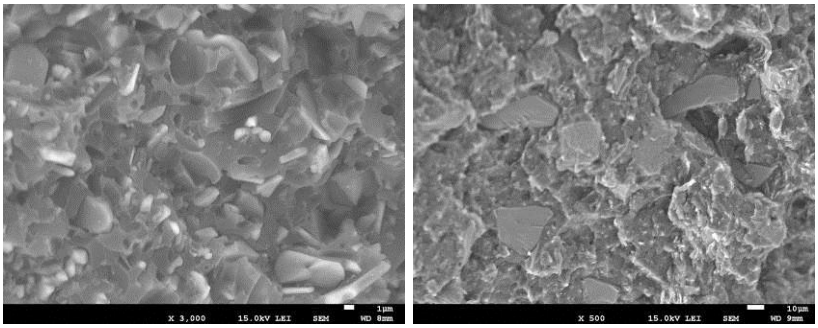

Fig. 2.38: SEM images of an epoxy-based system filled with 60 wt.% of Al_2O_3 microparticles and 60 wt.% of SiO_2 microparticles (left and right, respectively).

Figs. 2.39 and 2.40 depict a quantitative analysis of the samples. Every color dot virtually represents the atom of a specific element.
Fig. 2.39 shows the result of EDS measurement of ER-Al_2O_3-20. The red dots represent aluminum atoms.

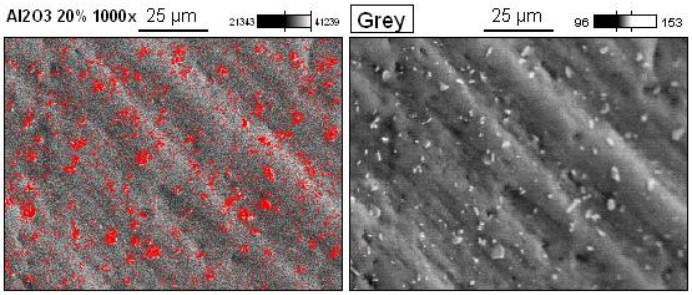

Fig. 2.39: SEM micrograph of ER-Al_2O_3-20 with 1000 times magnification.

Samples were broken and the resulting fracture roughness of the surface is observed on Fig. 2.40. The colour on the graphs depicts the presence of individual elements inside the composite. This is especially visible for silica particles, which are distributed inside the polymer matrix. The concentration of carbon and oxygen atoms is not even due to surface roughness. The EDS technique is more sensitive to the areas, which are close to the source, thus on the convex parts of the investigated area.

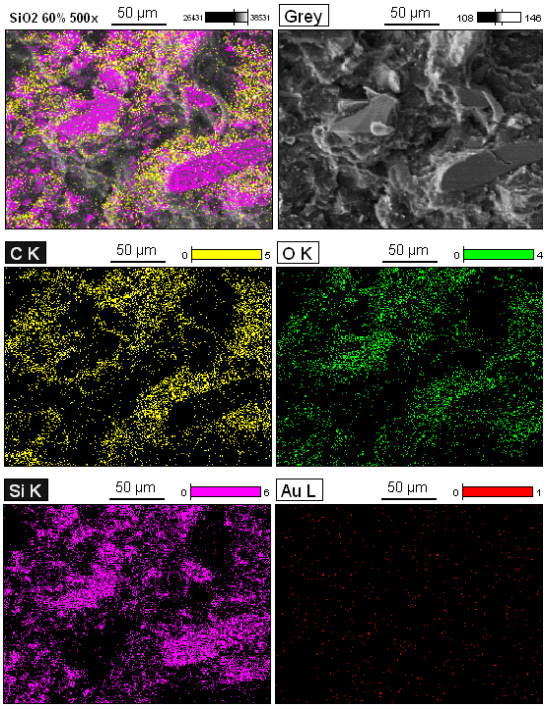

Fig. 2.40: SEM micrograph of ER-SiO_2-60 with 500 times magnification. Quantitative analysis shows the distribution of elements.

As it is illustrated in Fig. 2.40, the silica microparticles have a size ranging from a few micrometers to a couple of hundreds of micrometers. The silica particles are depicted by the purple colour, while the epoxy matrix (mostly carbon) is shown in yellow.
The SEM results and quantitative analysis indicate a good dispersion of micro-alumina and micro-silica for non-functionalized particles.

2.9.3 Particle concentration profile

In early experiments there were problems with sedimentation of particles on the bottom of the specimens due to gravitational settling. To investigate if sedimentation of nanoparticles takes place with the synthesis method, a cylindrical specimen was created. Due to some sedimentation at the bottom of nanocomposite specimens, we expected to see a difference of the particle concentration in weight percent, depending on the location. To investigate this, we divided the sample in 3 parts: upper, middle and bottom. In the course of TGA the organic part of the specimen is incinerated and the weight of the remaining inorganic particles that were in the matrix can be determined. If there would be a gravitational settling of the nanoparticles on the bottom, we should observe the majority of alumina on the bottom and only a small amount on the top of the sample. But what we obtained were quite similar results for all three parts and most of the aluminum oxide was not in the bottom part (see Fig. 2.41).

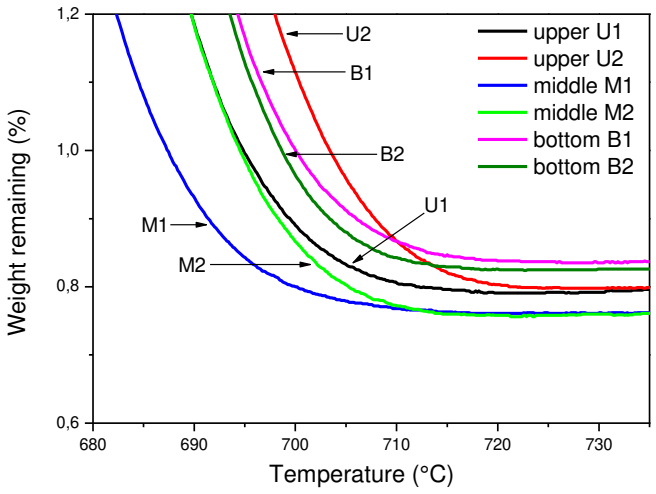

Fig. 2.41: Particle concentration profile: the differences between upper, middle and bottom part in wt.% are small.

The amount of alumina in the sample was also a bit higher than we calculated. We were trying to produce specimens with 0.5 wt% of alumina oxide, but as it can be seen we obtained about 0.8 wt % of alumina in the polymer matrix. The accuracy of this analysis is not high enough to measure such low fillgrades precisely. These results suggest that we do not have severe sedimentation on the bottom and the concentration of particles is almost constant for the whole sample.

2.10 Summary

The creation of nanocomposite materials is a complex task. A lot of literature research and experimental work has to be done to obtain nanocomposite samples with well dispersed nanoparticles. Thermosetting epoxy resin has been chosen as a host matrix because of its low viscosity before curing, which makes the mixing with filler easier, and because of the wide use in electrical engineering applications. One of the vital factors in nanocomposite fabrication is the surface modification of nanoparticles. Two methods have been applied to calculate an optimum amount of SCA needed for particle treatment. The nanoparticles were successfully functionalized with silane coupling agent. The successful functionalization was validated by examining the treated powder using TGA and FTIR analysis. Another crucial factor is the dispersion of nanoparticles inside the ER. First of all the dispersion has been checked in a solvent. It was important to find an appropriate solvent and mixing technique to get a fine dispersion, before ER was added to the suspension. The laser diffraction method showed that ethanol is an appropriate solvent in combination with an ultrasonic bath. The particles' size and dispersion inside the epoxy was verified using transmission and scanning electron microscopy. TGA showed that there is no nanoparticle sedimentation inside a cured nanocomposite specimen. Despite all the preventive measures that have been taken to avoid particle agglomeration, such as surface treatment and different mixing techniques, some of the nanocomposites have areas with agglomerates. All composites have been divided into three groups according to the size of individual particles and their aggregates inside the polymer matrix.

3

Thermal characterization

3.1 Introduction

The thermal conductivity has been important since the Stone Age, when humans started looking for materials, which can keep warm for a long time or the other way around – to cool down in a short period of time. Materials with a low thermal conductivity, such as animal leather or wool, have kept people warm for millennia. High thermal conductivity materials, such as metals, became extremely important during the industrial revolution. Copper, aluminum, silver and gold have been used for the creation of conductors for more than 2 centuries already. However, many applications require insulators to transfer the heat away from the conductor efficiently. Thermally conductive polymers and polymer-based composites are good candidates to satisfy such requirements.

This chapter contains the theoretical background about thermal conductivity, its behaviour in different materials and the processes

which limit the heat transfer in insulating materials. An explanation is given why polymers have a low thermal conductivity and how it can be improved. An overview of the available theories to predict and fit the thermal conductivity of composite materials is given in detail. The reasons are given why these models cannot be applied to the nanocomposites. It is shown that the filler-matrix interface plays a dominant role in the thermal conduction process of nanocomposites. The two-phase model was proposed as an initial step for describing systems containing 2 constituents, i.e. a cured epoxy matrix and an inorganic filler. The three-phase model was introduced to specifically address the properties of the interfacial zone between the host polymer and the surface modified nanoparticles. The influences of the size, shape, surface modification and concentration of filler on the thermal conductivity of a polymer-based system as well as the crystal structure of particles and their alignment are discussed.

3.2 Thermal conductivity, definition

Thermal conductivity (λ), along with radiation and convection is a mechanism of heat transfer. Convection is the energy transfer within liquids and gases by direct particle interaction. Radiation is the energy transfer by means of emission and absorption of energetic particles or waves. The focus of this work is on thermal conductivity, since it is the main mechanism of heat transfer within solid materials.
The thermal conductivity is the property of a material that indicates its ability to conduct heat. This physical constant is defined as the quantity of heat that passes through a unit cube of a material in a unit of time, when the difference in temperature between the opposite sides of the cube is 1K.

The first clear statement of the proportionality between heat flow and temperature gradient was made in 1822 by Fourier. When materials are subjected to a steady-state heat flow q, a temperature gradient (dT/dx) is produced in the materials along the direction of the heat flow. Both parameters are related by the equation:

$$q = -\lambda \frac{dT}{dx}, \tag{3.1}$$

where λ is a proportionality constant with the unit W/m·K and is referred to as the thermal conductivity of a material [182].
The concept of heat conduction in dielectric solids is often discussed with the help of the Debye kinetic model.

$$\lambda = \frac{1}{3} C \cdot \upsilon \cdot l \,, \tag{3.2}$$

where C is the specific heat per unit volume, υ is the average sound velocity (phonon propagation speed), and l is the mean free path of a phonon. l is in the order of a few nanometers at room temperature and of a few microns at low temperatures close to absolute zero. The speed of sound is relatively independent of temperature, while the mean free path decreases with increasing temperature.

The specific heat can be rewritten as $C = C_p \rho$, where C_p is the heat capacity and ρ is the density of a material. The product of velocity and mean free path of a phonon is known as thermal diffusivity D, i.e. $D = \upsilon \cdot l$.

Thus, the thermal conductivity is related to the thermal diffusivity as in [183]

$$\lambda = \frac{1}{3} C_p \rho D \,. \tag{3.3}$$

3.3 Thermal conductivity in metals, dielectrics, alloys & semiconductors

There are a few mechanisms by which heat can be transmitted through a solid. Thermal conductivity requires a transport of thermal energy. Different types of carriers like electrons, phonons (atom vibrations) or photons can be considered for this transport. In the nonmetal materials heat is conducted by phonons, the thermal vibrations of the atoms. In metals the thermal conduction is almost entirely due to electron transport. In alloys and semiconductors both transport mechanisms can make comparable contributions to the thermal conductivity [184].

The thermal conductivity of solids ranges over five orders of magnitude, varying at room temperature from about 400 W/m·K for copper or silver to 10^{-2} W/m·K for microporous materials such as plastic foams.

The thermal conductivity of a hypothetical infinitely large, isotopically pure dielectric crystal without any imperfections is infinite at all temperatures, if it is characterized by harmonic atomic vibrations.

An ideal crystal can be illustrated as an array of atoms connected by springs (see Fig. 3.1). Every atom is physically bonded to its neighbors in some way. If heat energy is supplied to one end of a solid, the atoms start to vibrate faster. As they vibrate more, the bonds between atoms shake more. This passes vibrations to the next atom, and eventually the energy spreads throughout the material.

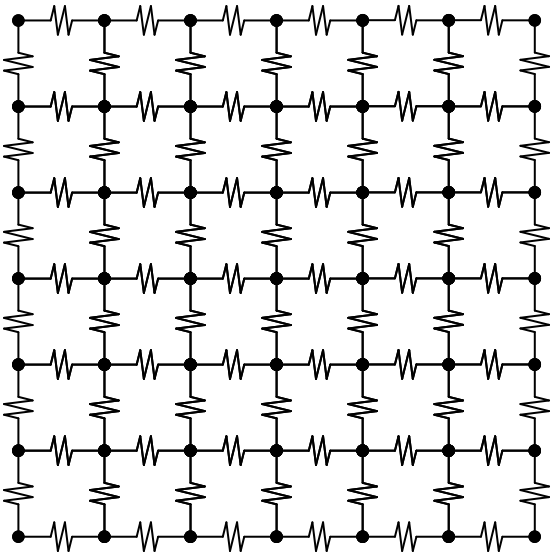

Fig. 3.1: A graphical representation of a two dimensional array of atoms connected by springs [185].

One of the most important features of this model of a solid, where the atoms are coupled to their neighbours, is that the vibrations are obeying the harmonic oscillator equations. These harmonic oscillators are found to possess energy only in discrete integer units of $h\nu = \hbar\omega$, where ν is the oscillator frequency, ω is the angular frequency, h is Planck's constant and $\hbar = h/2\pi$ is the reduced Planck constant. The energy of the oscillator is

$$E_n = \left(n + 1/2\right) \cdot \hbar\omega, \tag{3.4}$$

where n is an integer, and the half gives the inaccessible, but detectable, 'zero point' energy. These quanta $h\nu = \hbar\omega$ are called 'phonons' in solids by analogy with the photons of electromagnetic radiation. One point of view is that these phonons can be regarded as particles and the solid as a gas of such particles. Then heat conduction appears as a diffusion of phonons from a hotter region, where they are more numerous, to a colder region, where there are less of them.
Theoretically it has been shown that in a perfect single crystal of infinite size, where the lattice vibrations are strictly harmonic, there is no resistance to the flow of phonons [186].
Real crystalline solids have a finite size, contain imperfections in their material structure and exhibit anharmonicity in atomic vibrations. All

these factors cause different phonon scattering mechanisms, which in turn limit the thermal conductivity values of crystalline materials in practice.

3.4 Phonon scattering process

The effectiveness of the heat propagation depends on the scattering of phonons. The thermal resistance – reciprocal to the thermal conductivity - is caused by various types of phonon scattering processes, e.g. phonon-phonon scattering, boundary scattering, scattering from static point imperfections, dislocations of atoms, stacking faults, grain boundaries [187]. In order to maximize the thermal conductivity, these phonon scattering processes must be minimized. Phonons travel at the speed of sound. The scattering of phonons in composite materials is mainly due to the interfacial thermal barriers, resulting from acoustic mismatch and flaws associated with the filler-matrix interface.

Solid nonmetallic material must meet four criteria to be regarded as high thermal conductive:

a) low atomic mass;
b) strong interactions or chemical bonding;
c) simple crystal structure; and
d) low anharmonicity in the molecular vibrations.

Polymers do not satisfy any of these criteria and as a result their thermal conductivity values are low. Most polymers have a thermal conductivity between 0.1 and 0.6 W/m·K [188].

3.5 Thermal conductivity of polymers

Polymer materials show a weak thermal conductivity. Thermal conductivities of insulating polymer materials are usually 1-3 orders lower than those of ceramics and metals.
Due to the chain-like structure of polymers, the heat capacity consists of the contribution of two mechanisms: (a) lattice vibrations and (b) characteristic vibrations, which originate from internal motions of the repeating unit. The lattice (skeleton) vibrations are acoustic vibrations, which give the main contribution to the thermal conductivity at low temperatures. The characteristic vibrations of the side groups of the polymer chains are optical vibrations, which become visible at temperatures above 100 K [189].
Generally, the thermal conductivity of amorphous polymers increases with increasing temperature, if the temperature is in the glassy region and decreases slowly or remains constant in the rubbery region.

Numerous applications in the field of electrical engineering require high thermal conductivity, such as insulating materials for power equipment, electronic packaging and encapsulations, computer chips, satellite devices and other areas where good heat dissipation is needed. For polymers reinforced with different types of fillers this is even more important. Improved thermal conductivity in polymers may be achieved either by molecular orientation or by the addition of highly heat conductive fillers [190, 191].
Temperature, pressure, density of the polymer, orientation of chain segments, crystal structure, the degree of crystallinity and many other factors may affect the thermal conductivity of polymers [188]. It has been shown that the thermal conductivity is highly sensitive to the degree of crystallinity and the polymer chain segment orientation [191, 192].
K. Fukushima et al. [193] have developed a novel material design to improve the thermal conductivity, where polymer chains align themselves, by controlling the higher crystalline ordering. Fig. 3.2 shows the schematic representation of the higher order structure of the resin to achieve macroscopic isotropy and high thermal conductivity. The proposed resin has three features:

a) microscopic anisotropic crystal-like structures obtained via local alignment e.g. via oriented mesogens;
b) macroscopic isotropy of the epoxy due to disorder of the domains of the crystal-like structures; and
c) the oriented mesogens are connected with the amorphous structure via covalent bonds.

The thermal conductivity values of the new developed resin were up to 5 times higher than those of conventional epoxy resins, because the mesogens form highly ordered crystal-like structures, which suppress phonon scattering.

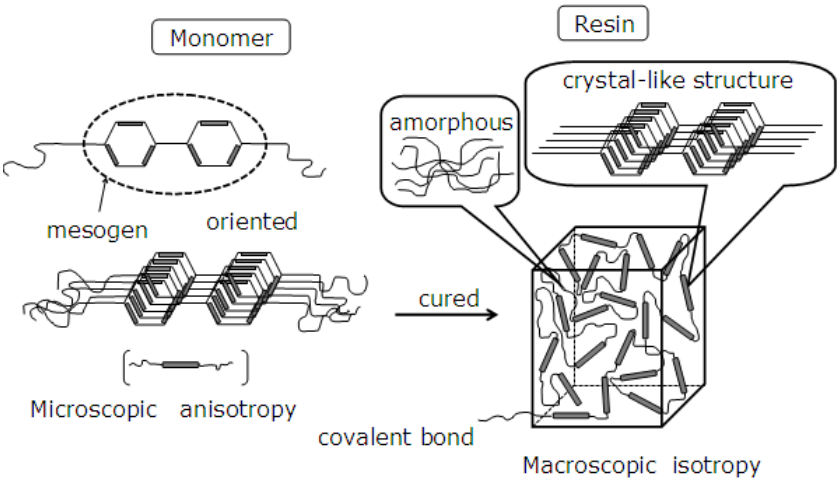

Fig. 3.2: Schematic representation of a macroscopically isotropic resin [193].

To improve the thermal conductivity of the polymer composites, Ekstrand and co-authors [96] proposed:

(a) decreasing the number of thermally resistant junctions;
(b) forming conducting networks by suitable packing; and
(c) minimize filler-matrix interfacial defects.

Z. Han et al. [97] discovered that an epoxy-filler composite with agglomerates of particles is more efficient in enhancing the thermal conductivity than a nanocomposite with well dispersed nanoparticles. This is presumably due to the formation of percolated pathways or networks.
The main approach to an effective improvement of the low thermal conductivity of polymers is to fill them with particles with high thermal conductivity.
Industrial companies, which are specialized in the production of polymer-based insulating materials, use a fillgrade up to 60 wt.% of silica or alumina. The thermal conductivity of these materials is not significantly high but the price is low [194, 195]. The more scientific approach has been taken by a number of researchers, who made attempts to create polymer systems filled with different types of high thermal conductivity microfillers [121, 145, 194, 195].

3.6 High thermal conductivity materials

A material is regarded as high thermal conductive if its thermal conductivity is larger than 100 W/m·K at room temperature [187]. The 12 semiconductors and insulators with the highest thermal conductivities are presented in Table 3.1a. The thermal conductivities of some metals and carbon-based materials are presented in Table 3.1b for comparison.

Table 3.1a: Values of λ for high thermal conductivity nonmetallic single crystals at room temperature [187].

Crystal	λ, W/m·K
Diamond	2000
BN (cubic)	1300
SiC	490
BeO	370
BP	360
AlN	320
BeS	300
BAs	210
GaN	170
Si	160
AlP	130
GaP	100

Table 3.1b: Values of λ for high thermal conductivity metals and carbon-based materials at room temperature [196-198].

Material	λ, W/m·K
Aluminum	237
CNT	2000-6000
Copper	401
Graphite	100-400
Gold	318
Silver	429

The thermal conductivity of high thermal conductivity nonmetallic materials can be expressed as follows [199, 200]:

$$\lambda(T) \approx \frac{D\overline{M}\Omega^{1/3}\Theta_D}{T\varpi^2}, \tag{3.5}$$

where T is the temperature, D is a constant, $\overline{M}$ is the average atomic mass, Ω is the volume of an atomic cell (average volume occupied by one atom of the crystal), Θ_D is the Debye temperature and ϖ is the average anharmonicity of bonds (Grüneisen's constant). The expression is valid for high temperatures ($T > \Theta_D$).

All high thermal conductivity crystals have low atomic mass, strong interatomic bonding between the constituents in the compound, simple crystal structure (a low number of atoms per unit cell) and low anharmonicity in the phonon vibrations [201-203].

3.7 Overview of the available theories to predict and fit the thermal conductivity of composite materials

Different theoretical and empirical approaches are available to predict and fit the thermal conductivity of two-phase systems.

The simplest three are the rule of mixture (parallel model, arithmetic mean):

$$\lambda_c = \phi \cdot \lambda_f + (1-\phi)\lambda_m , \tag{3.6}$$

the inverse rule of mixture (series model, harmonic mean):

$$\frac{1}{\lambda_c} = \frac{\phi}{\lambda_f} + \frac{1-\phi}{\lambda_m} , \tag{3.7}$$

and the geometric mean, giving the thermal conductivity as:

$$\lambda_c = \lambda_f^{\phi} \cdot \lambda_m^{(1-\phi)} . \tag{3.8}$$

In all formulas λ_c, λ_f, λ_m are the thermal conductivities of composite, filler material and polymer matrix, respectively, and ϕ is the volume fraction of the filler [204, 205].

The upper or lower boundaries of the thermal conductivity are given when filler particles are arranged either parallel to or in series with the heat flow. As soon as the particles have a random distribution and are not aligned in the direction of the heat flow in the polymer, the parallel and series model do not give a good prediction of the thermal conductivity of the composites. The parallel model typically overestimates the thermal conductivity of a composite and thus shows the upper limit, while the series model tends to predict the lower limit of the thermal conductivity of a two component system [206, 207].

Maxwell obtained a relationship for the electrical conductivity of randomly distributed and non-interacting homogeneous spheres in a homogeneous medium [208]. Eucken adapted the electrical conductivity equation to thermal conductivity [209]. Thus, the Maxwell-Eucken equation is presented as follows:

$$\lambda_c = \lambda_m \frac{\left[2\lambda_m + \lambda_f + 2\phi\left(\lambda_f - \lambda_m\right)\right]}{\left[2\lambda_m + \lambda_f + \phi\left(\lambda_f - \lambda_m\right)\right]}. \tag{3.9}$$

Frieke extended Maxwell's model and derived an equation for ellipsoidal particles in a continuous phase [210].
Using different assumptions for permeability and field strength than Maxwell, Bruggeman derived the theoretical model for a dilute suspension of non-interacting spheres dispersed in a homogeneous medium [211]. Later it was applied to the thermal conductivity of a composite system:

$$1-\phi = \left(\frac{\lambda_f - \lambda_c}{\lambda_f - \lambda_m}\right)\cdot\left(\frac{\lambda_m}{\lambda_c}\right)^{1/3}. \tag{3.10}$$

Most of the experimental results show [98, 121, 151, 212, 213] that Maxwell-Eucken and Bruggeman models as well as Frieke model do not predict the thermal conductivity of a composite correctly.
Tsao developed a model relating the thermal conductivity of a composite to two experimentally determined parameters which describe the spatial distribution of the two phases [214]. Cheng and Vachon extended Tsao's model by assuming the discrete phase in the continuous matrix [215]. The thermal conductivity of a composite, where $\lambda_f > \lambda_m$ according to Cheng-Vachon is given by

$$\frac{1}{\lambda_c} = \frac{1-B}{\lambda_m} + \frac{1}{\sqrt{K\lambda_d\left(\lambda_f + B\lambda_d\right)}}\cdot\ln\left[\frac{\sqrt{\lambda_m + B\lambda_d} + B/2\cdot\sqrt{K\lambda_d}}{\sqrt{\lambda_m + B\lambda_d} - B/2\cdot\sqrt{K\lambda_d}}\right], \tag{3.11}$$

where $B = \sqrt{3\phi/2}$, $K = -4\sqrt{2/3\phi}$ and $\lambda_d = \lambda_f - \lambda_m$.

Sundstrom and Lee [216] reported that the Cheng-Vachon model shows a reasonable agreement with experimental data obtained from polystyrene or polyethylene systems filled with glass, calcium oxide

(CaO), aluminium oxide (Al_2O_3) and magnesium oxide (MgO). Contrary to Sundstrom and Lee, Hill and Supancic showed that the results predicted by the Cheng-Vachon model have much lower thermal conductivity values, compared to experimental results [212].
All aforementioned models are based on the amount of filler loading and do not take into account the geometry of the particles and the size of filler particles.
Work of Hamilton and Crosser [217, 218] is based on Maxwell's and Frieke's theoretical models. They take into consideration the sphericity (ψ) of particles. The sphericity is defined as the surface area of a sphere with the same volume as the particle divided by the surface area of the particle. Hamilton and Crosser correlated various sets of data with a sphericity between $0.58<\psi<1.0$ with:

$$\lambda_c = \lambda_m \left(\frac{\lambda_f + (n-1)\lambda_m + (n-1)(\lambda_f - \lambda_m)\phi}{\lambda_f + (n-1)\lambda_m - (\lambda_f - \lambda_m)\phi} \right), \tag{3.12}$$

where n is an empirical constant $n = 3/\psi$. For a spherical particle n equals 3. For different type of particles (see Fig. 3.3) the sphericity is shown in Table 3.2.

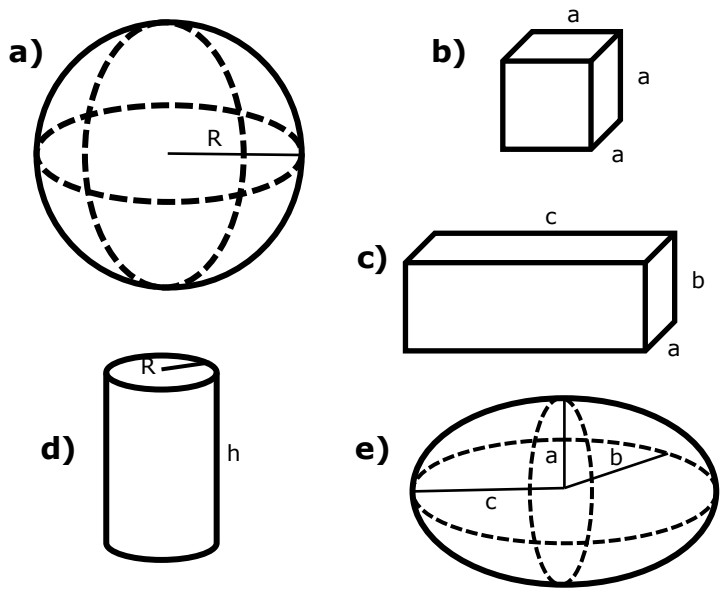

Fig. 3.3: Different shape of particles: sphere (a), cube (b), prism (c), cylinder (d) and ellipsoid (e).

Table 3.2: Type of particles, their dimensions and calculated sphericity.

Shape of a particle	Dimension	Sphericity, ψ
sphere	$R=1$	1
cube	$a=\left(\frac{4}{3}\pi\right)^{1/3}$	0.81
prism	$a=b=1,\ c=\frac{4}{3}\pi$	0.67
prism	$a=b=2,\ c=\frac{\pi}{3}$	0.77
cylinder	$R=1,\ h=\frac{4}{3}$	0.86
cylinder	$R=2,\ h=\frac{1}{3}$	0.43
cylinder	$h=1,\ r=\frac{2}{\sqrt{3}}$	0.80
ellipsoid	$a=b=0.75,\ c=1.778$	0.90
ellipsoid	$a=b=0.5,\ c=4$	0.64
ellipsoid	$a=b=0.1,\ c=100$	0.13

Hamilton and Crosser analyzed the composite systems of balsa wood and aluminum particles in rubber [217].
Hatta and Taya [219] proposed a model, which can be applied to systems filled with particles having a high aspect ratio or unidirectional fillers. The model assumes that all platelet-shaped particles are aligned either parallel or perpendicular to the direction of heat flow.

$$\lambda_{c,i}=\lambda_m+\frac{\lambda_m\phi}{S_i\left(1-\phi\right)+\lambda_m/\left(\lambda_f-\lambda_m\right)}, \tag{3.13}$$

where $\lambda_{c,i}$ is the thermal conductivity of the two-phase composite along one of the defined axes ($i=a,b,c$), S_i is a factor dependent on filler shape and direction. In case of platelet-like particles, if the measurement is performed in a direction parallel to the plane of aligned particles (a and b direction), $S_a=S_b=\pi d/4T$. If the measurement is

performed perpendicular to the plane of aligned platelets, defined as the c-direction, $S_c = 1 - \pi d / 2T$. Parameters d and T are the diameter and thickness of the disk-like particles [98, 212].
Meredith and Tobias [220] suggested a model for high-loaded systems

$$\lambda_c = \lambda_m \cdot \left(\frac{2A + 2\phi B}{2A - 2\phi B} \right) \cdot \left(\frac{(2-\phi)A - 2\phi B}{(2-\phi)A + \phi B} \right), \tag{3.14}$$

where $A = 2 + \lambda_f / \lambda_m$ and $B = 1 - \lambda_f / \lambda_m$.

Lewis and Nielsen [220-223] adopted the Halpin-Tsai [224] mechanical model to obtain a model for the thermal conductivity. The semi-empirical Lewis-Nielsen model is based on the particle size, geometry, and the manner of particle packing in the matrix. Using the following formulas one can do the basic estimations regarding the thermal conductivity. According to Lewis-Nielsen theory for composites:

$$\lambda_c = \lambda_m \frac{1 + \xi \eta \phi_f}{1 - \Phi \eta \phi_f}, \tag{3.15}$$

where $\eta = \frac{(\lambda_f - \lambda_m)}{(\lambda_f + \xi \lambda_m)}$ and $\Phi = 1 + \frac{(1 - \phi_M)}{\phi_M^2} \phi_f$.

The constant ξ is the shape factor, which depends on the shape, orientation and aspect ratio of the dispersed particles. The factor ϕ_M represents the maximum packing fraction of the dispersed particles, which is sensitive to the filler shape. The relation $\eta = (\lambda_f - \lambda_m)/(\lambda_f + \xi \lambda_m)$ is coupling the conductivities of the components and the geometry of the filler. The factor Φ was introduced to take into account the maximum concentration of particles that is possible. For randomly packed spherical particles, $\xi = 1.5$ and $\phi_M = 0.637$ [225].
At the limits of $\xi \to 0$ (for particles with low aspect ratio) and $\xi \to \infty$ (for particles with high aspect ratio), the Lewis-Nielsen equation reduces to the series $\lambda_c^{-1} = \lambda_f^{-1} \phi_f \Phi + \lambda_m^{-1} (1 - \phi_f \Phi)$ or parallel $\lambda_c = \lambda_f \phi_f + \lambda_m (1 - \phi_f)$ thermal conductivity models. The limits show that the maximum packing conditions (Φ) only affect the series model. The Lewis-Nielsen model

reduces to the Maxwell equation by using a constant value for the shape factor of 2 and the maximum packing factor of $\Phi = 1$ [209]. Not surprisingly, the value of the shape factor for the Maxwell model is the closest to the one of spherical particles, and therefore is the best for predicting the thermal conductivity of nanocomposites filled with isolated spherical objects.

Agari and Uno [226-228] proposed a model, which is based on the generalization of both parallel and series models for filled composites

$$\log \lambda_c = \phi C_2 \log \lambda_f + (1-\phi)\log(C_1 \cdot \lambda_m), \tag{3.16}$$

where C_1 and C_2 are adjustable constants, which can be determined from experimental data. C_1 indicates the effect of the filler on the secondary structure of the polymer matrix, e.g. crystallinity and the crystal size of the polymer. The parameter C_2 indicates how easily the particles can form conductive paths inside the polymer. The closer C_2 comes to 1, the more easily conductive chains are formed in composites. So, if the dispersion state of the filler is different, the thermal conductivity of composites may be different even if the composites are of the same type [54, 98, 229, 230]. Generally, the Agari&Uno semi-empirical model fits experimental data well. However, experimental data is needed for each type of composite in order to determine the parameters C_1 and C_2. The Agari & Uno model does therefore not predict the thermal conductivity, but is basically a fit function.
To extend the overview of the thermal conductivity modelling, numerous different models can be mentioned, such as Russell [231], Topper [232], Jefferson-Witzell-Sibitt [233], Springer-Tsai [234], Budiansky [235], Baschirow & Selenew [236], McCullough [204] and McGee [237], and many others, including mathematical numerical methods [238, 239].
Summarizing all aforementioned models, no single correlation or technique accurately predicts the thermal conductivity for all types of composites. The theories listed above are good for prediction of the thermal conductivity in a few particular cases. The thermal properties become more complicated with the addition of fillers to polymers.
There are many types of composites, in which a polymer is filled with different particles. The thermal conductivity of a composite is the highest when predicted by the parallel model. This can be visualized as if all particles are gathered to form a block, which is arranged parallel to the block of polymer and in the direction of the thermal flux (Fig 3.4a).

The thermal conductivity is the lowest and can be described by a series model, if those blocks are arranged in series relative to the direction of the thermal flux (see Fig. 3.4b).

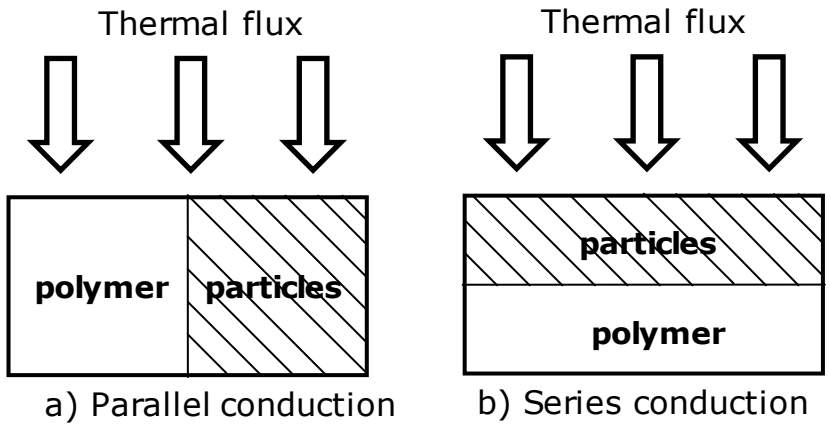

Fig. 3.4: Schematic representation of the systems, which can be described by a) parallel and b) series thermal conductivity models.

Maxwell-Eucken and Bruggeman equations are used for ideal systems that consist of randomly distributed and non-interacting spheres in a homogeneous matrix. Cheng and Vachon derived a model for the discrete phase in the continuous medium. Parallel, series and geometric mean as well as Maxwell-Eucken, Frieke, Bruggeman and Cheng-Vachon models are based on the amount of the filler loading. Hamilton and Crosser introduced the sphericity of particles. Hatta and Taya proposed a model for the systems filled with particles having high aspect ratio particles. Meredith and Tobias suggested a model for high-loaded systems. Lewis and Nielsen proposed a model, which is based on the particle size, geometry and the manner of the packing of particles in the matrix. The Lewis-Nielsen model can be used for nanocomposite systems, taking into account the thermal resistance (section 3.12). The Agari & Uno semi-empirical model is basically a fit-function that requires constants, that are derived from experimental data.
Table 3.3 shows the list of models, which can be used to describe the thermal conductivity of composite systems and when the particular model can be applied.

Table 3.3: The list of thermal conductivity models and when they can be applied.

Model	Terms of use
Series, parallel	particles are aligned either parallel or perpendicular to heat flow
Maxwell-Eucken, Frieke, Bruggeman	ideal system, non-interacting spherical / spheroidal particles in homogeneous medium
Geometric mean, Cheng-Vachon	discrete phase in continuous matrix, taking into account only filler loading
Hamilton-Crosser	sphericity is taking into consideration
Hatta-Taya	for the systems filled with high aspect ratio particles
Meredith-Tobias	for high-loaded composites
Lewis-Nielsen	size, geometry and manner of particle packing is taking into account
Agari-Uno	fitting function with adjustable constants
Russell, Topper	for porous composites, containing voids of gas

The effect of nano-reinforcement on the thermal conductivity of polymer composites is still under investigation [40].

3.8 Towards nanocomposites

The thermal conductivity of composites containing microparticles can be calculated by taking into account the shape and volume of the incorporated particles, assuming diffusive heat conduction in both phases. This approach cannot be applied to a system with nanoparticles inside. Various factors have to be taken into consideration for nanocomposites, which can be disregarded when dealing with microscale particles. Interface resistance and phonon scattering become increasingly important in case of nano-scale particles [240].
For nanocomposites, a thermal expansion mismatch and poor chemical adhesion of the polymer to the particle surface may lead to inefficient transport of phonons through the interface. This is the so-called interfacial thermal resistance (Kapitza's resistance of an interphase boundary) [241, 242]. It provides a temperature discontinuity at the particle-polymer interface, which vanishes when the particle size is above about 100 nm.

The effect of the thermal resistance was implemented into the two-phase Lewis-Nielsen (LN) model, by introducing Kapitza's resistance R_K to be in series with the particle resistance, d/λ_f, where d is the particle size. The equivalent resistance then is $d/\lambda_F' = d/\lambda_f + R_K$, and the effective thermal conductivity of a particle including interfacial resistance can be written as [243]:

$$\lambda_F' = \frac{\lambda_f}{1+\frac{R_K \lambda_f}{d}}. \tag{3.17}$$

In case of very small particles, the term R_K/d converges to infinity, $R_K/d \to \infty$, the filler is not involved in the thermal conduction process and the effective thermal conduction of particle is zero ($\lambda_F' = 0$). For large particles the interfacial resistance is not important, since $R_K/d \to 0$.

The thermal conductivity of filled polymer systems can be affected to a great extent by surface treatment of the particles. The surface treatment improves the contact between particles and the polymer matrix, decreasing the interfacial thermal resistance. Therefore, the transport of energy through the filler-polymer interface increases. In addition, the modified polymer forms a structure around the particle, which may differ from the structure of the polymer matrix in the bulk [8]. The interfacial layer, which can be defined as a transition layer between a host material and incorporated filler, has different crystallinity, glass transition temperature, crosslink density, permittivity and thermal conductivity [244]. In some cases the physico-chemical micro- and macro-properties of the interfacial layer play a more important role than the properties of the individual components. The properties of the interfacial layer might match neither the properties of the matrix nor the properties of the incorporated filler [245].

We assume that the aligned layer does not depend on the size of the particles. Therefore, the layer volume is negligibly small for large particles with respect to the particle volume, and will be significant for particles of nanosized filler. The three-phase model is well accepted in the nanofluid community. In three-phase models for nanofluid, the particles are also subjected to Brownian motion and clustering, in addition to the layering of the liquid at the particle-liquid interface [246, 247]. For polymer composites, the high viscosity of the matrix before

curing significantly slows down the Brownian motion. The effect of the interfacial shell on the conductivity of nanofluids has been analyzed by introducing the "complex nanoparticle": the effective particle with thermal properties of the nanoparticle itself and the surrounding interfacial layer [248]. This modification has been done to the original Maxwell [249] and Bruggeman [250] models, although other approaches are reported as well [246], to account for the shape of the particles, clustering and the interfacial thermal resistance [251, 252].

In our case, a composite material can be represented by composite particles embedded into the polymer matrix. We define a "composite particle" (CP) as a particle itself and the polymer close to the particle surface, which is organized by the surface modification. A CP has a volume $v = v_f + v_l$, where v_f is the volume of a particle and v_l is the volume of the layer surrounding this particle. Inspired by the thermal resistance model, the thermal conductivity can be modeled after the series model for the filler-layer composite particle

$$\frac{1}{\lambda'_F} = \frac{v_f}{\lambda_f\left(v_f + v_l\right)} + \frac{v_l}{\lambda_l\left(v_f + v_l\right)}, \tag{3.18}$$

where $\frac{v_f}{\left(v_f + v_l\right)}$ is the volume fraction of the filler in the composite particle. For large particles, i.e. $v_f >> v_l$, we come to $\lambda'_F = \lambda_f$.

The second aspect, which is important in modeling the interfacial layer is the volume fraction of the CPs, which also includes the volume fraction of the polymer layer. Therefore we can write $\phi_m + \phi_f + \phi_l = 1$, where the first contribution is from the matrix, the second and the third are from the filler and the interfacial layer, respectively. For spherical particles of a radius r, the volume of the interfacial layer is proportional to the volume of the particle. Therefore the volume of CPs will be written as $\phi_{cp} \equiv \phi_f + \phi_l = \phi_f \delta$, where $\delta = \left(1 + l/r\right)^3$, with l being the thickness of the interfacial layer. In this case, the Lewis-Nielsen expression for a two-phase model (Eq. 3.15) together with Eq. 3.17 will be modified in the three-phase LN model, where $\phi_f \delta$ appears instead of ϕ_f, and $\lambda_f \mapsto \lambda'_F$.

To emphasize aforementioned, we should stress the fact that at small concentrations the condition $\lambda_m = \lim_{\phi_f \to 0} \lambda_c$ must remain valid, so that no aggregates or networks of particles are formed in that case.

3.9 Measurements of the thermal conductivity

Experimental methods for measuring the thermal conductivity can be divided into 2 groups, depending on whether the temperature distribution within the sample is time dependent. The first group of methods which are based on the principles of steady state measurements, and the second group consists of unsteady state methods [253-256].

The thermal conductivity measurements were performed with a Thin Heater Apparatus System (THASYS), produced by Hukseflux Thermal Sensors (Fig. 3.5). THASYS is based on the steady state measurement principle. This system works according to the ASTM 1114-98 standard and performs a direct measurement which allows the determination of the absolute value of the thermal conductivity. With a combination of a thin heater, two samples of similar thickness and two heat sinks it is possible to generate a homogeneous thermal field with a well defined heat flux through the samples. The thermal conductivity can be calculated by measuring the heat flux value derived from the heat power, effective sample thickness and the temperature difference that can be measured across the samples during heating, compared to the situation without heating. Glycerol eliminates the problem of contact resistance by filling out potential gaps between heater and samples [257].

A straightforward calculation of the thermal conductivity was made using the following equation:

$$\lambda = \varphi \cdot H_{eff} / \Delta T , \tag{3.19}$$

where λ is the thermal conductivity, φ is the heat flux derived from the heater power, H_{eff} is the effective sample thickness and ΔT is the temperature difference across the samples.

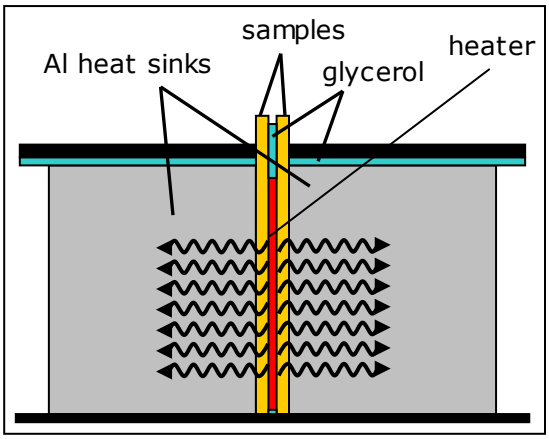

Fig. 3.5: Schematic representation of the working principle of the THASYS.

The thermal conductivity data represents the average value for the thermal conductivity of both samples. The measurements were performed in a climate chamber at a constant temperature of 18°C, to avoid any influence due to changes of the ambient temperature during measurement. The accuracy of the measurements is 6%. Each data point corresponds to an average value of 4 measurements. The scatter of the results was negligible, i.e. 0.001 W/m·K maximum.

3.10 The effect of fillgrade on the thermal conductivity of systems filled with micro- SiO_2 and Al_2O_3 particles

Adding fillers with a thermal conductivity higher than the epoxy improves the heat transfer of epoxy-based composites [97, 101, 258]. The thermal conductivity of the ER-Al_2O_3 and ER-SiO_2 microcomposites as a function of the filler concentration is shown in Fig. 3.6. With an increase of the filler content, the thermal conductivity gradually increases, as anticipated. Incorporation of Al_2O_3 particles in an epoxy matrix resulted in a steady increase of the thermal conductivity by about a factor of 3 at the volume fraction of 0.312. However, to reach the same effect with SiO_2 particles (factor of 3.4), a volume fraction of about 0.45 is required. By adding the same weight amount of microparticles (60 wt.%), we get a different volume fraction because of the different densities of silica and alumina. For the same volume fraction of microparticles, an ER-Al_2O_3 compound will result in a higher thermal conductivity value than an ER-SiO_2 system.
To determine the volume fraction of the filler for a given weight fraction, the following relation was used:

$$\phi = \frac{W}{W + (1-W)\frac{\rho_f}{\rho_m}}, \tag{3.20}$$

where ϕ is the volume fraction of the filler additives, W is the weight fraction, ρ_f and ρ_m are the densities of the filler and matrix, respectively [259].

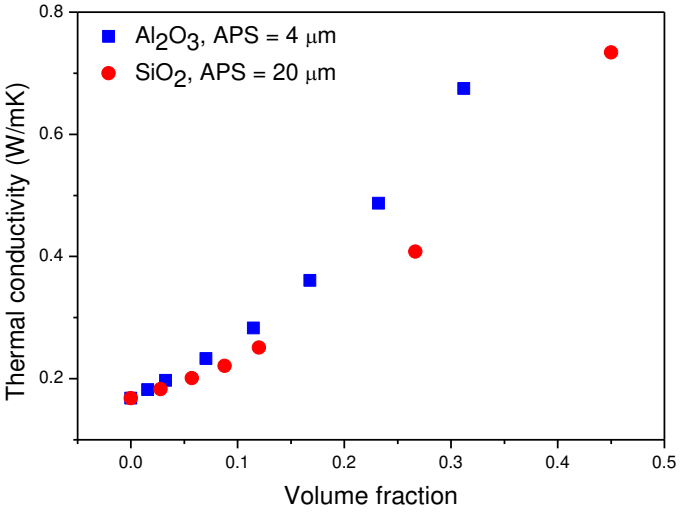

Fig. 3.6: Thermal conductivity of investigated microcomposites as a function of filler volume fraction.

The size of the particles and their shape play an important role in the heat transfer between polymer matrix and the incorporated filler [152, 190, 260]. Fillers with a higher thermal conductivity than ER improve the heat transfer of composites, since heat conduction mainly occurs through the fillers. The epoxy is a thermal barrier for heat propagation, while the filler material transmits the heat much faster [261]. The thermal conductivity of the mineral alumina, e.g. is more than 10 times higher than that of epoxy [194]. The resulting values are however much lower than the values of bulk crystalline silica or alumina would suggest, because the thermal conductivity of powders is significantly lower than their crystalline bulk counterparts [187]. Since the thermal conductivity of bulk Al_2O_3 is higher than SiO_2, microparticles of alumina will transfer heat more effective in the compound at the same volume fraction of filler inside the polymer [195, 262].

3.11 Thermal conductivity of nanocomposites

The thermal conductivity of nanocomposites might have a completely different mechanism in contrast to microcomposites. In case of microcomposites the heat is transported by microparticles much faster than in epoxy resin. Phonons, which are responsible for heat conduction in dielectric materials, are scattered at the interface between dissimilar materials. The heat dissipates on the surface of nanoparticles to a higher degree than on the surface of microparticles. In case of nanocomposite systems with surface modified filler, the heat transport is controlled by the interface provided by a coupling agent that connects inorganic particles on one side and the polymer host on the other side. The surface modified nanoparticles lead to a restructuring of the polymer host and alignment of polymer chains perpendicular to the nanoparticle surface [8].

Fig. 3.7 shows the thermal conductivity behaviour of nanocomposites filled with different types of particles. The thermal conductivity of neat ER varies in the range 0.170 ± 0.02 W/m·K. These variations are attributed to the minor differences in the ratio between epoxy and hardener, polymerization time and temperature of individual samples. With a filler loading of 3.9 vol.% for AlN, the thermal conductivity of the composite reached 0.205 W/m·K, which is the highest recorded value for the nanocomposites studied.

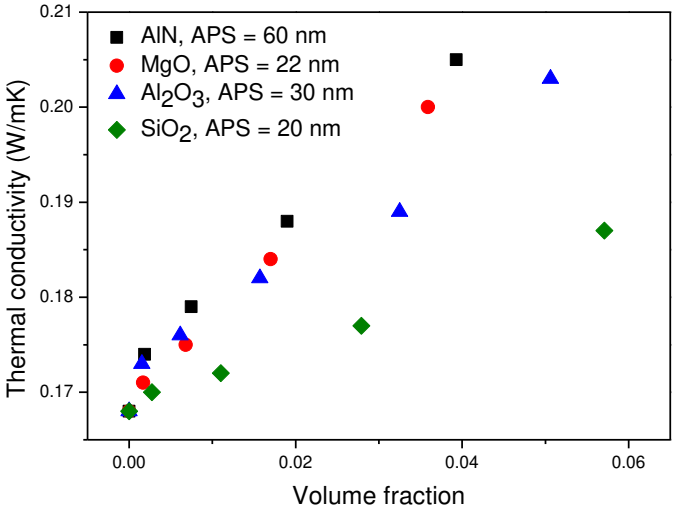

Fig. 3.7: Thermal conductivity of composites with different type of filler vs. volume fraction.

The higher heat conduction of AlN filled samples can be due to a combination of several factors. First of all, the structure of AlN suits the criteria for high-thermal conductive materials [187] better than alumina, silica or MgO, which is explained in sections 3.4 and 3.6. Secondly, the higher values of AlN-mesocomposites can be attributed to a large amount of agglomerates, which promote fast heat conduction. In addition, the small size of Al_2O_3, SiO_2, and MgO particles leads to large interfacial areas and interfacial thermal resistance, which cause higher levels of phonon scattering. Furthermore, the shape of alumina and silica particles is spherical, while that of AlN is hexagonal and cubic. Particles with an aspect ratio > 1 exhibit better heat conduction in one direction, compared to spheres (aspect ratio = 1), with the same volume fraction. The lowest value of thermal conductivity for ER-SiO_2 nanocomposites may be due to the small size of the particles with a nonmodified surface. Due to the lack of modification, the contact between filler and matrix is not fully achieved, thus hindering the thermal transport across the interface. During the composite preparation, the surface modification of particles does not only improve the filler's contact with the matrix, but also changes the structure of the polymer in the proximity of a particle.

3.12 Modelling (Lewis-Nielsen model)

3.12.1 2-phase system

All the data have been fitted to the two-phase and three-phase LN model as introduced in section 3.8. The three-phase model includes the matrix, the filler and the interfacial layer between the matrix and the filler as phases with distinct thermal conductivity and volume. The thermal conductivity and the volume of the interfacial phase are unknown, but we made an attempt to predict those values. It is important to note that the precise value of the thermal conductivity of the filler is also unknown. The three unknown quantities (λ_f , λ_l and v_l) are estimated by fitting the experimental data to the model.

As a representative example, Figs. 3.8 and 3.9 display the fitting of the two-phase LN model (Eq. 3.15) to the experimental data of SiO_2 micro- and nano-particle composites. The best fitting was obtained with values for the parameters as presented in Table 3.4. The average shape factor of the silica microparticles from fitting appears to be ξ =4.9, which indicates the formation of aggregates. This value is obtained from fitting the model over all fractions of particles, and therefore may reflect a value averaged over all concentrations. In contrast, the data for the nanocomposites is well described by the model with the shape factor value equal to 1.5, which corresponds to homogeneously dispersed

spheres. Therefore, we may conclude that SiO_2 nanoparticles do not form clusters, which was also found from TEM observations (Fig. 2.34). The thermal conductivity values for micro-SiO_2 and micro-Al_2O_3 fillers that we obtained using the two-phase model are higher, compared to those for nanoparticles made of the same material. The reason is the higher heat loss on the larger surface area of nanoparticles. The maximum packing fraction ϕ_M of the dispersed particles was assumed 0.637 according to the data in literature [206] available for SiO_2 nanoparticles. This results in a value of 0.89 for the term $\frac{(1-\phi_M)}{\phi_M^2}$, as shown in Table 3.4. Only these particles are well dispersed for all concentrations, they are spherical and have a narrow size distribution. The value of ϕ_M for microparticles was chosen smaller, since they have a wider size distribution or a shape different than a sphere, which reflects in the values $\frac{(1-\phi_M)}{\phi_M^2}$ found in Table 3.4.

Table 3.4: The fitting parameters of the 2-phase LN models.

Composite	λ_m, W/m·K	ξ	λ_f, W/m·K	$\frac{(1-\phi_M)}{\phi_M^2}$
ER-Al_2O_3 micro	0.168	10 (7.36)	5 (2.45)	1.34
ER-SiO_2 micro	0.168	4.9	2	1.16
ER-SiO_2 nano	0.168	1.5	1.36	0.89

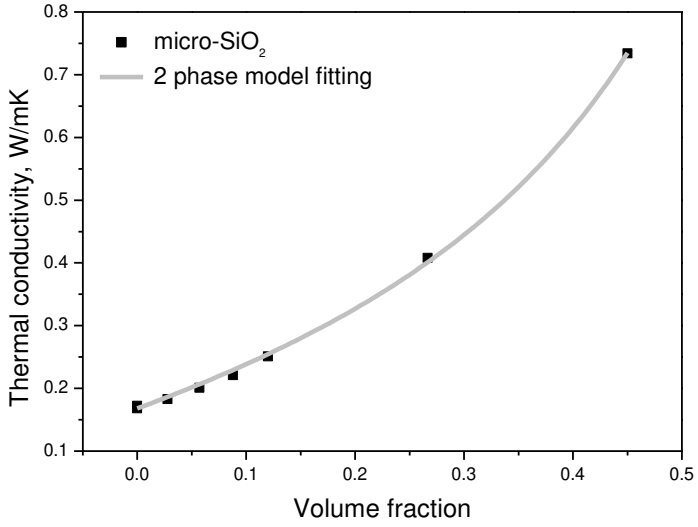

Fig. 3.8: Thermal conductivity of ER-SiO_2 microcomposite as a function of the filler loading (squares) fitted with the 2-phase LN model (solid line).

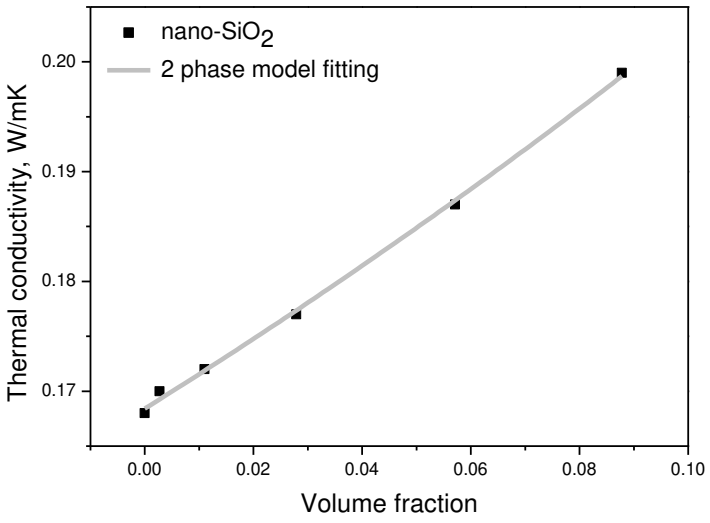

Fig. 3.9: Thermal conductivity of ER-SiO_2 nanocomposite as a function of the filler loading (squares) fitted with the 2-phase LN model (solid line).

3.12.2 3-phase system

The results of fitting the three-phase (Eq. 3.15 and Eq. 3.17) LN models to the experimental data for surface modified Al_2O_3, AlN and MgO are displayed in Figs. 3.10-3.12. For the three-phase model, the effective volume of the CP is $v_f + v_l$, and the effective value of the filler fraction becomes $\phi_f + \phi_l$. Estimations show that the volume of the interfacial layer takes about 10-40% of the nanoparticle volume. The width of the layer is mostly determined by the surface modification of the particle, rather than its size. For the nonspherical particles we assumed agglomeration in form of a rod-like shape. The thermal conductivity of the composite was calculated by averaging over the isotropic agglomerate orientations, as it was done in literature for the Young modulus estimated by the Halpin-Tsai model [263].

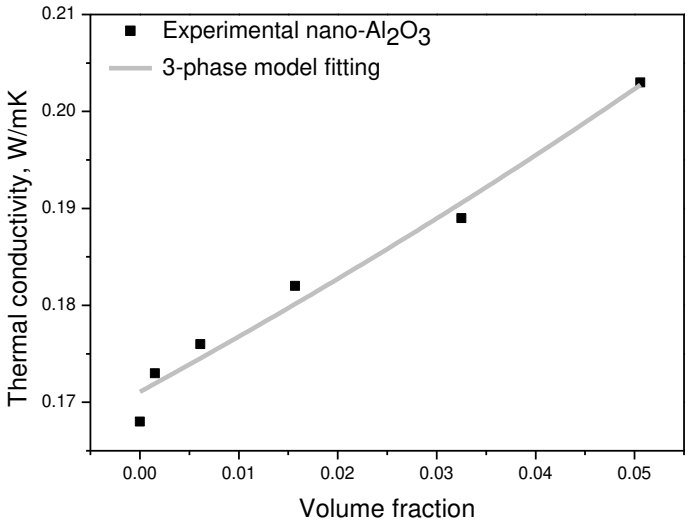

Fig. 3.10: Experimental values of the thermal conductivity of ER-Al_2O_3 composites as a function of the filler loading (squares) fitted with the 3-phase Lewis-Nielsen model (solid line).

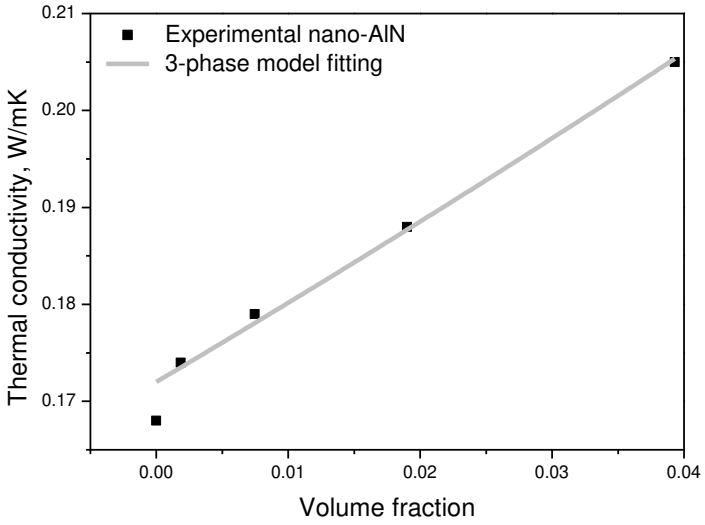

Fig. 3.11: Experimental values of the thermal conductivity of ER-AlN composites as a function of the filler loading (squares) fitted with the 3-phase Lewis-Nielsen model (solid line).

We propose the three-phase LN model for nanocomposites containing surface modified nanoparticles because of several reasons. First of all, it takes into consideration the third phase, which is the aligned layer of polymer chains in the vicinity of nanoparticles. Secondly, if the nanocomposite is described by the two-phase LN model, the parameters of the model become unrealistically high. For example, the thermal conductivities of nanoparticles are much higher than theoretically possible. In contrast, the three-phase model predicts realistic values of the thermal conductivity of nanoparticles and their shape factor. The three-phase model was proposed specially for nanocomposite systems, which have a third phase of polymer aligned layer that was created in the synthesis stage.

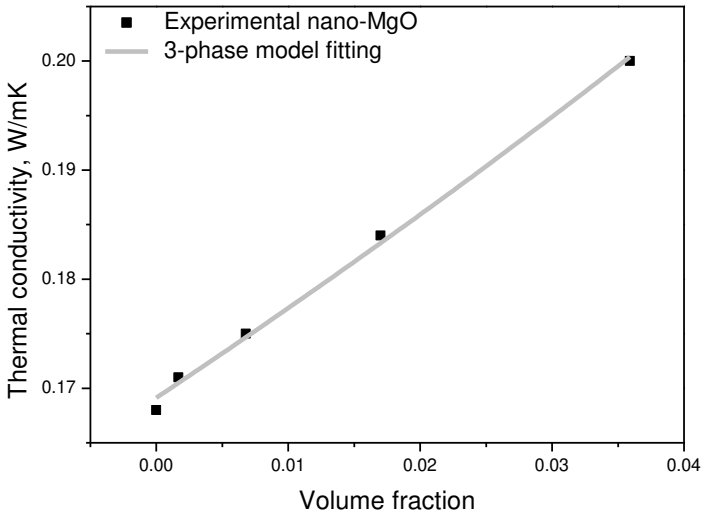

Fig. 3.12: Experimental values of the thermal conductivity of ER-MgO composites as a function of the filler loading (squares) fitted with the 3-phase Lewis-Nielsen model (solid line).

The fitting parameters of the 3 phase LN model are shown in Table 3.5.

Table 3.5: The fitting parameters of the 3-phase LN model.

Compo-site	λ_m, W/m·K	ξ	λ_F', W/m·K	$\frac{(1-\phi_M)}{\phi_M^2}$	$\frac{(\nu_l+\nu_f)}{\nu_f}$	l, nm
ER-Al_2O_3 nano	0.171	3.0	2	1.1	1.17	1.6
ER-AlN nano	0.171	3.6	22	1.1	1.10	1.9
ER-MgO nano	0.169	4.3	2	1.0	1.38	2.5

The three-phase model predicts small values of the thickness l for the interfacial layer (1.6-2.5 nm). For polymers with nanosized clay this layer was estimated by electron spin resonance to be between 5-15 nm [264]. Chen et al. [265] deduced that the thickness of the interfacial layer was 5-10 nm for poly(vinyl alcohol)/silica and dependent upon composition. The other estimations [266] for the interfacial thermal conductance between a single crystal silicon and amorphous polyethylene have shown that the interfacial layer of the polymer has a

thickness of 16 nm. Calculating the three-phase model with the same interface thickness for our experimental systems, we can derive that the effective thermal conductivity of the particle + interfacial layer, i.e. CP, becomes smaller as the size of the composite particle decreases. As shown in Table 3.6, the thermal conductivity λ_F' becomes smaller if the size of the CP decreases, e.g. 0.36 for 22 nm MgO particles opposed to 1.11 for 60 nm AlN particles.

Table 3.6: The fitting parameters of the 3-phase LN model assuming a 16 nm interfacial layer thickness.

Composite	λ_m, W/m·K	ξ	λ_F', W/m·K	$\frac{(1-\phi_M)}{\phi_M^2}$	$\frac{(\nu_l+\nu_f)}{\nu_f}$
ER-Al_2O_3 nano	0.171	2.5	0.38	1.1	3.62
ER-AlN nano	0.171	3.1	1.11	1.1	2.03
ER-MgO nano	0.169	4.3	0.36	1.1	5.15

The Kapitza thermal resistance, R_K, caused by different phonon scattering processes, is effectively present in the measured value for the thermal conductivity of the CP. In a multiphase system there can be a strong scattering of phonons, which occurs when the phonons propagate through a boundary separating one phase from another. The large interfacial area plays a dominant role for the phonon scattering mechanisms inside a polymer composite. This effect is vanishing with increasing filler size. However, the effective value for the thermal coefficient of the CP (λ_F') and the size of CP gives an estimation for R_K. The structure of the equation for the effective thermal conductivity of the CP assumes that we deal with a three-phase model, where the interfacial layer has thermal conductivity λ_l, and a layer thickness l. Although the thermal conductivity of nanoparticles is unknown, the thermal resistance of the layer is $R_K = l/\lambda_l$, effectively introducing the thickness l and the thermal conductivity of the layer. Therefore,

$$\lambda_F' = \lambda_f \Big/ \left(1 + \frac{l\lambda_f}{d\lambda_l}\right). \tag{3.21}$$

3.13 The effect of the size

The effect of size on the thermal conductivity is revealed in Fig. 3.13, where SiO_2 particles are used as filler. The epoxy-based composites filled with SiO_2 microparticles have much higher thermal conductivity values, compared to those filled with nanosized particles. This effect is attributed to the phonon scattering on the much larger surface areas of the nanoparticles.

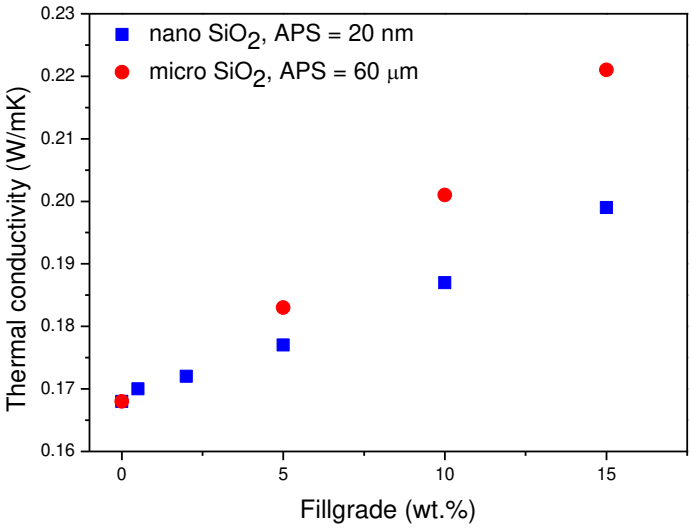

Fig. 3.13: Thermal conductivity of composite with nano- and microparticles of SiO_2 vs. fillgrade.

3.14 Surface modification and aspect ratio

In order to check the influence of surface modification of incorporated particles on the thermal conductivity, various types of the epoxy-BN filled systems have been fabricated. In order to enhance the thermal conductance of the filler-matrix interface, a SCA in the form of GPS was applied for some samples [151, 195]. The thermal resistance of the interface is not known and cannot be measured on the nanoscopic scale. But the boundary thermal resistance is dependent on the quality of the interface and the acoustic mismatch between a polymer and filler. The mismatch determines the degree of phonon scattering at the interface. A SCA helps to decrease the mismatch by creating a polymer layer, which has different properties. The quality of the interface between dissimilar materials can also be improved by grafting a SCA on the surface of nano- or microparticles [98, 267].

The specimens, details about the modification of the particles, the measured thermal conductivity values and the relative improvement of the thermal conductivity, compared to the reference sample, are summarized in Table 3.7.

Table 3.7: Influence of surface functionalization on the thermal conductivity.

Specimen	SCA	λ, W/m·K	Improvement, %
Neat ER		0.168	-
ER-70BN-10	no	0.234	39
ER-0.5BN-10	no	0.264	57
ER-1.5BN-10	no	0.236	40
ER-70BN-10	yes	0.240	43
ER-0.5BN-10	yes	0.274	63
ER-1.5BN-10	yes	0.242	44

Differences in the thermal conductivity can be seen for epoxy resin filled with BN particles, depending on filler size, shape and modification. The thermal conductivity measurements show that the addition of 10 wt.% BN filler enhances the thermal conductivity by about 39-57%, depending on the filler size and its morphology. The surface modification of BN particles with silane coupling agent can increase the thermal conductivity additionally by up to 7%, for the composite filled with submicron particles of BN (0.5 μm). The increase in thermal conductivity is due to a decrease in the thermal contact resistance between the filler and matrix, due to the improvement of the interface between host and particles [182].

We can witness an increase of the thermal conductivity for a different particle shape. The shape of the particles of 70 nm and 1.5 μm diameter is spherical. If spherical particles are homogeneously dispersed into a polymer matrix, the average distance between them is the maximum possible. If the aspect ratio is differing from one, in case of platelets or needles, the average distance between particles becomes smaller for the same volume percentage of filler material. The high aspect ratio particles greatly exhibit the bridging phenomenon which assists in the formation of the conducting network by lowering the percolation threshold [139].

The BN filler of 0.5 μm size has a platelet-like structure with an aspect ratio larger than one. This leads to a smaller average distance between particles. Since the thermal conductivity is much lower in the polymer than in the filler, the reduced distance between the particles could be the reason for the more efficient heat transfer [271].

3.15 Crystallinity

Nanoalumina in the α, γ and δ phases with different average particle size were introduced into epoxy resin, using a conventional mechanical mixing method and ultrasonication processing. Surface treatment of the particles was realized by silanization, in order to improve the compatibility of the host polymer and the ceramic filler, by organizing physical and chemical bonding between the dissimilar materials. Five types of alumina-epoxy composites were fabricated with an average particle size ranging between 20 and 80 nm. The filler loading was 2 wt.% for all composites.

Al_2O_3 can exist in several crystalline phases, which all revert to the most stable hexagonal alpha phase at elevated temperatures [269]. Besides α-phase Al_2O_3 with APS of 40 and 80 nm, we investigated γ-phase Al_2O_3 with APS of 20 and 40 nm supplied by IoLiTec. We also prepared a composite using 30 nm δ-phase Al_2O_3 particles obtained from Sigma-Aldrich. Microscopy revealed the different structure of the filler material: alumina particles supplied by IoLiTec have an irregular shape (see Fig. 2.32), while Al_2O_3 obtained from Sigma-Aldrich consists of spherical particles.

The thermal conductivities of neat ER and nanocomposites filled with different types of alumina are presented in Table 3.8.

Table 3.8: Influence of crystallinity and particle size on the thermal conductivity.

Specimen	Nanofiller	APS, nm	λ, W/m·K
Neat ER	None	-	0.1686
ER-Al_2O_3-2	γ- Al_2O_3	20	0.1739
ER-Al_2O_3-2	δ- Al_2O_3	30	0.1745
ER-Al_2O_3-2	α- Al_2O_3	40	0.1755
ER-Al_2O_3-2	γ- Al_2O_3	40	0.1757
ER-Al_2O_3-2	α- Al_2O_3	80	0.1762

As it was expected, the addition of the inorganic filler raised the thermal conductivity of the epoxy matrix, but not by much. The thermal conductivity was improved by 3% with the incorporation of 20 nm γ-Al_2O_3 and by 4.5% by adding 80 nm α-Al_2O_3 particles, compared to the neat polymer. We conclude that the influence of the crystal structure of the incorporated alumina particles on the thermal conductivity is negligible for such small particles. The thermal resistance, which is caused by phonon scattering processes, plays a dominant role in limiting the thermal conductivity. The scattering of phonons in composite materials is mainly due to the existence of a thermal barrier, originating from an acoustic mismatch at the interface between the organic polymer

host and ceramic filler [98, 207, 270]. The composite containing the largest nanoparticles, which means lowest particle surface area, has the highest thermal conductivity value. This is because the interfacial thermal barrier is relatively small compared to other nanocomposites [271].

3.16 Alignment

Engineers have been working for decades to develop efficient heat transfer from conductor to environment. The operating life and power rating of high voltage machines, apparatuses and cables can be prolonged by improving thermal conductivity of electrical insulation material. The orientation of nanoparticles could be a good solution to improve the thermal conductivity in one direction. It is well known that thermal transport increases significantly in the direction of orientation of the nanoparticles and slightly changes in the direction perpendicular to the orientation [54]. The anisotropic behaviour of the thermal conductivity will lead to the cooling of the conductor, for example in a cable.

The theory behind the alignment of nanoparticles and the experimental results are presented in Appendix A.

3.17 Summary

Polymer materials have good insulating properties and processability but the thermal conductivity is rather weak. The microparticles, which have been used for more than 50 years as filler, change the property of a polymer considerably. The study of nanostructured materials might help in developing a new branch of polymer-based nanocomposites, which can be used in special applications. It has been found that filler size, geometry, concentration, dispersion, orientation, crystal structure, and interface between the polymer matrix and filler affect the thermal conductivity of the host polymer. Different models, which are used to predict and fit the thermal conductivity of a two-phase system, have been discussed. There is not a single model that can be used to describe the thermal conductivity of all composites. All proposed models are good in particular cases. The heat conduction mechanism of nanocomposite materials is completely different from that in a matrix that has been reinforced by conventional sized microfiller. In case of microcomposites, the heat is conducted mainly via the highly conductive filler. In case of nanodielectrics, the surface modified nanoparticles reorganize the polymer matrix in such a way that the interface polymer layer in the proximity of the particles changes its properties significantly. The interface polymer layer, which is created by surface modified nanoparticles, has semicrystalline properties. It means that polymer chains are not chaotically distributed. They are perpendicular to the

particle surfaces. This interfacial polymer layer has to be considered as a separate phase in addition to filler and polymer, which has not been affected by nanoparticles. A three-phase Lewis-Nielsen model has been proposed and used to describe the behaviour of epoxy filled with surface modified nanoparticles. The model fits very well the experimental data and takes into account the interface thermal resistance. The creation of nanoparticle paths is possible in practice if the relative permittivities of the matrix and filler have quite different values and if the polymer matrix has a low electrical conductivity. Our system does not satisfy these requirements and therefore can be studied only in theory.

4

Dielectric response of nanocomposites

4.1 Introduction

Dielectric Spectroscopy (DS) is a powerful tool for investigating a variety of dielectric processes for both electrical and non-electrical applications. The dielectric properties of materials play a fundamental role in the description of physical phenomena in many branches of modern science and engineering [272]. Dielectric spectroscopy provides a link between the dynamics of molecular motion of the individual constituents of a complex material and the characterization of its bulk properties [273]. Polymer nanocomposites are interesting because of their unique behaviour especially at low concentrations of nanofiller. It has been reported that the presence of a small amount of inorganic filler can affect the real and imaginary parts of the complex permittivity [116, 267,

274, 275]. The influence of nanofillers is unique in the sense that the incorporation of clay [72], alumina, titania or zinc oxide [74, 93, 276] into a polymer can reduce the relative permittivity compared to the value of the neat polymer material. The dielectric spectroscopy results show a behaviour that cannot be explained by rules of mixture and therefore a qualitative model is proposed for the explanation of the low values of the relative permittivity.

4.2 Measurement principle

DS is a commonly used technique to record the behaviour of the complex permittivity as a function of frequency and temperature. The measurement is based on the interaction of an electric field with the electric dipole moment of the test specimen, which is often expressed by the complex permittivity. In other words, the technique is based on the application of a voltage of varying frequency to a test specimen and on the measurement of the resulting current and the phase shift between the current and the applied voltage. From these data, the real and imaginary parts of the complex permittivity are derived [277].

4.3 Measurement setup

A fully automated Alpha-A dielectric analyzer from Novocontrol has been used, which allows measuring the complex permittivity (and deduced quantities such as conductivity, impedance or $\tan(\delta)$) of a dielectric as a function of frequency and temperature [278]. Fig. 4.1 shows a schematic representation of the DS setup. The system consists of a ZGS Alpha active cell and includes an automatic temperature control unit (Quatro cryosystem) with a precision of 0.1°C [279, 280]. The sample lies within a cryogenic cell, which can be heated up to 400ºC and cooled down to -160ºC with 0.01ºC temperature stability. A sinusoidal voltage of 3 V_{rms} was applied across the sample. The diameter of the measuring electrodes is 20, 30 or 40 mm depending on the sample size.

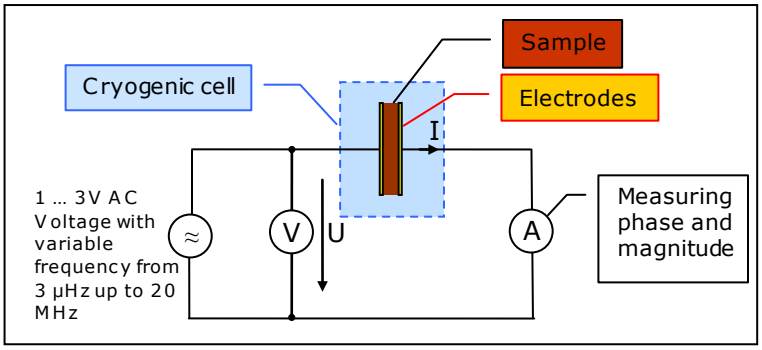

Fig. 4.1: Equivalent circuit diagram of the DS setup.

The main part of ZGS Alpha active cell, the sample holder, is shown in Fig. 4.2.

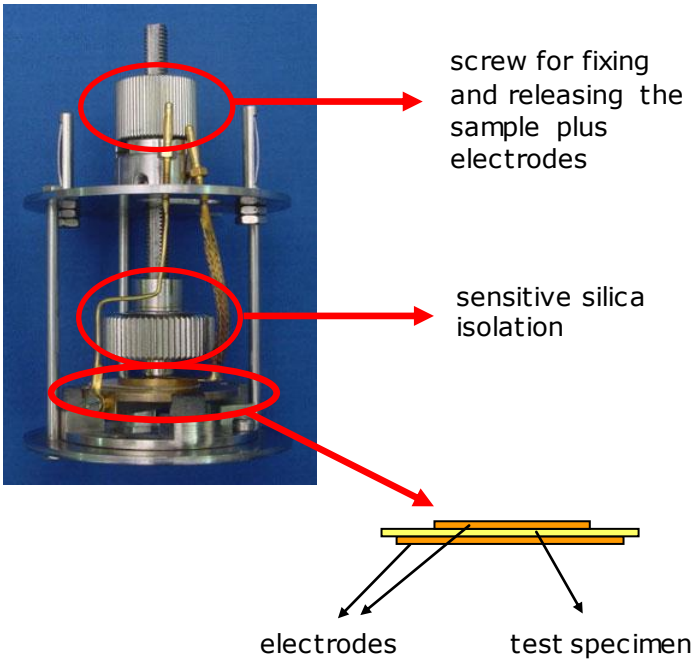

Fig. 4.2: Low frequency (<20 MHz) sample holder (image by Novocontrol).

Specimens with a diameter of 42 mm and a thickness of about 0.5 mm were created using the synthesis process explained in Chapter 2. Prior to dielectric characterization, aluminum or gold electrodes were deposited onto both sides of the specimens by sputtering, in order to

achieve a good contact between the samples and measuring electrodes [281]. In order to minimize the amount of absorbed water in the specimens, which may affect the measurement data [117], all samples were dried at 140°C for 2 days before the measurements and stored in nitrogen gas to keep them dry. The measurements were performed in a cryogenic cell under a nitrogen atmosphere to prevent any influence of humidity.
The dielectric properties were measured in the frequency range of 10^{-2}-10^{7} Hz and at temperatures between -20°C and 120°C. The temperature was increased in steps of 20°C. The values of the complex permittivity for each data point are the average values of 3 measurement values with an error of 2-3%.

4.4 Polarization spectrum

A dielectric material in its simplest form can be represented as a capacitor and a resistor in parallel. The current through such a sample must have both a real and imaginary component [31]. This can be taken into account by defining the complex permittivity (ε^*), which relates to a material's ability to respond to the electric field by its polarization.

$$\varepsilon^* = \varepsilon' - j\varepsilon'' \tag{4.1}$$

ε' is what we know as the relative permittivity, it is a measure of the amount of polarization. The imaginary part ε'' represents the loss component, it is a measure of the losses involved in the polarization processes.
The behaviour of the permittivity as a function of frequency and temperature is sensitive to material changes, such as aging processes, absorbed moisture or the addition of fillers [8]. Any change of the molecular structure of a dielectric will show up if the related polarization phenomena are occurring in the measured frequency range.
The loss tangent tan(δ) is directly related to the real and imaginary parts of the complex permittivity:

$$\tan(\delta) = \frac{\omega\varepsilon'' + \sigma}{\omega\varepsilon'}, \tag{4.2}$$

where σ is the electrical conductivity.

In practice tan(δ) is frequently used for the testing of high voltage components at 50 Hz. However, a lot more information about the structure and condition of a dielectric material is available when the complex permittivity is measured in a broad frequency range [282].

Even though DS generally yields complex dielectric relaxation spectra, the data analysis and discussion of the dielectric properties is mainly based on the dielectric loss spectrum ε''. This has two reasons:

- Dielectric dispersion curves often show more details and make visual evaluation easier. For example: every time ε' varies rapidly – at the relaxation or resonance frequency – a peak can be seen in the ε'' curve.
- The real and imaginary part of ε^* are related through the Kramers-Kronig relations (4.3 and 4.4), since the two spectra are fully equivalent in terms of information about relaxation processes [283].

$$\varepsilon'(\omega_0) = 1 + \frac{2}{\pi}\int_0^\infty \frac{\omega \cdot \varepsilon''(\omega)}{\omega^2 - \omega_0^2} d\omega \tag{4.3}$$

$$\varepsilon''(\omega_0) = -\frac{2\omega_0}{\pi}\int_0^\infty \frac{\varepsilon'(\omega)}{\omega^2 - \omega_0^2} d\omega \tag{4.4}$$

The frequency dependant polarization spectrum of a dielectric is the superposition of all active polarization mechanisms (see Fig. 4.3):

- For very high (i.e. optical) frequencies even electrons cannot keep up with the changing field, the result is a relative permittivity equal to 1.
- At high frequencies (IR, UV) electronic and atomic polarizations are dominating.

  - ❖ Electronic polarization is a resonant process which occurs in a neutral atom when the electric field displaces the electron density relative to the nucleus it surrounds.
  - ❖ Atomic polarization is a resonant process, which arises from the change in dipole moment accompanying the stretching of chemical bonds between unlike atoms in molecules

In most applications we stay well below these frequencies.

For electrical engineering applications frequencies below 100 MHz are important.

- At intermediate frequencies (1 Hz … 100 MHz) orientational polarization shows up. In this frequency range, molecules, parts of molecules or molecular chains orient in the changing electrical field. In this region changes in the material composition affect

the polarization, for instance because of the introduction of filler materials.

- ❖ Dipole relaxation originates from permanent and induced dipoles aligning to an electric field. Dipole relaxation is heavily dependent on the temperature and chemical surrounding.
- ❖ Ionic relaxation comprises of ionic conductivity, interfacial and space charge relaxation.

- At low frequencies two mechanisms may become visible (< 1 Hz):
  - ❖ Interfacial polarization – the polarization of interfaces between materials, with a relaxation time in the range of seconds to hours. The losses caused by interfacial polarization are relatively high compared to losses, which are originated from other polarization mechanisms.
  - ❖ DC conductivity – this gives rise to ohmic losses that show up in a linear reciprocal relation between ε'' and the frequency. This is especially visible at higher temperatures, where the conductivity strongly increases.

The polarization processes at low frequencies and high temperatures are obscured by the effect of the DC conductivity. For a fast approximation of ε'', Wübbenhorst and van Turnhout [284] proposed a simplified version (4.5 and 4.6) of the Kramers-Kronig relations, which can be used to remove the effect of the conductivity.

$$\varepsilon''_{cond}(f) = \frac{\sigma_{dc}}{2\pi f \varepsilon_0} + \varepsilon''_{pol}(f), \tag{4.5}$$

$$\varepsilon''_{pol}(f) = -\frac{\pi}{2} \cdot \frac{\mathrm{d}\,\varepsilon'(f)}{\mathrm{d}\ln(f)}. \tag{4.6}$$

Dielectric relaxation as a whole is the result of the movement of dipoles and electric charges due to an applied alternating field. Relaxation mechanisms are relatively slow compared to resonant electronic transitions or molecular vibrations, which are usually in the Terahertz frequency range.

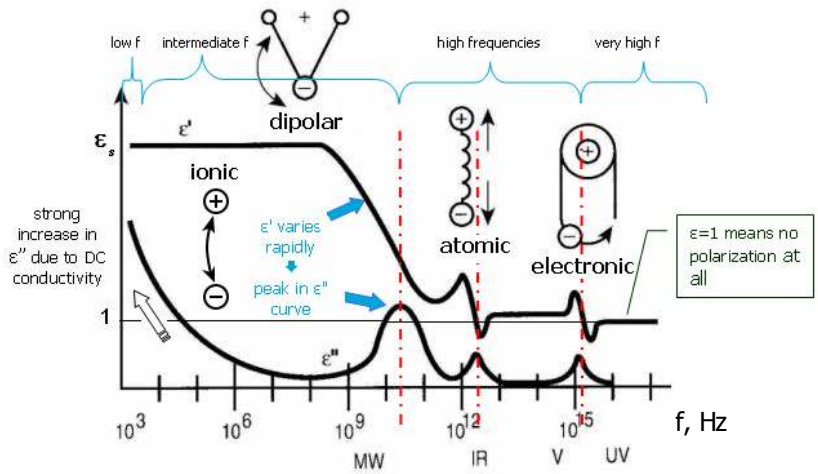

Fig. 4.3: The polarization spectrum over a wide range of frequencies [285].

The complex permittivity exhibits several types of relaxation, each of them characterized by their own relaxation parameters. The most pronounced, α- and β-relaxation and DC conductivity, are shown for an epoxy example in Fig. 4.4.

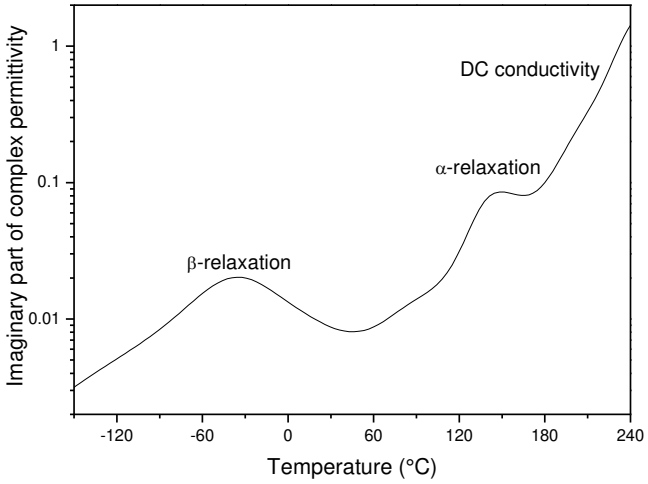

Fig. 4.4: Schematic representation of the polarization spectrum of a polymer-based composite as a function of temperature.

The α-relaxation has a high and narrow peak in comparison to other relaxations. In polymers, the α-relaxation is associated with the glass

transition temperature T_g. Sometimes it is difficult to determine the α-peak, because it can be overshadowed by the DC conductivity (see Fig. 4.4). The β-relaxation is characterized by a broad relaxation peak, which can have a width of several decades. It originates from localized fluctuations of the side groups of a polymer.
When considering real polymers, it becomes clear that the polarization spectrum is much more complicated. A spectrum is always a superposition of the relaxation mechanisms and sometimes it is difficult to discern the individual relaxation processes [31]. Havriliak and Negami proposed an empirical expression to describe the dielectric relaxation of some polymers [286, 287]:

$$\varepsilon'(\omega,T)-\varepsilon_\infty=\frac{\varepsilon_s-\varepsilon_\infty}{\left\{1+\left[j\omega\tau(T)\right]^a\right\}^b}, \tag{4.7}$$

where ε_∞ is the relative permittivity at $\omega\to\infty$, ε_s is the static relative permittivity at $\omega\to 0$, $\tau(T)$ is the relaxation time, and the exponents a and b are values between zero and unity.

4.5 Dielectric response of neat epoxy

The real and imaginary parts of the complex permittivity of the neat ER samples as a function of frequency are shown in Figs. 4.5 and 4.6, respectively. The high values of ε' at low frequencies and high temperatures can be attributed to the proximity of the α-relaxation peak. The broad peak on ε''(f), which can be seen at 1 kHz for -20°C, moves to higher frequencies with increasing temperature and is attributed to a β-relaxation process. The β-relaxation is linked to the mobility of the side chains in the polymer [113].
The imaginary part of the complex permittivity of the reference neat ER sample as a function of frequency is shown in Fig. 4.7. The α-relaxation peak is not clearly visible at high temperatures because it is obscured by the DC conductivity, which increases greatly above the T_α [8]. The location of the α-relaxation peak can be confirmed with DMA (dynamic mechanical analysis).

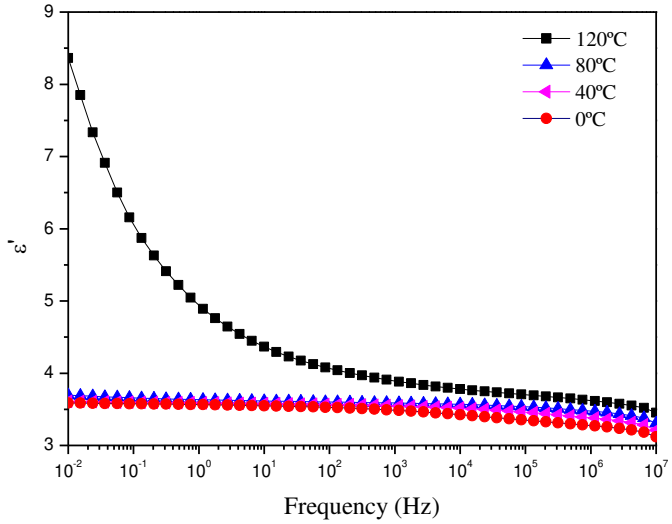

Fig. 4.5: ε' of the reference neat ER samples for different temperatures as a function of frequency.

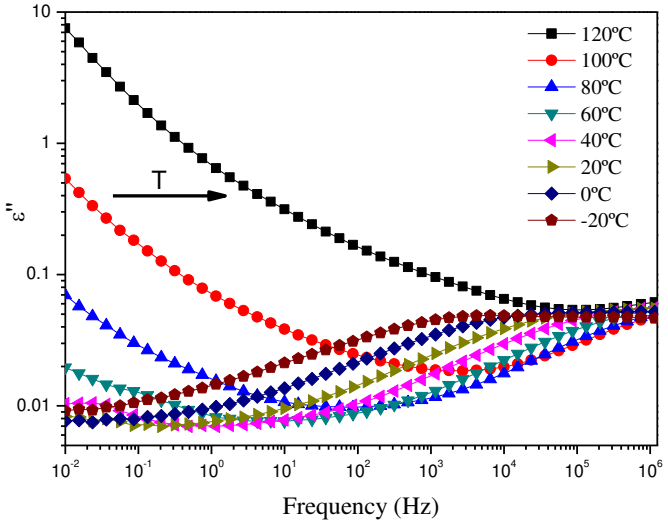

Fig. 4.6: ε'' of the reference neat ER samples for different temperatures as a function of frequency.

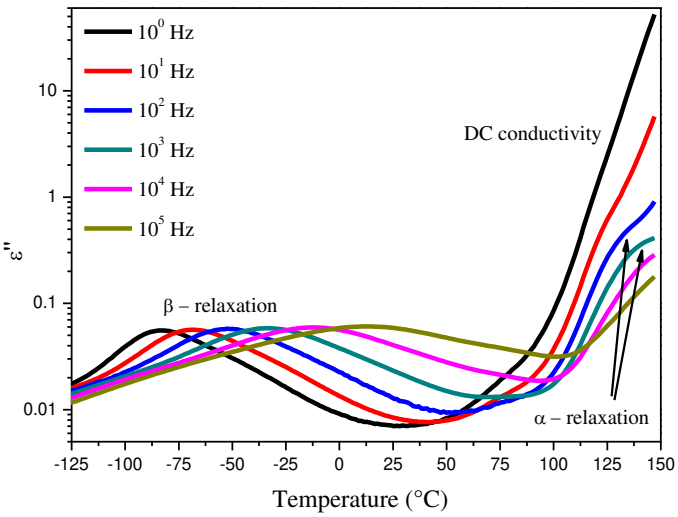

Fig. 4.7: ε'' of the reference neat ER samples for different frequencies as a function of temperature.

4.6 Influence of filler type and concentration

Figs. 4.8-4.11 show the real part of the complex permittivity of Al_2O_3 -, AlN-, MgO- and SiO_2 - epoxy composites as a function of frequency for different filler contents at 20°C. With an increase in frequency, ε' decreases monotonically in all samples. As the frequency increases, some dipolar groups, e.g. larger molecules, can not keep pace with the applied field. Therefore the contributions of these inert dipolar groups to the permittivity disappear, which leads to a decrease of the amount of polarization in the system [288].

The modified nanoparticles with coupling agents on the surfaces have different microscopic properties compared to the bulk polymer matrix, which is relatively far away from the particle surface. A SCA affects the amorphous structure of epoxy and leads to some alignment of the polymer chains, which are perpendicular to the particle surface [8] (see Fig. 4.12).

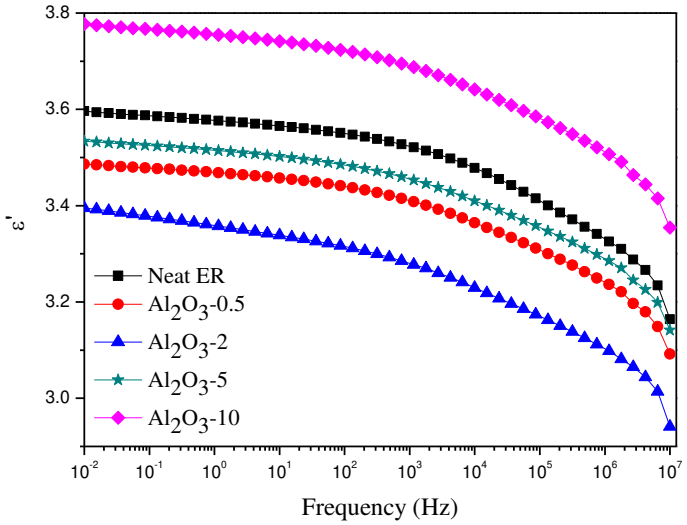

Fig. 4.8: ε' of ER-Al_2O_3 samples as a function of frequency at 20°C.

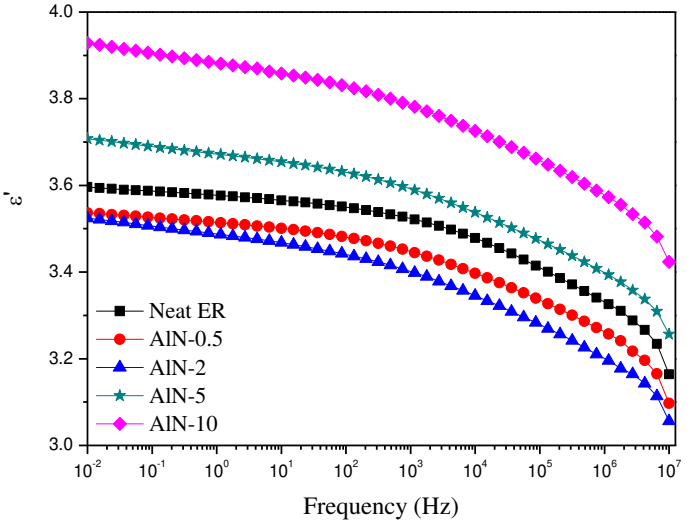

Fig. 4.9: ε' of ER-AlN samples as a function of frequency at 20°C.

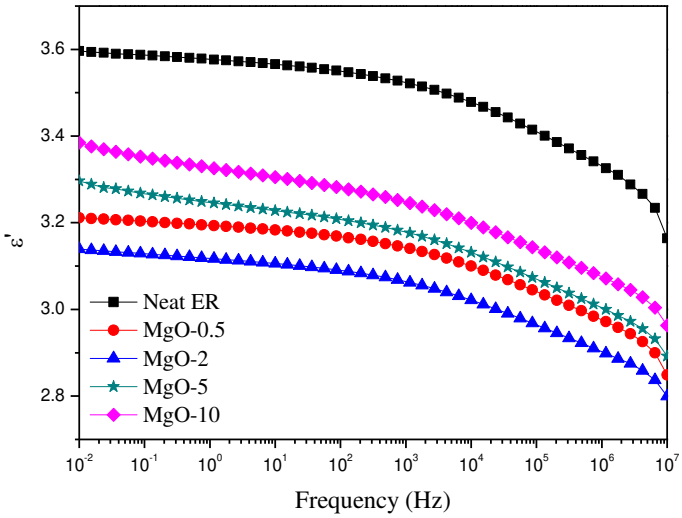

Fig. 4.10: ε' of ER-MgO samples as a function of frequency at 20°C.

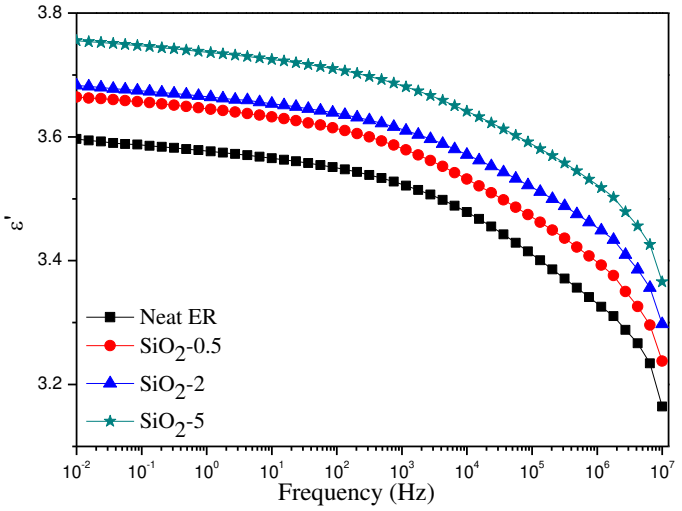

Fig. 4.11: ε' of ER-SiO_2 samples as a function of frequency at 20°C.

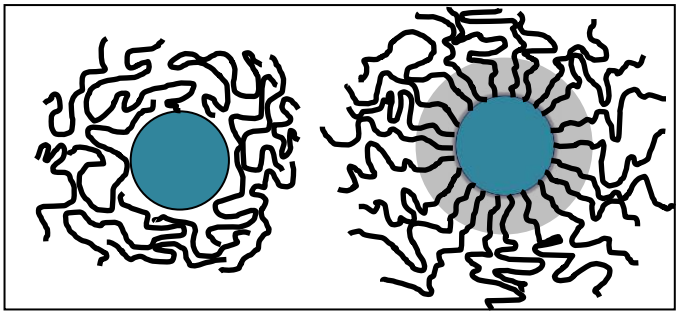

Fig. 4.12: A particle without surface modification (left) and a particle with surface modification (right). The grey area around the surface treated particle is a layer of aligned polymer chains.

The ε' spectra of composite materials containing surface modified particles (Al_2O_3, AlN and MgO) show a similar trend. The composites with 2 wt.% of modified particles have the lowest ε' values. The value of ε' at 0.5 wt.% is the second lowest. An incorporation of 5 wt.% and further 10 wt.% gives a rise in ε' above the value of the reference epoxy.

We assume two mechanisms, which affect the polarization of ER. The first mechanism is the restriction of the chain mobility in the vicinity of the nanoparticles, within a few nanometers of the filler surface. This mechanism is caused by the interface polymer layer with modified molecular structure and chain dynamics, compared to the neat polymer matrix. The dipolar groups are immobilized in the proximity of the nanoparticles [29]. The first effect explains why the relative permittivity drops down. The second mechanism is the effect of the relative permittivity of the filler itself. The relative permittivity of any material we used as a filler is higher than the ε' of ER. The second effect explains why the relative permittivity increases for fillgrades above 2 wt.%. The first effect is predominating up to 2 wt.%, while the second one becomes stronger for higher concentrations.
Singha and Thomas investigated the systems based on ER and filled with 0.1, 0.5 and 1 % of TiO_2, ZnO and Al_2O_3 [74, 93, 289]. The higher filler concentration is reflected in the higher relative permittivity values of the composites. We explain the difference between our results and the results of Singha and Thomas by a different surface modification, which influences the dielectric behaviour of the final nanocomposite. It can also be explained by variations in the synthesis process, for example using different times for ultrasonication and curing. The epoxy system the samples were based on is also not the same. Variations in the chemical structure of the ER can lead to a different thickness of the

interfacial layer, thus to a different response of the polymer to an external electric field.

The higher values of ε' for Nanopox-based composites (Fig. 4.11), compared to the neat polymer and composites filled with other particles, are assumed due to the different specimen preparation process. Nanopox composites were produced using an in-situ polymerization process. The surface modification is not part of this synthesis method, therefore we assume that there is no interfacial layer of aligned polymer chains in the proximity of the SiO_2 nanoparticles. Thus, immobilization of the epoxy chains does not take place, which would explain why a reduction of ε' could not be observed. Another reason why Nanopox-based composites have higher relative permittivity values can be due to byproducts, which are present inside the polymer after in-situ precipitation of nanosilica [290]. These byproducts are assumed to be very mobile and lead to a higher ε' of the composite material overall.

4.6.1 Restriction of chain mobility

ER samples filled with MgO nanoparticles have the lowest relative permittivity values of all nanocomposites tested. An interesting feature is that the MgO (APS is 22 nm) nanoparticles are the smallest within the group of tested nanoparticles, i.e. Al_2O_3 and AlN (APS is 30 nm and 60 nm, respectively), not taking into account the composites filled with SiO_2 due to missing surface modification. All $\varepsilon'(f)$ curves of ER-MgO have lower values than neat epoxy samples. Since the ε' of the bulk material of MgO, Al_2O_3 and AlN is approximately the same, namely 8.5-10 depending on the structure [150, 291], we conclude that the interaction between the MgO nanoparticles and the host is the strongest. Since MgO nanoparticles are the smallest, they have the highest surface-to-volume ratio, which leads to larger amounts of OH groups on the surface. The evidence of larger amounts of hydroxyl groups on the surface of MgO nanoparticles, compared to e.g. Al_2O_3 nanoparticles, can be found in TGA spectra of as-received and GPS-treated particles of these types (see Figs. 2.21 and 2.22, Chapter 2). The larger weight loss for MgO in Fig. 2.22 indicates a larger amount of GPS molecules that reacted with the OH groups on the surface of the nanoparticles. The reaction of hydroxyl groups with GPS creates stronger bonds between particles and host. Therefore more dipolar groups will be immobilized in the vicinity of the MgO nanoparticles. The importance of the size of the particles and therefore the interfacial region is underlined by results for ER-BN composites shown in Section 4.7.

AlN particles have the largest APS and therefore smallest interface volume (see Section 4.7). Since the volume of interfaces decreases for increasing filler size at constant weight percentage, the move to larger filler results in smaller zones of immobilization. The larger the particles

are, the larger the influence of the filler properties becomes, compared to the changes to the polymer structure. Therefore the influence of the immobilization layers diminishes.

The ε' values of ER-AlN-5 are higher than of neat ER, while ER-Al_2O_3-5 values are still lower. The amount of hydroxyl groups on the surface of alumina is larger than on the surface of AlN. Hence, more GPS groups connect to the surface of Al_2O_3 particles. In turn, more dipole groups of the epoxy will be immobilized in the interface polymer layer. The properties of the filler become predominant at 10 wt.% of Al_2O_3 or AlN. Therefore the ε' of ER-Al_2O_3-10 and ER-AlN-10 have higher values than neat ER.

The ε' values of all specimens at 1 kHz and the difference compared to neat ER are shown in Table 4.1. Neat ER has an ε' equal to 3.52. Specimens with MgO nanoparticles have values between 3.06 and 3.25, which is a reduction by 8.5% to 15%, compared to the neat ER. The addition of 2 wt.% of alumina nanofiller leads to a 7.4% reduction of ε'. The lowest value for ER-AlN composites is 3.4, which is a 3.6% reduction. ER-SiO_2 samples have a higher ε' for all fill grades, compared to the reference sample.

Table 4.1: The relative permittivity of the specimens at 1 kHz and the difference compared to neat ER.

Composite	Relative permittivity ε'	Difference (%)
Neat ER	3.52	-
ER-Al_2O_3-0.5	3.41	-3.3
ER-Al_2O_3-2	3.28	-7.4
ER-Al_2O_3-5	3.45	-2.0
ER-Al_2O_3-10	3.69	+4.7
ER-AlN-0.5	3.44	-2.2
ER-AlN-2	3.40	-3.6
ER-AlN-5	3.59	+1.9
ER-AlN-10	3.78	+7.4
ER-MgO-0.5	3.14	-12.1
ER-MgO-2	3.06	-15.0
ER-MgO-5	3.18	-10.9
ER-MgO-10	3.25	-8.5
ER-SiO_2-0.5	3.58	+1.6
ER-SiO_2-2	3.61	+2.5
ER-SiO_2-5	3.68	+4.5
ER-BN-10 70nm	3.47	-1.4
ER-BN-10 500nm	3.90	+10.8
ER-BN-10 1500nm	4.09	+16.0
ER-BN-10 5000nm	4.33	+22.9

Fig. 4.13 shows the effect of different nanoparticle types with a fillgrade of 2 wt.% on the ε' of the nanocomposites as a function of frequency. Nanocomposites with 2 wt.% are shown, because the reduction of ε' is the most pronounced at this fillgrade for all investigated nanocomposite types, except for SiO_2 nanoparticles. As the volume of the filler material increases, the influence of the material properties of the particles on the ε' of the matrix becomes more pronounced. The surface of AlN, Al_2O_3 and MgO was treated with GPS, which creates better adhesion and aforementioned interfacial layer.

4.6.2 Effect of the relative permittivity of the nanoparticles

The ε' becomes higher if the concentration of the filler exceeds 2 wt.% or 0.5 wt.% for SiO_2. It was mentioned above that the relative permittivity of any material that we add as filler, is relatively high, compared to the ε' of ER. The higher volume fraction of the filler with higher ε' results in a higher relative permittivity of the composite. If the volume fraction increases, the amount of the material with high relative

permittivity is increasing along with the overlapping of the interfacial layers, which leads to the higher relative permittivity of the whole nanodielectric system. The overlapping is possible at high filler loadings (≥ 10 vol. %) or large interface layer around the nanoparticles.

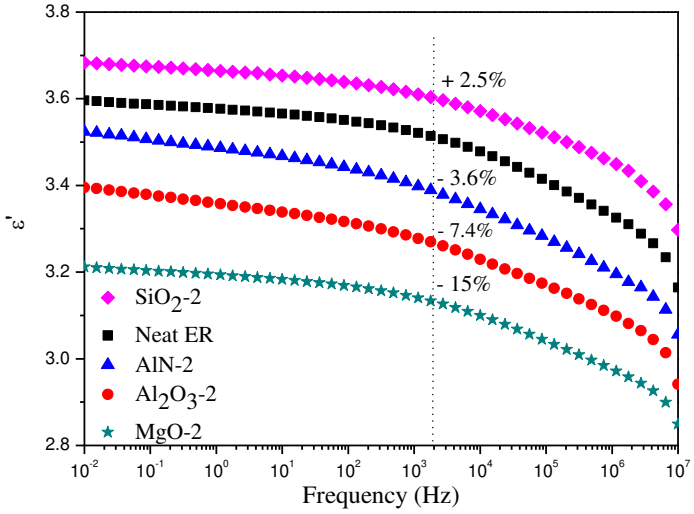

Fig. 4.13: The effect of the filler type on the ε' of nanocomposites with 2 wt.% for 20°C as a function of frequency.

The dielectric losses of the composites containing up to 5 wt.% of nanoparticles do not differ much from those of the neat polymer (see Figs. 4.14 and 4.15). The mechanism why the losses appear to be slightly reduced at low and at high frequencies is not well understood yet.

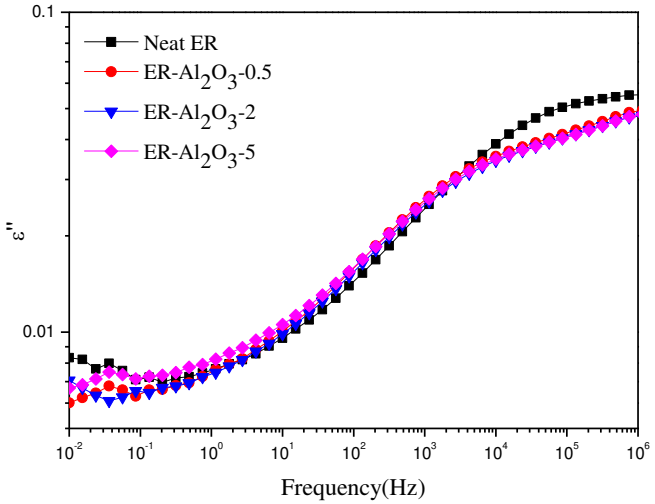

Fig. 4.14: ε'' of ER-Al_2O_3 samples as a function of frequency at 20°C.

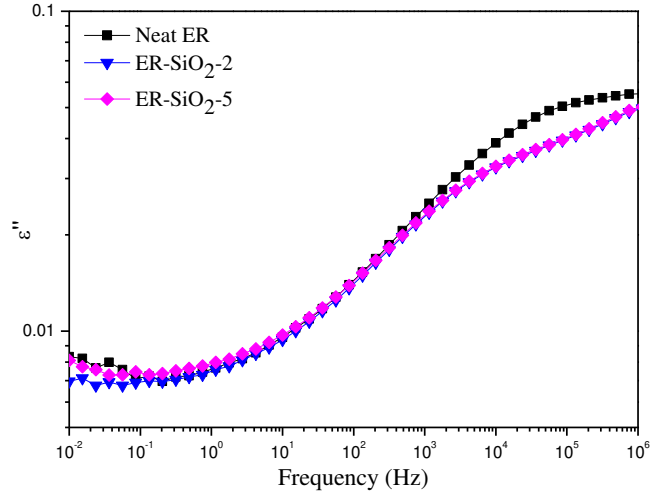

Fig. 4.15: ε'' of ER-SiO_2 samples as a function of frequency at 20°C.

The main difference in the dielectric spectroscopy spectra of composites with nanoparticles is observed at frequencies higher than 1 kHz. The polarization of epoxy dipolar groups is more pronounced in the high frequency region, which causes higher losses in this region. The lower losses of nanocomposites can be an indication for the presence of the interfacial layer. The side chains, which are responsible for the

β– relaxation peak, are restricted in the vicinity of nanoparticles, while in unfilled polymer all side chains can move in respect to the applied field, which increases the losses of the system. However, the ε'' at 50 Hz is almost the same as for ER. That means that ER filled with small amounts of nanoparticles can be used for electrical insulation applications and the losses are much lower compared to microcomposite systems filled with 60 wt.% of conventional sized alumina or silica filler.

4.7 Effect of filler size

The complex permittivity of composites filled with 10 wt.% of surface modified BN particles was investigated. BN particles with different APS have been chosen in order to study the effect of filler size on the real and imaginary parts of the complex permittivity.

The ε' increases if the size of particles increases, while the particle concentration remains constant. The relative permittivity of epoxy-based compounds with 10 wt.% of modified micro- and submicron-BN particles is higher than of the neat ER, while ε' of ER filled with 10 wt.% of 70 nm particles is lower compared to the reference sample (see Fig. 4.16). XRD analysis showed that the structure of BN is the same in all cases (see Chapter 2.9.1.2 Fig. 2.25). Thus, the difference can be explained by the size of the particles, their aspect ratio and their surface modification.

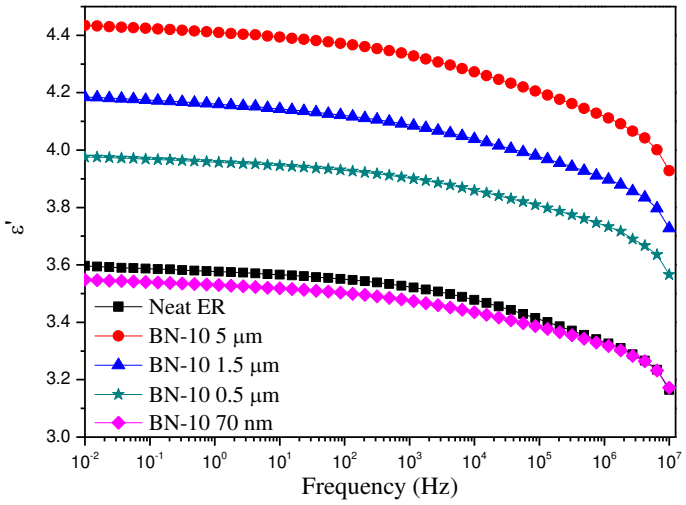

Fig. 4.16: The effect of the filler size on the ε' of composites with 10 wt.% BN particles for 20°C as a function of frequency.

The imaginary part of the complex permittivity ε'', which represents the dielectric losses, is shown in Fig. 4.17. The dielectric losses of composites filled with BN are higher compared to ER in the low frequency region (<1 kHz) and lower for frequencies higher than 1 kHz, with the exception of BN with 5 μm APS. The broad dielectric loss peak in the high frequency region (10 kHz) is attributed to a β-relaxation process of the epoxy network. It moves to a higher frequency with increasing temperature.

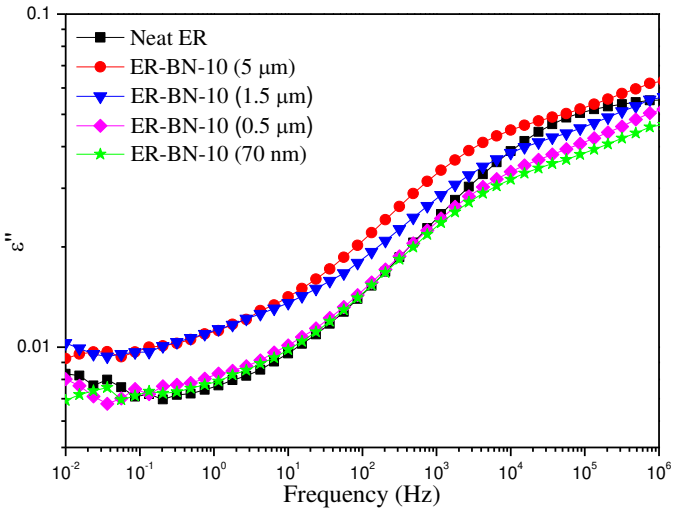

Fig. 4.17: The effect of the filler size on the ε'' of composites with 10 wt.% BN particles for 20°C as a function of frequency.

The ε' of BN filled composites was shown to be dependent on the APS. Composites with larger particles show a higher permittivity. An explanation for this behaviour could be found in the structure of the interface between the filler and polymer matrix. Every modified particle has an interfacial layer of constant thickness. For larger particles this interfacial layer is relatively thin compared to the particle dimensions, as illustrated in Fig. 4.18. Smaller particles with the same weight percentage lead to a larger interfacial volume. In our case we have a directly proportional relationship between the overall volume of the interfacial layer and the amount of polarization. The movement of the dipoles in the layer close to the particle is restricted. Since the movement of dipoles is limited, the ε' of the system is lower for smaller particles.

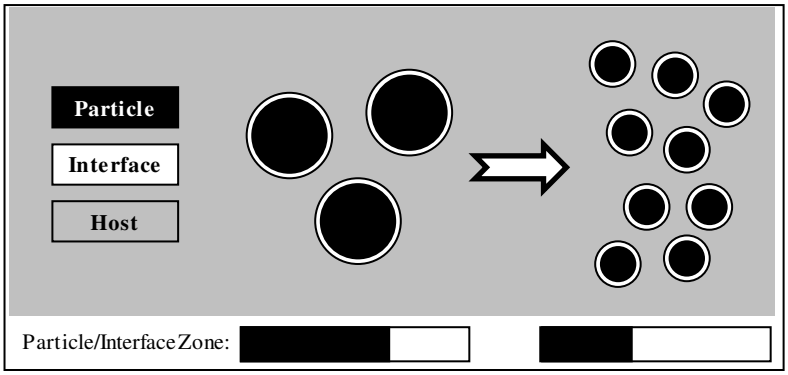

Fig. 4.18: Illustration of the change of the ratio between particle and interface volume as a function of particle size [78].

The increase of the relative permittivity might be attributed to the macroscopic polarization of the BN particles as well. This effect is possible if larger particles consist of agglomerates of nanoparticles. The individual particles in the clusters may have ionic species with a high mobility and DC conductivity on their surface, which adds to the polarization of the entire system.
The dielectric losses of the samples with 1.5 μm and 5 μm particles are high compared to the reference sample. The ε'' of the specimens filled with 70 nm and 0.5 μm particles do not differ much from neat epoxy.

4.8 Relative permittivity as a function of temperature

Fig. 4.19 shows the ε'' of ER filled with 2 wt.% of AlN as a function of temperature at different frequencies. ER-Al_2O_3-2 shows a behaviour very similar to ER-AlN-2. The β– relaxation process is similar to neat epoxy, but the β-peak is shifted to a slightly higher temperature (see Fig. 4.7). In MgO the shift is more pronounced, which reflects in the Arrhenius plot (Fig. 4.20). Composites filled with SiO_2 on the other hand saw a shift of the β-peak to lower temperatures compared to unfilled reference sample.

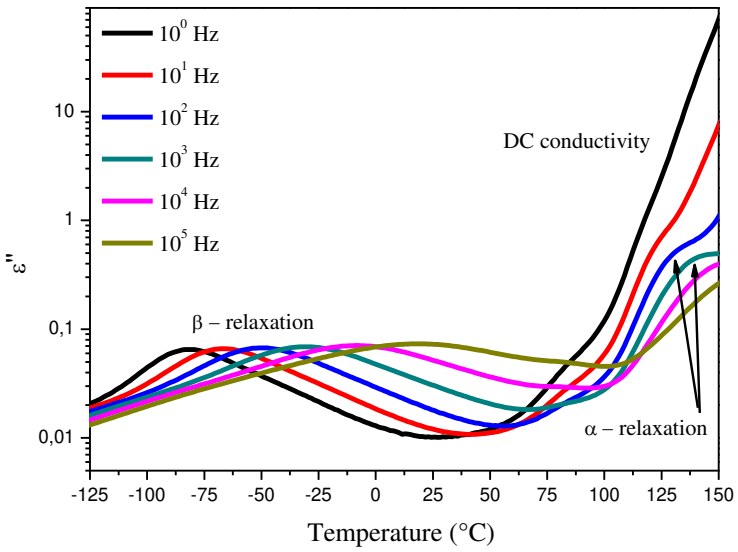

Fig. 4.19: ε'' of ER-AlN-2 samples for different frequencies as a function of temperature.

From the Arrhenius plot (Fig. 4.20) the activation energy for unfilled ER could be determined as 2.79 eV. Activation energies of the side chains of nanocomposites filled with 2 wt.% of filler are summarized in Fig. 4.20 and have only minor differences compared to the unfilled reference sample.

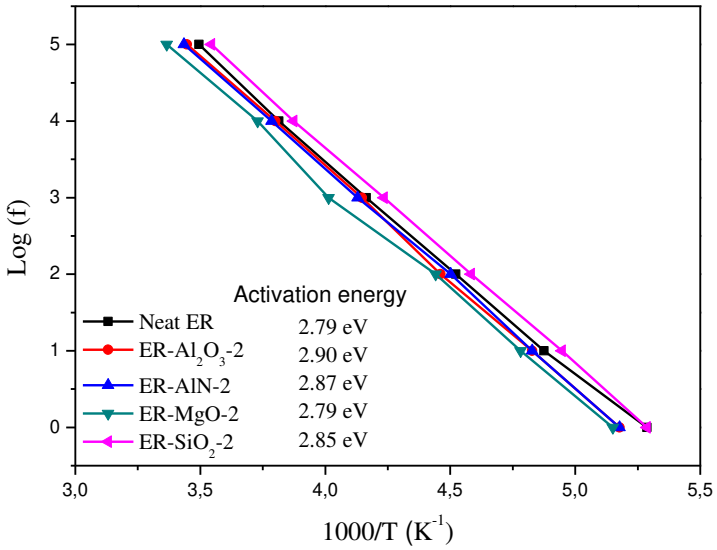

Fig. 4.20: Arrhenius plot and derived activation energies for unfilled ER compared to nanocomposites filled with 2 wt.% of different filler types.

4.9 Analysis and modelling

It is generally accepted that the surface-to-volume ratio of the nanoscale fillers and the interface-polymer layer in the vicinity of the filler plays a significant role for the decreased ε' that has been observed [36, 292].

Tanaka et al. [293] proposed the multi-core model, where he divided an interfacial layer into 3 layers (bonded, bound and loose layers). Andritsch [8] proposed the polymer chain alignment model and introduced 2 layers (aligned and affected). Rätzke & Kindersberger [59] and Todd & Shi [294] proposed a single interface polymer layer or interphase. All models have in common the assumption that the molecular structure in the interface layer is reorganized, which results in a change of the morphology and of the chain dynamics around the particles.

In our model, we assume the existence of an interface layer between the filler and matrix, which has different properties than filler or matrix. This interfacial layer is introduced to illustrate the effects of surface modified nanoparticles on the dielectric properties of nanocomposites. The interfacial layer was investigated and its size estimated in prior work of Miwa et al. [264], Chen et al. [265] and Hu et al [266]. We use their work as a basis to describe a nanodielectric system filled with different

types of surface modified nanoparticles [95]. Our explanation model has its limits however, since current measurement techniques do not offer insight in the exact nature of the interface, e.g. the value for the permittivity of the interfacial zone. As soon as the physical properties of the interfacial layer, for example the thickness or relative permittivity, can be measured the qualitative model will be more accurate.
Due to the large surface area of nanoparticles, the interface layer can occupy a significant volume of the polymer in a nanocomposite [40]. We assume that the interface layer plays a role for the properties of a composite, which is more important than the nature of the particles themselves. The total interface volume would occupy a larger space if the size of the particles becomes smaller for the same fillgrade.
The rules of mixture, which are used to predict the relative permittivity values of composites filled with conventional microsized particles, cannot be applied to the systems containing nanoparticles. T. Andritsch et al. [8, 295] tried to use the Looyenga formula [296] and semi-empiric models [119, 274] to predict the relative permittivity of nanocomposites, but did not succeed in fitting experimental data. The interface layer which is created by the aligned polymer chains has to be taken into account with an entirely different permittivity [297]. The immobilization caused by the surface treatment of the nanoparticles seems to be the main factor determining the ε' of composites with fillgrade below 5 wt.%.
In our hypothesis we assume that the interfacial polymer layer, which has different properties compared to the bulk polymer, acts as a third phase. A third phase, i.e. interfacial polymer layer, immobilizes the epoxy chains around the particles. The dipolar groups in these immobilized chains are not able to follow the external field like the polymer chains in the amorphous zones do. This leads to lower polarization of the interfacial volume and as a result to lower polarization of the whole composite. The lower polarization of a material reflects on the macroscopic properties of a material, such as the relative permittivity. The highest degree of epoxy chain immobilization and as a result, lowest relative permittivity value is observed for systems filled with 2 wt.% filler. The smaller the particles are, the larger the relative interfacial layer is and the larger the total interface volume. We notice that the smallest MgO nanoparticles (APS 22 nm) create systems with the lowest relative permittivity values. Even the system containing 10 wt.% of MgO filler has a lower ε' than neat ER whilst the addition of 5 wt.% of AlN particles (APS 60 nm) shows already a higher ε' than neat ER.
The relative permittivity of a nanocomposite system is a measure of the polarization of the polymer host, filler and interface layer. If the ε' of the layer is much lower than either of epoxy or filler, the contribution would lower the value of ε' for the entire system. The relative volume of

this layer in the composite with nano-BN is larger than in any of the composites with bigger particles. Thus, the impact of the low value of ε' in the interface layer is more pronounced in the case of the system filled with 70 nm particles, therefore the $\varepsilon'(f)$ values are lower than for ER and composites filled with larger particles.
Typically, the interface thickness is in the order of 5 to 20 nm [8, 264, 298]. If we assume the interface polymer layer equal to 5 nm, which is constant for all BN-filled systems, then the interface region volume fraction will occupy 12% of the whole volume for 10 wt.% of the BN particles having APS 70 nm. For the system with APS 1.5 μm the interface volume will be 0.5% for the same fillgrade. For 5 μm particles this value is even reduced to 0.1%. If we make the same calculations, assuming an interface layer of 20 nm, then the overall interface volume will occupy 70%, 2% and 0.6% for APS of 70 nm, 1.5 μm and 5 μm, respectively (see Fig. 4.21).
We can conclude that the size of nanoparticles and the thickness of the interfacial layer, which can be created by surface modification of nanoparticles, act as a main characteristic determining the dielectric behaviour of composites at low filler concentrations.

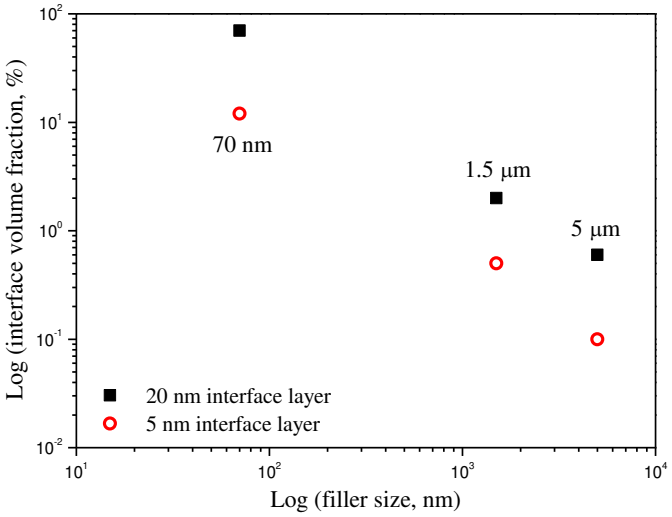

Fig. 4.21: Log-log dependence of the filler size on interfacial volume fraction, assuming different interface layer between matrix and filler.

The simplest approach to calculate the relative permittivity of a two-component system is to use linear rule of mixtures:

$$\varepsilon_c = \varphi\varepsilon_p + (1-\varphi)\varepsilon_m, \tag{4.8}$$

Birchak formula [299]:

$$\varepsilon_c^{1/2} = \varphi\varepsilon_p^{1/2} + (1-\varphi)\varepsilon_m^{1/2}, \tag{4.9}$$

Landau-Lifshitz-Looyenga formula [296]:

$$\varepsilon_c^{1/3} = \varphi\varepsilon_p^{1/3} + (1-\varphi)\varepsilon_m^{1/3} \tag{4.10}$$

or Lichtenecker-Rother formula [300]:

$$\log\varepsilon_c = \varphi\log\varepsilon_p + (1-\varphi)\log\varepsilon_m, \tag{4.11}$$

where φ is the volume fraction of particles, ε_c, ε_p and ε_m are the real parts of the complex permittivity of the composite, particles and matrix, respectively.

All formulas show that the relative permittivity of a composite ε_c should vary monotonically. But measurements show that the relative permittivity of nanocomposites has a local minimum depending on the volume fraction. This behaviour cannot be explained by a two-phase theoretical approach. A key feature of nanocomposites is the high surface area of the particles, and, consequently, the large volume fraction that can attribute to interface regions.

As a working hypothesis the existence of an interface polymer layer in the vicinity of a particle is assumed, which has different properties from those of the unaltered polymer further away from the particle surface. We further assume that homogeneously dispersed nanoparticles have the same diameter and are surrounded by interface polymer layers of a constant thickness, which are not overlapping [59].

Using aforementioned conditions, we can introduce the third term, which is responsible for the affected interfacial layer. In order to get the reduced values and the minimum in the relative permittivity, we have to assume that the relative permittivity of an affected layer is lower than that of both epoxy and particles. The location of the local minimum is strongly dependent on the thickness of an interfacial layer and its relative permittivity. In order to fit the experimental values the thickness of this layer should be more than 100 nm [297]. Alternatively,

the relative permittivity could be below 1, but that is physically incorrect. Based on our findings, we can assume that we deal with a global restructuring of the host polymer and a change of its macroscopic properties, rather than having a confined interfacial zone. This is another hypothesis to explain the dielectric behaviour of nanocomposite systems.

4.10 Impact of curing and water absorption

One of the vital factors, which contribute to the outstanding properties of nanocomposites, is the large interface area of a nanoparticle relative to its size. The drawback of the large interface area is the large amount of water that nanoparticles can take up from the environment. The nanoparticles absorb moisture during nanocomposite synthesis and afterwards when the material is used as a dielectric. Previous research about epoxy resin and epoxy resin composites has shown that the water absorbed into the materials has a large influence on the dielectric behaviour [301-303]. In order to find out the influence of moisture uptake and postcuring process on the relative permittivity and dielectric loss factor, nanocomposites were investigated containing surface modified magnesium oxide nanoparticles.

Dielectric spectroscopy measurements were performed on test specimens that were cured for 4 hours and had been stored under ambient conditions for one month (the "wet" samples). The second round of tests was performed after subjecting the same specimens to a heat treatment at 160°C for 2 days (the "dry" samples). In Figs. 4.22-4.26, the relative and imaginary parts of the complex permittivity are shown as a function of frequency. Two different temperatures (20°C and 100°C) have been chosen to check the influence of the heat treatment (or postcuring).

As it can be seen in Figs. 4.22 and 4.23, the values of ε' and ε'' became lower after the postcuring (PC) process, the effect is depicted by arrows. A possible explanation for this behaviour is the absorption of humidity in the "wet" samples. The MgO nanoparticles and the ER matrix itself absorb water from the environment. The hydrophilic nature of the inorganic nanofiller surface tends to attract moisture.

After the postcuring, the relative permittivity of the nanocomposites became lower since a large part of the water, which has a much higher value of ε' than MgO and ER, was evaporated during the postcuring process. Beside the reduction in the amount of hydroxy groups in the composite system due to the evaporation of the moisture, the further polymerization can play a significant role in the molecular dynamics [304]. If the reaction between diepoxide-bisphenol-A and the curing agent has only partly finished after 4 hours of curing, it will finalize during the postcuring period. Also the dielectric losses significantly

decrease after heat treatment (see Fig. 4.23). This is noticeable for most of the samples with higher filler loadings, since they contain more nanoparticles, which have in turn a larger overall surface area and thus are more susceptible to water uptake. High dielectric losses at low frequencies (see Fig. 4.23 and 4.25) can be attributed to the ionic conductivity, which is linked to the water uptake. Fig. 4.24 exhibits a very similar dielectric behaviour in the dielectric relaxation for all postcured specimens in the frequency region 50Hz-1MHz at 20°C. The differences of the loss factor in the low frequency region (0.01-50 Hz) can be attributed to the interfacial polarization between ER and the incorporated MgO filler. The influence of the water uptake is more pronounced at low frequencies for high temperatures, e.g. 100°C (see Figs. 4.25 and 4.26). The water molecules act as mobile ions, which in turn is reflected in high values of ε' and ε'' [305].

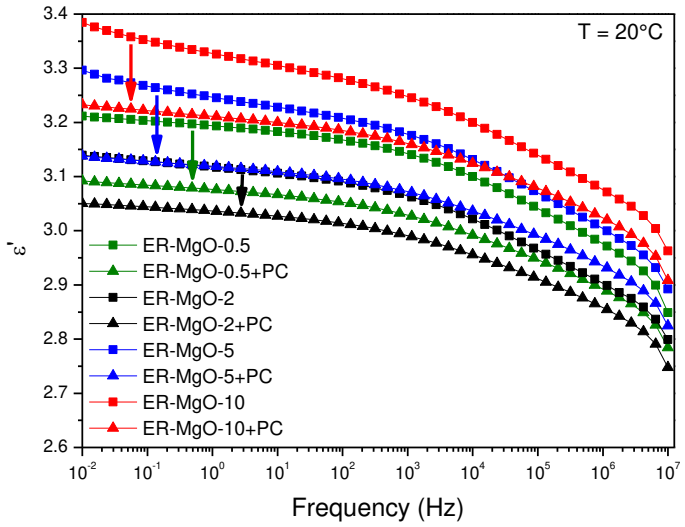

Fig. 4.22: ε' of ER-MgO samples as a function of frequency at 20°C.

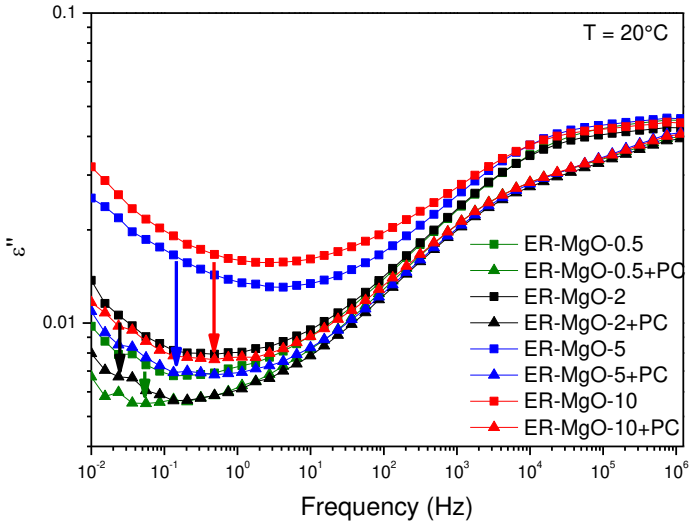

Fig. 4.23: ε'' of ER-MgO samples as a function of frequency at 20°C.

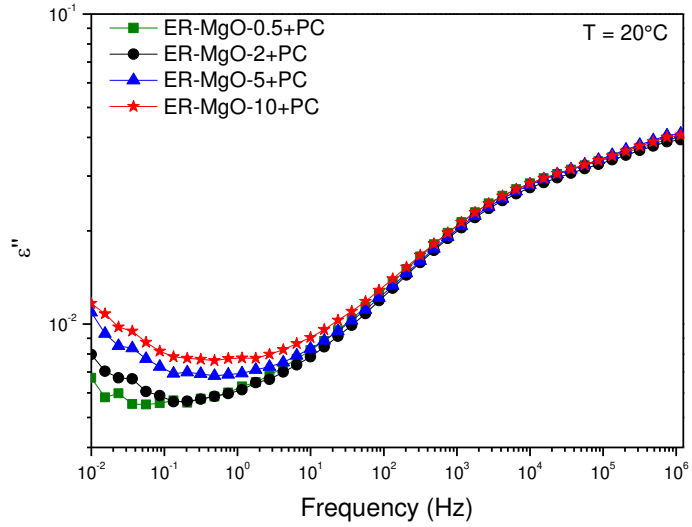

Fig. 4.24: ε'' of ER-MgO samples that that have been postcured.

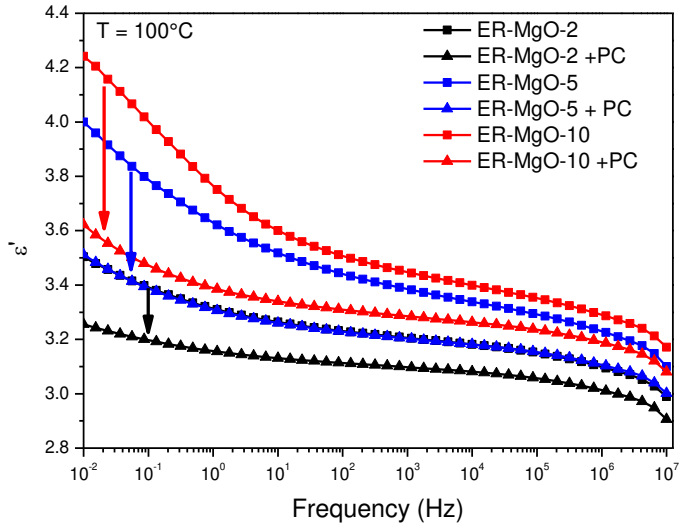

Fig. 4.25: ε' of ER-MgO samples as a function of frequency at 100°C.

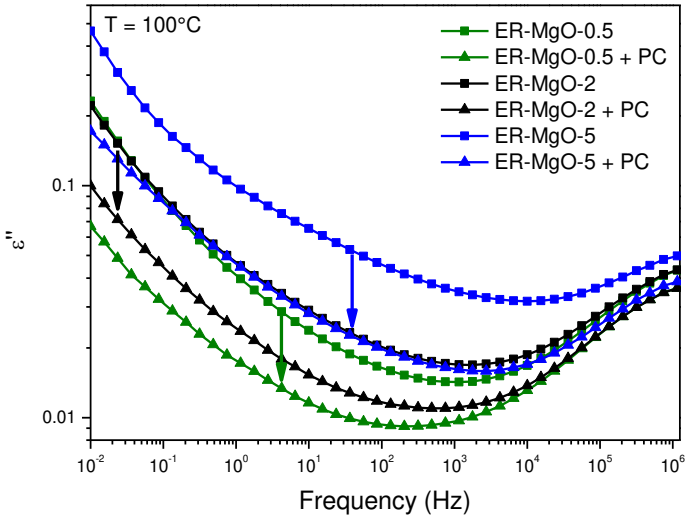

Fig. 4.26: ε'' of ER-MgO samples as a function of frequency at 100°C.

4.11 Summary

Measurements of the complex permittivity revealed that the relative permittivity of epoxy filled with 0.5, 2, 5 wt.% of alumina, 0.5, 2, 5 and 10 wt.% of magnesium oxide and 0.5 and 2 wt.% of aluminum nitride was lower than for the pure epoxy, despite the fact that the relative permittivity of Al_2O_3, MgO and AlN is higher than of the epoxy. On the other hand, epoxy-silica composites showed higher values of ε' compared to neat ER. The dielectric behaviour of nanocomposites was explained by the existence of a strong interface layer between polymer matrix and inorganic filler, and its influence on the macroscopic properties of the composite. The dielectric losses of the epoxy resin did not change significantly with the addition of nanofiller up to 5 wt.%.

The reduction of the relative permittivity compared to neat ER at low filler concentration is explained by the immobilization of epoxy chains in the proximity of nanoparticles. The immobilization is possible due to the interface polymer layer that was created by surface modification of the nanoparticles. The relative permittivity was noticed to have a minimum at 2 percent by weight, when the average distance between the modified nanoparticles is large. If the distance is large enough, their interface layers do not overlap and the lower relative permittivity can be solely attributed to the intrinsic properties of the interfacial volume around the nanoparticles.

Differences of the imaginary part ε'' between the neat ER and the nanocomposites can mainly be seen at the frequencies above 1 kHz. Below 1 Hz some nanocomposites show slightly increased losses. The ε'' at 50 Hz is almost the same as for ER. This indicates that ER filled with small amounts of nanoparticles can be used for electrical insulation applications and the losses are much lower compared to microcomposite systems filled with 60 wt.% of conventional sized alumina or silica filler. The ε'' does not change significantly for nanocomposites as a function of fillgrade. The activation energy of the $\beta-$relaxation for nanocomposites show only minor differences compared to unfilled epoxy, where the activation energy is 2.79 eV.

The relative permittivity of epoxy-based compounds with 10 wt.% of modified BN particles is in all cases higher than in neat ER, when the particles have submicron and micron-size dimensions.

The dielectric losses of epoxy-based compounds with nano- and submicron BN filler are only slightly different compared to neat ER. The losses are lower in the high frequency region because the dipolar polarization of epoxy groups is predominant. Losses are higher for composites filled with micron-sized particles. This is explained by the influence of interfacial polarization and absorbed humidity.

The dielectric spectroscopy investigations demonstrated a reduction of the relative and imaginary parts of the complex permittivity for all samples after subjecting the samples to postcuring.
The hydrophilic nanofiller and polymer matrix tend to attract moisture from the environment. Samples with a higher filler loading take up more moisture, since the particle surface area is bigger. The influence of highly mobile water molecules and its ions is visible primarily at low frequencies and higher temperatures.
The ε'' of the samples was reduced after postcuring. That is most noticeable for samples with higher filler loadings, since they contain more nanoparticles, which have a large overall surface area. The behaviour of ε'' is similar for all ER-MgO systems at frequencies higher than 50 Hz.

5

Synthesis optimization

5.1 Introduction

Nanotechnology deals with the creation, measurement, modelling, control and manipulation of matter at dimensions below 100 nm. The unique phenomena, which are inherent to the materials produced, using nanotechnology, enable novel applications. The physical and chemical properties of materials at this length scale can differ greatly from the properties of bulk matter. Nanotechnology is directed towards understanding and fabricating improved materials, devices and systems that exploit these new properties [306]. By creating nanometer-scale structures, it is possible to control the fundamental properties of materials, such as melting (or glass transition) temperature, charge capacity, complex permittivity and magnetic properties. Making use of this potential will lead to new, high-performance products and technologies that were not possible before. The properties are radically different compared to those of the traditional filled polymer materials.

The technical approach involves the incorporation of nanoparticles into a selected polymer matrix. There are two main challenges in developing polymer-based nanostructured materials after the desired nanoparticles have been selected for the polymer of interest. First, the choice of nanoparticles requires an interfacial interaction and/or compatibility with the polymer matrix. Second, the proper processing technique should be selected to uniformly disperse and distribute the nanoparticles or nanoscale clusters within the polymer matrix [11].

5.2 Incorporation of nanoparticles

The incorporation of nanoparticles in a polymer matrix can be realized in different ways. For solid thermosetting prepolymers or thermoplastic polymers with solid nanoparticles, the following processing methods are recommended:

- ✓ Solution blending [307, 308],
- ✓ Melt intercalation [309-311],
- ✓ Roll milling [312, 313].

For liquid thermosetting prepolymers or thermoplastic polymers with solid particles, the following processing methods are recommended:

- ✓ In-situ polymerization [314-316],
- ✓ Electrospinning [317],
- ✓ Emulsion polymerization [318, 319],
- ✓ High-shear mixing [116, 320, 321].

The surface of nanoparticles can be modified with coatings, surfactants and coupling agents to improve the nanoparticle dispersion in all these methods.
Nanocomposite materials hold the potential to redefine the field of traditional composite materials in terms of performance and possible applications. Developing the processing-manufacturing technologies in terms of quantity and value for commercialization will be one of the main challenges [322].

5.3 Synthesis optimization

The production procedure can be introduced to the market, if it provides samples with a good dispersion of nanoparticles and reproducible properties of a composite.
In our nanocomposite synthesis we combine solution intercalation and high shear mixing together with surface modification of the nanoparticles. The surface modified nanoparticles, which were modified in ethanol, were dispersed inside ER. The suspension of surface modified

nanoparticles, solvent and epoxy was subjected to high shear mixing to disperse the nanoparticles inside the polymer matrix. Subsequently, the ethanol was evaporated at 115°C. The boiling point of ethanol is 78°C but it can only be slowly evaporated at that temperature because it is trapped on a molecular level. Alternative might be solvents that have a lower boiling point like acetone or methanol. The boiling point of acetone and methanol is 56°C and 65°C, respectively. Preliminary results show that acetone is not a good candidate since the dispersion of nanoparticles is not stable and nanoparticles settle in this solvent. Methanol is a good solvent for the particles we use but it is more toxic than ethanol [323]. Water has a few advantages compared to ethanol such as being more environment friendly, better dispersion in a shorter time span (see section 2.5.1) and lower price. The main disadvantage is the higher boiling point. Therefore, water cannot be used as a solvent to make the synthesis of nanocomposites faster.

Degassing is another crucial problem while processing a nanocomposite. The air trapped in the sample because of insufficient degassing may initiate cracks and mechanical failure of a specimen under low strains [324].

5.4 Separation of the particle modification from the fabrication procedure

The separation of the particle modification from the rest of the production process will reduce the synthesis time. The nanoparticles can be modified in a suitable solvent, e.g. ethanol, water or methanol. The surface modified nanoparticles can be filtered out from the solvent. The problem in this case is choosing the proper filter. If the grain size of the filter is too big, the particles can seep through the filter. If the grains are too small, the particles might clog the filter.
In a next step, the solvent can then be evaporated. Surface modified particles are hydrophobic and stick together in the absence of a solvent. Afterwards they can be separated mechanically and introduced to the polymer as a dry filler (see Fig. 5.1).
Large amounts of nanoparticles can be functionalized, dried and stored for a long period of time. The dispersion of dried, surface modified nanoparticles inside an ER can be realized by high shear force mixing.

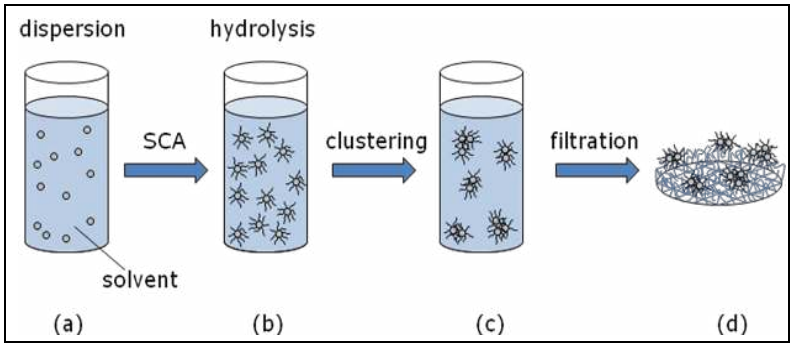

Fig. 5.1: Surface modification of nanoparticles for long term storage. (a) Dispersion of nanoparticles in a solvent; (b) surface modification with SCA; (c) agglomeration of modified hydrophobic particles; (d) filtration.

5.5 Sol-gel method for production of nanocomposites

Another method for the faster creation of nanocomposites can be realized through the fabrication of a master batch with a high concentration of nanoparticles. This method is well suited for thermosetting polymers. A high concentration of surface modified nanoparticles can be introduced to a polymer and stored for indefinite time. A nanocomposite with the required concentration of nanoparticles can be obtained by melting a part of the masterbatch and diluting it with a neat polymer. This approach is used e.g. by the company called Nanoresins®. They fabricate an ER with a high concentration of silicon dioxide nanoparticles. The required concentration of nanoparticles can be obtained by addition of neat epoxy and hardener.

Among the various processes available for synthesizing nanomaterials, sol-gel synthesis appears to be one of the most versatile and cost-effective for producing nanomaterials. Nanostructures can be synthesized in various shapes and forms, such as monoliths, films, fibers, and monodispersed nanocrystalline oxide powders [133, 134].

The sol-gel preparation involves mixing of different precursor chemicals in either liquid or solid form. The precursors generate a solution containing a stable dispersion of colloidal particles, known as sol.

Epoxy-silica nanocomposites have been successfully produced using this method [133]. This method has one major disadvantage. Some by-products of nanoparticle precipitation remain in the final composite. The by-products can influence the macroscopic properties of a composite, for example the relative permittivity or space charge accumulation of the system. We attribute the increase of the relative permittivity discussed in Chapter 4 to this effect [295].

5.6 Nano-microcomposites

Many polymer nanocomposites can be created in ways similar to conventional polymer microcomposites, making them particularly attractive from a manufacturing point of view. But, the replacement of high loaded microcomposites by low concentration nanocomposites probably won't happen in one step. First of all there is the cost involved: more epoxy is needed to replace the conventional sized silica, and nanosilica is more expensive than microscale SiO_2. The switch will be realized gradually.

Research interest within high voltage and power engineering is now focused on nano-micro-composites (NMC) [76, 155, 157, 325]. NMC could be the transition from micro- to nanocomposite materials in electrical engineering equipment. In most of the cases microcomposites cannot be completely replaced by nanocomposites because of the reasons explained above. However, nanocomposites could find a niche market because of the unique properties they have. A good example is the relative permittivity, which can be lower than the relative permittivity of a host polymer material at low fillgrade.

The implementation of nanocomposites depends on the balance between the price and difficulties, which must be solved to produce a device at the one hand side, and the advantages that could be achieved by using nanoparticles instead of conventional sized microparticles.

Because of the challenges, which must be solved to produce nanocomposites, the academia and industry have to work together to investigate new materials and implement nanocomposites to the market. Nanocomposites are already used for fire retardant materials by the company Nanocor® [326]. The company Nanoresins® offers nanocomposite products with improved scratch and abrasion resistance and better electrical properties [327]. The Japanese company J-Power Systems is planning to implement 500 kV DC cables using XLPE doped with MgO nanoparticles [328]. Nanocomposites exhibit superiority in terms of partial discharge (PD) resistance compared to neat polymers and microcomposites [61, 68, 156]. This effect is inherent to nanocomposites since composites of smaller particle size are more resistant to PD than that of larger size [66].

Nanocomposite materials can be further explored and used for special applications. Insulation materials play an important role in electrical apparatuses and cables. One of the first applications for nano-microcomposites could be in HV cable terminations or in cast resin transformers, where improved thermal conductivity is required for better heat transfer from the conductors to the environment [80, 329]. Another possible application of NMC is epoxy-based insulation material for switchgear [330, 331]. NMC is preferable in this case because large thermal expansion coefficients of PNC will cause exfoliation component - insulation material interfaces due to thermal cycling [332]. Therefore,

epoxy-based NMC, which have a little weight percentage of nanofiller and approximately 60 wt.% of microfillers, have been developed in recent years [277].

5.7 Alignment of nanoparticles

The alignment of nanoparticles in the composite matrix can be critical in order to maximize anisotropic properties such as the mechanical properties and the thermal conductivity [333]. The alignment of nanoparticles in one direction can be realized by the application of an electric or magnetic field and depends on the nature of the filler [334]. The field-nanostructuring can be used to enhance the mechanical strength, BD strength, thermal conductivity or to control the relative permittivity along one axis [335, 336].
The anisotropic behaviour of nanocomposites could be realized for a system, where the values for the relative permittivity of matrix and filler differ from each other by at least one order of magnitude. The relative permittivity of epoxy resin that we used in our study does not differ much from the relative permittivity of the filler, therefore the formation of nanoparticle paths is hard to realize (see appendix A). The alignment can be easily formed by $BaTiO_3$ or $PbTiO_3$ nanoparticles, which have relative permittivities higher than 100 [337, 338]. The structuring of the particles inside a polymer may provide an opportunity to create composites with variable relative permittivity depending on the filler loading and paths formation [335].

5.8 Nanofluids

Much attention has been paid to a new type of liquid composite material, which is called nanofluid. The enhanced properties are mainly associated with improved heat transfer and a higher breakdown voltage compared to conventional transformer oil [339-343].

5.9 Summary

All mentioned methods of nanocomposite production have been tried out at a laboratory scale. It is needed to scale up the process to fabricate large quantities of nanomaterials. There is still lack of real time industrial characterization methods, tools and infrastructure like facilities, equipment and skilled personnel. To move nanotechnology forward, education is needed for both scientists and engineers in academia and industry [322].

6

Health and environmental aspects

6.1 Possible harmful effects of nanoparticles

The introduction of novel materials into industry applications requires safety evaluations as well as an understanding of the impact of the nanomaterials on the environment, human health and other biological species [322, 344, 345]. Humans continually come into contact with small and tiny particles, for example pollen or dust, and they are generally not seriously hurt by being exposed to these particles. A pure wax candle can release 250.000 nanoparticles per cubic centimeter in one evening. Smoke released by one cigar may contain more than 70.000 nanosized particles [346, 347]. The processes that apply to ultrafine particles in principle are applicable for nanoparticles as well. Airborne particles can be divided by size into three groups [348]:

- ✓ Small particles (APS < 80 nm) are in the agglomeration mode, they are short-lived and tend to rapidly agglomerate and form large particles;
- ✓ Large particles (APS > 2000 nm) are in coarse mode and subject to gravitational settling;
- ✓ Intermediate particles (80 nm < APS < 2000 nm) are in accumulation mode and can remain suspended in air for a longer time up to several weeks. They can be removed from the air via dry or wet deposition [349-351].

As it can be seen from the classification, the biggest danger (concerning the life-time of nanoparticles) comes from intermediate particles rather than particles with APS < 100 nm. Since these particles can stay in the air for weeks, the basis for bioaccumulation in the food chain is given. Major targets where these particles usually accumulate are lungs, bones and the brain. This is considered a serious occupational health hazard in chronic inhalation exposures [352].
Besides inhalation, nanoparticles may enter the body via skin contact or by ingestion. The nanoparticles penetrate the human body during inhalation, either through nasal cavity or the alveolar-capillary barrier in the lungs [353-355]. Once nanoparticles enter a body via the digestion system with food, they can penetrate into the blood stream and accumulate in the liver and spleen [343, 356]. The risk of skin penetration is rather small since skin is much thicker compared to alveolar membrane [357, 358]. Carbon and graphite nanoparticles may cause skin diseases and respiratory infections, which have been reported in literature [359, 360]. Studies investigating the toxicology of carbon nanotubes showed that, once they reach the lungs, they are more toxic than carbon black or quartz [361-363]. The high aspect ratio of CNT makes them more dangerous, since this leads to sharp ends due to the needle-like shape [364]. Strict industrial precautions measures should be taken to protect the health of humans [365].
The unique health hazards are attributed to nanoparticles since their size is comparable to human cells. The result of that is that the human immune system may not work against them [366, 367].
The surface chemistry and the surface area of nanoparticles play a significant role in the increased toxicity of nanoparticles [368]. Thus, the size of the particles, shape, charge and their treatment are important considerations [322]. The toxicity of TiO_2 on the other hand has not been found to be dependent on particle size or surface area [369, 370]. TiO_2 nanoparticles were shown to be solely deposited on the outermost surface of the skin and were not detected in deeper layers of the human epidermis and dermis skin layers [359]. However, chemically modified titania nanoparticles from over-the-counter sunscreen products

have been shown to induce the formation of hydroxyl radicals and oxidative DNA damage. Additionally, sunlight-illuminated TiO_2 was shown to cause catalyzed DNA damage in human cells [322, 359, 371].

6.2 Requirements and precautions on working conditions

The nanoparticles that we use in our study are only harmful for the human body if they accumulate in the internal organs, for example lungs. The nanoparticles are not dangerous as soon as they are mixed into a polymer host, because of the strong bonding between filler and matrix. Safety measures are necessary to prevent the release of nanoparticles into air [372]. Fume hoods and respiratory masks are needed to be used at the factories which produce nanocomposites, in order to protect lungs against airborne nanoparticles. A small under-pressure in the working area is recommended to prevent escape of nanoparticles to other working areas. Ventilation systems have to be equipped with nanocertified filters to prevent outflow of nanoparticles to the environment [343, 373]. Toxicological aspects have to be taken into account, when the lifetime of a composite is over and it has to be recycled or disposed. One has to be aware of the possibility of nanosized particles being released into the atmosphere as a result of combustion and then being inhaled by humans [374].

The determination of toxicity of nanoparticles is a quite expensive, complicated and time consuming research [375, 376]. The cost of a toxicological study is high but insignificant compared with the fines and penalties paid by the companies in asbestos victims trials. More work is needed on all new nanomaterials to assess their toxicity and health hazards [377].

Another issue is the correct interpretation of the data obtained using these complex bio/nanomaterial systems. A worthy goal for toxicologists and material scientists is the joint development of 'green' nanomaterial formulations – those optimized for function and minimal health impact. The European Commission considers safety issues and precautionary principles for nanotechnology application on daily basis [378].

7

Conclusions and recommendations

7.1 Conclusions

One of the biggest challenges of this project was to synthesize dielectric nanocomposites with various filler types. In order to make an organic polymer and inorganic filler compatible with each other, it is essential to create a chemical bonding between the constituents. To obtain a good dispersion of the nanoparticles, treatment with a coupling agent is a vital factor. Surface modified aluminum oxide, aluminum nitride, boron nitride and magnesium oxide nanoparticles were introduced into an epoxy resin using ultrasonic bath and high shear mixer for further improvement of the particle dispersion.

The heat conduction mechanism of nanocomposite materials is completely different from that in a matrix that has been reinforced by a conventional sized microfiller. In case of microcomposites, the heat is conducted mainly via the highly conductive filler. It has been shown that nanoparticles reorganize the polymer structure in such a way, that epoxy chains are aligned perpendicular to the particle surface. The alignment is possible because of surface functionalization by a coupling agent. It was postulated that the interface polymer volume, which is affected by the alignment of polymer chains, conducts the heat much better than an amorphous polymer that is not affected by nanoparticles. We proposed a three-phase Lewis-Nielsen model and used this model to describe the behaviour of epoxy filled with surface modified nanoparticles. The model fits the experimental data very well and takes the interface thermal resistance into account.

Besides the thermal properties, the dielectric characteristics are affected by the interfacial layer as well. The interfacial polymer layer immobilizes the epoxy chains around the particles. The dipolar groups in these immobilized chains are not able to follow the external field, which leads to a lower polarization of the interfacial volume and as a result to lower polarization of the whole composite. The lower polarization of a material reflects on the macroscopic properties of a material, such as the relative permittivity. The highest degree of epoxy chain immobilization and as a result, lowest relative permittivity value is observed for the systems filled with 2 wt.% of the nanoparticles. The smaller the particles are, the larger the relative interfacial layer is and the larger the total interface volume. We notice that the smallest nanoparticles (MgO with an APS of 22 nm) create the system with the lowest relative permittivity values. Even the system containing 10 wt.% of MgO has a lower ε' than neat ER. Conversely, the addition of 5 wt.% of the largest particles (AlN with an APS of 60 nm) results in a higher ε' than for the neat ER. If the volume fraction increases, the amount of material with a high relative permittivity is increasing, and leads to a higher relative permittivity of the overall nanocomposite.
The relative permittivity of epoxy-based compounds with 10 wt.% of modified BN particles is in all cases higher than neat ER, when the particles have submicron and micron-size dimensions. However, the ε' of the composite with nano-BN is lower than that of the reference polymer. This is attributed to the influence of interfacial volume, which is a function of the particle size.
We can conclude that the size of nanoparticles and the thickness of the interfacial layer that is created by surface modification of nanoparticles, act as a main characteristic determining the dielectric behaviour of composites at low filler concentrations.

The dielectric spectroscopy investigations demonstrated a reduction of the real and imaginary parts of the complex permittivity for all samples after subjecting the samples to postcuring. The postcuring leads to the evaporation of water and finalizes the process of epoxy curing.

An overview was given how to improve the ex-situ polymerization process as well as different methods of nanocomposite production. It was described how nano- micro-composites can be used beneficially for industrial application in the near future.

7.2 Recommendations

For the future work we would recommend to verify some of the concepts that have been brought up in the course of this project:

- Thermal treatment of nanofillers in vacuum before surface functionalization may free up the hydroxyl groups on the surface of the nanoparticles to make them available for hydrogen bonding with the SCA and further with the polymer matrix. The effect of temperature treatment can be considered as an additional step in order to improve the contact between the polymer matrix and introduced filler.

- In the three-phase Lewis-Nielsen thermal conductivity model, the thermal conductivity of the filler and the interfacial layer were estimated as well as the thickness of the layer. Direct measurements of the interfacial layer and the thermal conductivity of individual particles will be helpful to understand the nature of the thermal conductivity of nanocomposites and make the fitting model more accurate.

- One of the possible ways to improve the thermal conductivity of polymer materials is the creation of micro-nano-composite systems. It is common practice to add up to 60 wt.% of low-price inorganic filler such as silica, quartz or alumina to the epoxy insulation used for HV equipment. This improves the thermal conductivity up to 0.75-0.9 W/m·K, compared to 0.15-0.25 W/m·K of neat epoxy [195, 379]. The thermal conductivity can be further improved by surface modification of microparticles with silane coupling agent. The other solution is to use high aspect ratio microparticles. The most effective way to improve the thermal conductivity could be the production of a material system, which combines several methods.

- First of all, the amount of microfiller should be optimized.
- Secondly, the particles have to have a high aspect ratio.
- Thirdly, the surface should be modified in order to minimize the thermal resistance between epoxy and filler.
- In addition, the surface modified nanoparticles with high aspect ratio can be added to create thermally conductive channels between microparticles.

❖ Previous measurements [8, 78, 79] on epoxy-based nanocomposites saw a drastic increase of the short-term DC breakdown voltage. The short and long term AC BD tests are of vital importance for practical applications and need to be considered for the future research.

❖ Using a finite-element program, like COMSOL, or Molecular Dynamics simulation software, to model an optimal system with maximal achievable thermal conductivity. Furthermore, to check the influence of different parameters such as the thermal conductivity of particles, their shape, aspect ratio and thickness of the aligned polymer layer.

Appendix A

Formation of nanoparticle paths

A.1 Theory

Anisotropic material properties can be induced in ceramic/polymer composites by applying an alternating electric field of moderate strength during processing. Under suitable conditions, particles of an inorganic filler material with high thermal conductivity that are randomly dispersed in a liquid pre-polymer can be polarized and organize the paths consisting of particles in the electric field (see Fig. A.1).

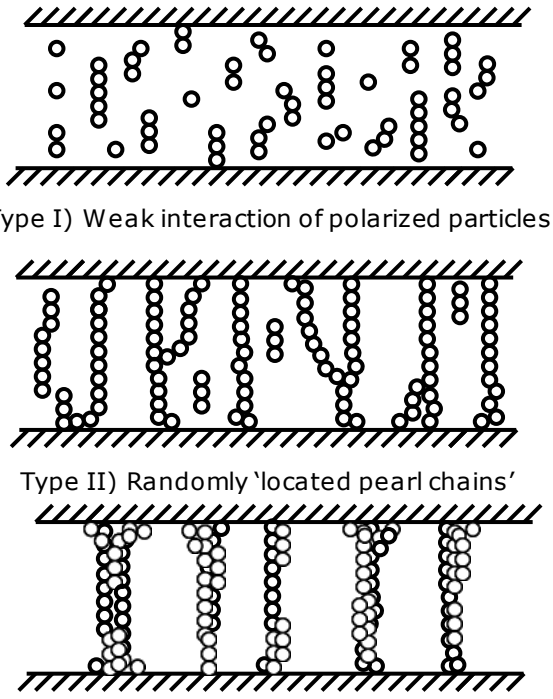

Fig. A.1: Types of electrically induced structure observed to form in low volume-fraction suspensions of lead titanate in a curing epoxy resin [380].

When a single particle suspended in a fluid medium is exposed to an electric field, two phenomena can possibly occur:

1. electrophoresis;
2. dielectrophoresis.

Electrophoresis is defined as the translational motion of charged matter within any electric field (uniform or nonuniform). Dielectrophoresis is defined as translational motion of neutral matter caused by the induction of polarization in a nonuniform electric field. The major differences between the electrophoresis and dielectrophoresis effects are given as:

1. The dielectrophoretic effect is not dependent on the polarity of the applied electric field, while the electrophoretic effect is dependent on both the field direction and the polarity of the particle charge.

2. The dielectrophoretic force depends on the dielectric permittivities of both – particles and surrounding fluid and on the difference between them. Higher field strengths are required for fluids of low dielectric permittivity. Electrophoresis operates under relatively low fields.
3. The dielectrophoretic effect is proportional to the particle volume and is more pronounced as the particle size increases. In contrast, the electrophoretic effect is relatively independent of particle size.
4. Dielectrophoresis requires very divergent nonuniform electric fields for pronounced effects while electrophoresis is observed in both uniform and nonuniform electric fields [381, 382].

A.2 Dielectrophoresis

The interaction potential between particles in the suspension can be expressed as:

$$V(r) = 2\pi\varepsilon_0\varepsilon_m a\zeta^2 \ln\left[1+\exp\left(-\kappa r\right)\right] - \frac{Aa}{12r}, \tag{A.1}$$

where $V(r)$ is total interaction potential, ε_0 is permittivity of vacuum, ε_m is relative permittivity of the medium, a is average particle radius, ζ is zeta potential, κ is Debye reciprocal length, r is interparticle radius, and A is Hamakar constant [383].

The first term in Eq. A.1 represents a repulsive potential due to the Stern and Gouy-Chapman charge layers surrounding a particle in suspension. The second term is an attractive potential based on van der Waals forces of attraction.

If the electric field is applied to the suspension, a third term must be introduced. This term is the solution to the Laplace equation and is included in the interaction potential equation to yield:

$$V^*(r) = 2\pi\varepsilon_0\varepsilon_m a\zeta^2 \ln\left[1+\exp\left(-\kappa r\right)\right] - \frac{Aa}{12r} + \frac{\upsilon\left(1-3\cos^2\theta\right)}{r^3}, \tag{A.2}$$

where $\upsilon = \dfrac{\left(\beta a^3 \varepsilon_f E_{loc}\right)^2}{\varepsilon_f}$ and $\beta = \dfrac{\varepsilon_f - \varepsilon_m}{\varepsilon_f + 2\varepsilon_m}$,

where θ is orientation angle of particles, β is effective polarizability, ε_f is relative permittivity of the filler, and $E_{loc} \approx E_{applied}$ [384, 385].

The orientation angle dependence of Eq. A.2 shows why the particles form the well recognized chains exclusively along the electric field. The orientation angle θ is defined as the angle between a vector parallel to the applied field and a vector connecting the centers of two particles in suspension (see Fig. A.2). The contribution to the attractive interaction potential is maximal when $\theta = 0°$. At a critical angle of approximately 55°, the dipole-dipole potential switches from an attractive to a repulsive potential. Hence, particles existing at an orientation greater than 55° will experience a repulsive potential. The result is the formation of distinct chains parallel to the applied field direction.

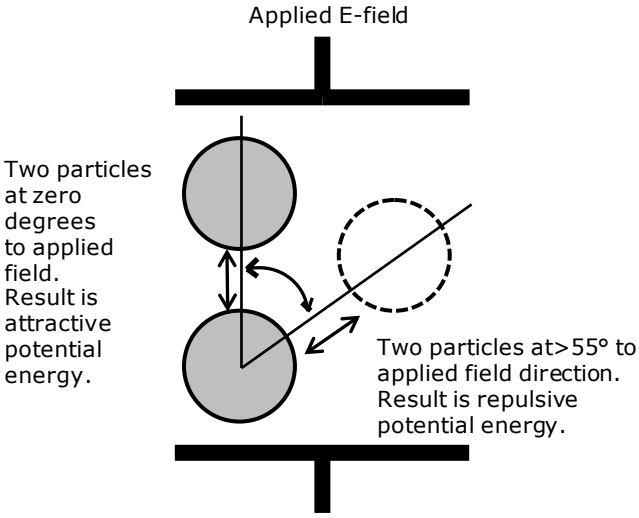

Fig. A.2: Schematic of the orientational relationship of the interaction potential under an applied electric field [381].

There are several requirements necessary for the matrix materials in the dielectrophoretic composite:

- ✓ The matrix must be an insulating material of low dielectric constant that can easily transform from a liquid-like to a solid state. The liquid-like state is necessary for easy orientation of the particles. The matrix must be insulating in order to allow the generation of a polarization field and the relative permittivity is desired to be low so the effective polarizability, β is maximized for a given particular filler material.
- ✓ The polymer matrix should have a high breakdown strength in the uncured state.

- ✓ The viscosity of the uncured polymer matrix must be low enough to allow dielectrophoretic migration of particles into the chained structure but high enough to prohibit settling of the particles due to gravitational forces. If particles of the filler component have a higher density than that of the surrounding fluid, they tend to settle down under the influence of gravity. The rate of sedimentation depends on particle size and shape and also on the viscosity of the surrounding fluid. However, the forces acting on different sized particles are not of the same magnitude.
- ✓ A further difficulty concerns the viscosity of the surrounding fluid, which is not constant over the course of the processing cycle. For example, thermosetting polymers such as epoxy resins exhibit a progressive increase in viscosity with time as polymerization proceeds. At the same time, the polymerization reaction itself is exothermic and heat is generated. The fluid experiences a rise in temperature and consequently its viscosity decreases.
- ✓ The matrix should cure rapidly and easily to allow for a rapid production rate and lower production costs.

Theoretically, any material with a dielectric constant higher that that of the matrix ($\beta > 1$) can be aligned and chained through the dielectrophoretic effect [381].

A.3 Electrorheological effect

The electrorheological effect was first discovered by Winslow in 1949 [386]. Winslow discovered that in certain suspensions a change in viscosity can be observed on application of an electric field to these suspensions. The application of AC or DC electric field leads to a redistribution of the dispersed particles into chains of aggregates.
The origins of the electrorheological effect are still unclear. It is generally accepted that the electric field induces a space charge separation on the suspended particles to form a dipole. The induced dipoles on one suspended particle then interact with each other in accordance to electrostatic dipolar-dipolar attraction. The dipolar interactions drive the particles to form the chains.
Using the electrorheological effect of chain formation, it is possible to align particles between electrodes. It is possible to manipulate a uniformly dispersed uncured mixture to one that has nonuniform mixing of volume fraction and connectivity [387].
The electrorheological effect and dielectrophoresis/ electrophoresis take place at the same time, since they appear at similar conditions. It is hard to distinguish which effect plays the dominant role, therefore the formation of paths of nanoparticles can be equally attributed to both of these effects.

The dipole interaction leads to the formation of chains, which are parallel to the applied electric field. Dielectrophoretic assembly can be induced by applying a high alternating field across a particle suspension in uncured thermoset polymers.
The results described in literature [388] obtained on aligned samples are far from the values predicted by the parallel mixing rule. The reason for this discrepancy is that the particles within each chain are not actually touching, but are separated by a thin polymer layer between them. These thin polymer interfaces disrupt the continuity of the filler phase and result in substantial disagreement with the parallel mixing rule.
In a dielectrophoretic process, a dispersion of filler particles in a liquid pre-polymer is exposed to an AC electric field. Under suitable conditions, the filler particles become polarized and exhibit a mutually attractive force, which causes them to form chain-like structures between the electrodes. The liquid can then be solidified by means of a chemical reaction or a change in temperature and the newly formed structures fixed in place to form a composite material with anisotropic properties.
The frequency of the applied electric field is dictated by the dielectric properties of the fluid and the filler. In a polyurethane matrix optimum alignment can be established with frequencies ~ 10 Hz, whereas in an epoxy the higher conductivities require frequencies ~ 700 Hz to produce alignment [389].

A.4 Experiment

For the experiment on the alignment of nanoparticles a special mold was designed and produced. Basis was the mold that has been used for casting samples for the thermal conductivity measurement. Custom made PTFE bushings were introduced to separate the HV and ground electrodes.
The experimental setup consisted of the following parts (see Fig. A.3):

- Function generator, to generate the initial sine wave
- AC amplifier, for increasing the power of the sine wave
- Oscilloscope, to measure amplitude and frequency of the input and output voltages and output current
- Aforementioned mold, where the epoxy with functionalized particles was cast
- Oven, for curing of the sample during voltage application

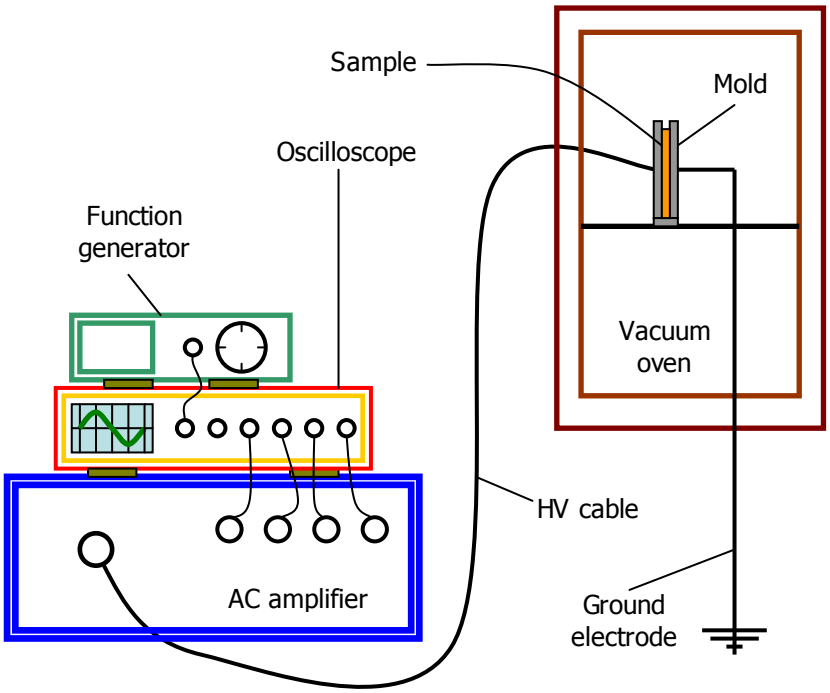

Fig. A.3: Schematic representation of the experimental setup for chain formation of nanoparticles.

The frequency of the sine wave was 1 kHz and the voltage amplification was 1000 times with an input voltage of 1V. Hence we expected the output voltage to be 1 kV. But, the output voltage was initially only 50V. This voltage level was stable for approximately 15 minutes. Since the mold with the liquid composite was inside the oven at 140°C, the polymerization process of the epoxy started at some point. The epoxy resin undergoes a change in conductivity as a result of the curing process, consequently the output voltage started growing. Within 8 minutes the output voltage reached 1 kV, which was the set-point from the beginning, and remained constant afterwards.
Unfortunately, the thermal conductivity value of the produced sample was approximately the same as in the sample that was created without voltage application (normal production procedure).
We did not check the morphological structure with TEM, but it seems that the attempt of particle alignment failed. The reason is probably the high electrical conductivity of the epoxy resin in it's liquid state. Ceramic particles can be aligned if their dielectric constant is considerably higher than that of the matrix, i.e. $\beta = \frac{\varepsilon_f - \varepsilon_m}{\varepsilon_f + 2\varepsilon_m} > 1$. If we assume that the

relative permittivity of the epoxy resin $\varepsilon_m = 3.3$ and the relative permittivity of the filler (AlN or Al_2O_3) $\varepsilon_f \approx 9$ [194, 390], the effective polarizability will be $\beta \approx 0.36$. Since the effective polarizability is less than 1, this is not enough to organize nanoparticle paths inside the polymer host.

Fig. A.4 and Table A.1 illustrate the input and output voltages and output current, in cyan, purple and orange lines, respectively, at different stages of the experiment. Figs. A.4.a to A.4.e have been captured in time intervals of 1 minute. Here the transformation of the output voltage from rectangular to sinus can be witnessed. After 8 minutes of voltage application, the voltage remains constant (Fig. A.4.f), while the current is slowly dropping down.

Table A.1. Changing parameters as a function of time during the experiment of alignment of nanoparticles.

Time, min	Output Voltage, V	Output current, mA
0	47.2	19.82
1	62.7	19.8
2	90.7	19.78
3	143	19.72
4	255	19.58
5	475	18.96
6	852	17.32
7	1.040	8.58
8	1.050	4.4
10	1.050	3.9
15	1.050	3.68
75	1.050	3.4

a)

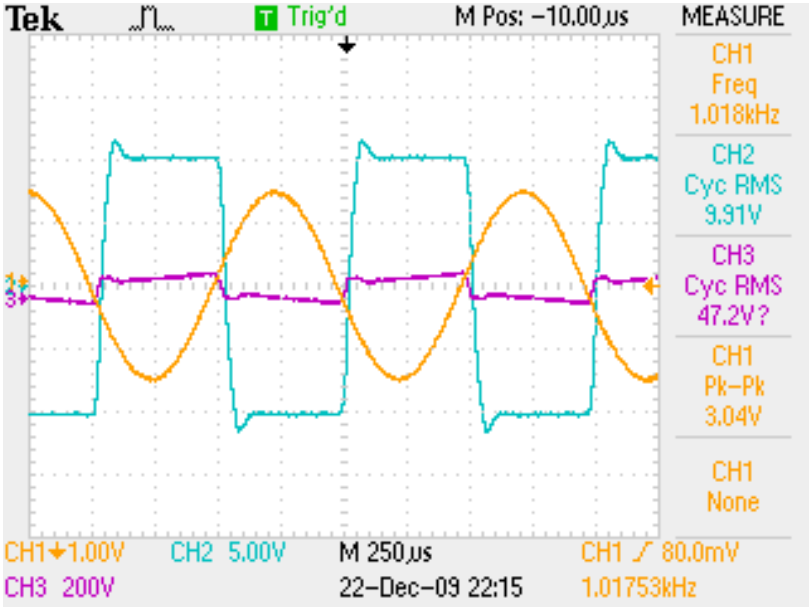
Tek
Trig'd
M Pos: -10.00µs
MEASURE
CH1
Freq
1.018kHz
CH2
Cyc RMS
9.91V
CH3
Cyc RMS
47.2V?
CH1
Pk-Pk
3.04V
CH1
None
CH1 1.00V
CH2 5.00V
M 250µs
CH1 80.0mV
CH3 200V
22-Dec-09 22:15
1.01753kHz

b)

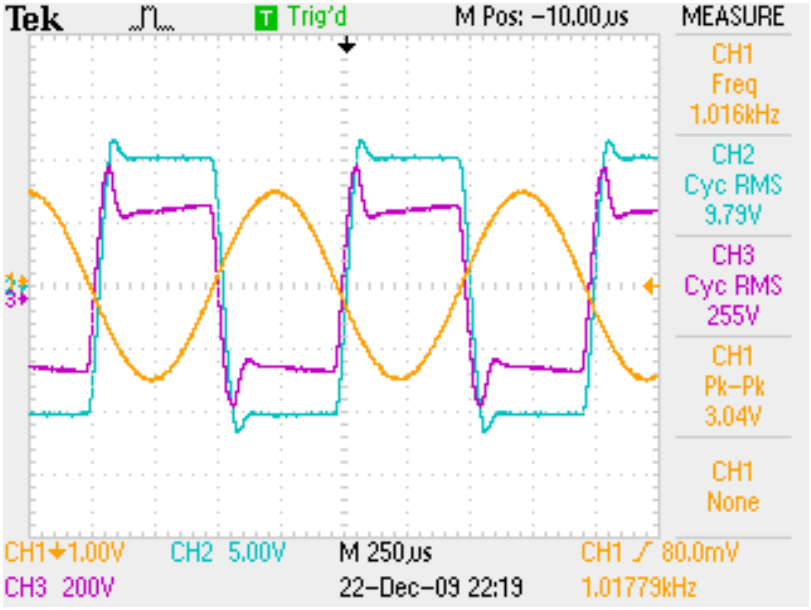
Tek
Trig'd
M Pos: -10.00µs
MEASURE
CH1
Freq
1.016kHz
CH2
Cyc RMS
9.79V
CH3
Cyc RMS
255V
CH1
Pk-Pk
3.04V
CH1
None
CH1 1.00V
CH2 5.00V
M 250µs
CH1 80.0mV
CH3 200V
22-Dec-09 22:19
1.01779kHz

c)

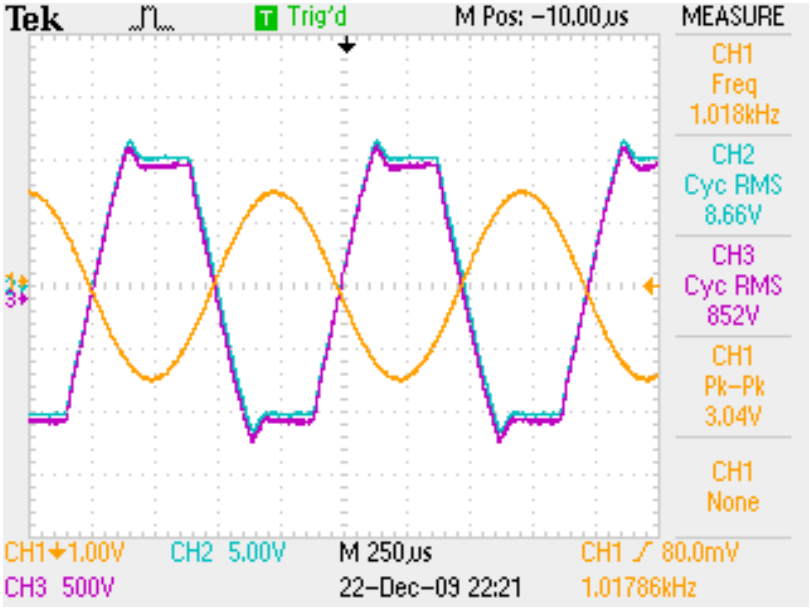
Tek
Trig'd
M Pos: -10.00µs
MEASURE
CH1
Freq
1.018kHz
CH2
Cyc RMS
8.66V
CH3
Cyc RMS
852V
CH1
Pk-Pk
3.04V
CH1
None
CH1 1.00V
CH2 5.00V
M 250µs
CH1 80.0mV
CH3 500V
22-Dec-09 22:21
1.01786kHz

d)

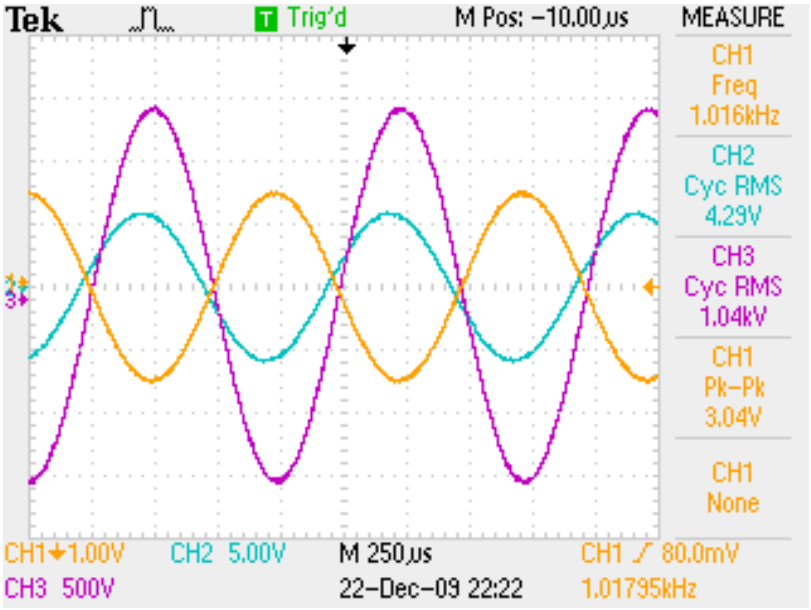
Tek
Trig'd
M Pos: -10.00µs
MEASURE
CH1
Freq
1.016kHz
CH2
Cyc RMS
4.29V
CH3
Cyc RMS
1.04kV
CH1
Pk-Pk
3.04V
CH1
None
CH1 1.00V
CH2 5.00V
M 250µs
CH1 80.0mV
CH3 500V
22-Dec-09 22:22
1.01795kHz

e)

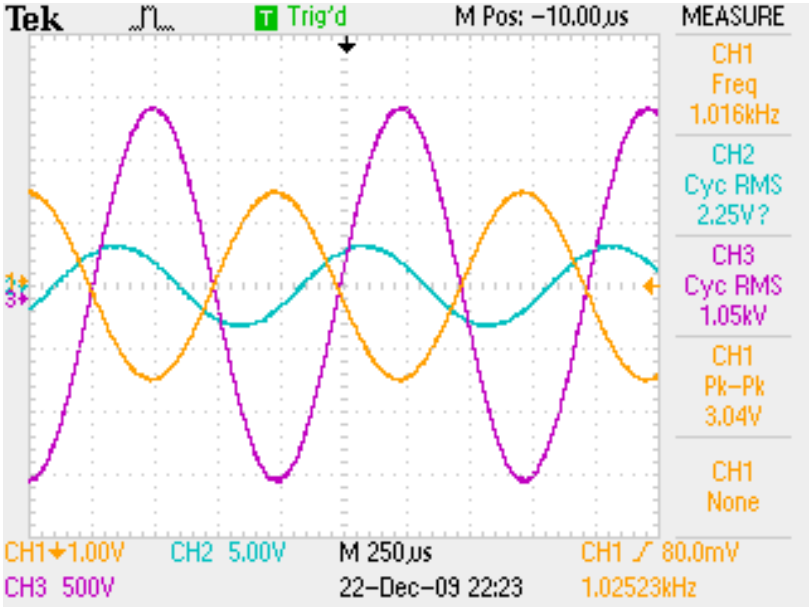

f)

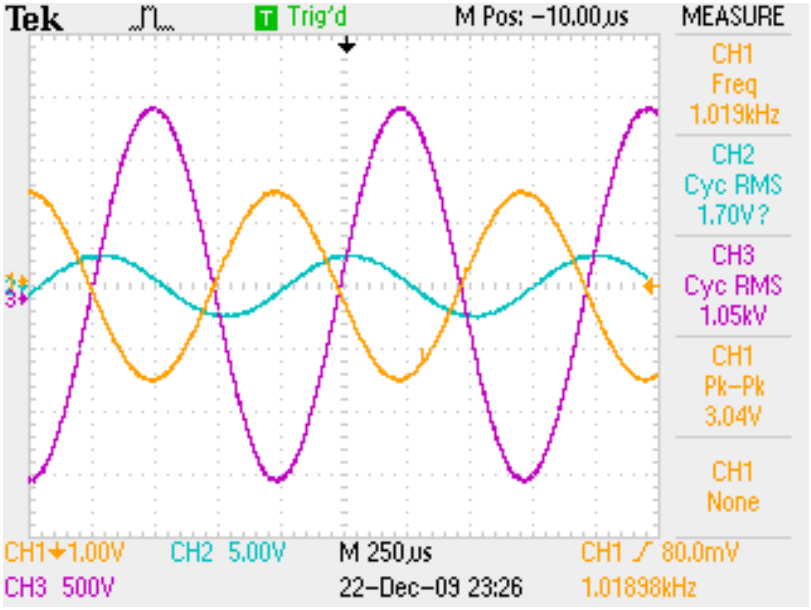

Fig. A.4: Input voltage, output current and output voltage at different moments of time.

List of abbreviations

Abbreviation	Description
AC	Alternating current
AlN	Aluminum nitride
Al_2O_3	Aluminum oxide
$Al(OH)_3$	Aluminum hydroxide
AlO(OH)	Aluminum oxide hydroxide
AlP	Aluminum phosphide
APS	Average particle size
BAs	Beryllium arsenide
$BaSO_4$	Barium sulfate
$BaTiO_3$	Barium titanate
BD	Dielectric breakdown
BeO	Beryllium oxide
BeS	Beryllium sulfide
BN	Boron nitride
BP	Boron phosphide
C_2H_6OH	Ethanol
CA	Coupling agent
$CaCO_3$	Calcium carbonate
CaO	Calcium oxide
$CaSO_4$	Calcium sulfate
CP	Composite particle
CNT	Carbon nanotube
DGEBA	Diglycidyl ether of bisphenol-A
DC	Direct current
DMA	Dynamic mechanical analysis
DS	Dielectric spectroscopy
EDS	Energy dispersive spectroscopy
ER	Epoxy resin
FESEM	Field emission scanning electron microscopy
FTIR	Fourier transformed infrared spectroscopy
HDPE	High density polyethylene
HV	High voltage
GaN	Gallium nitride
GaP	Gallium phosphide
GLYMO	γ-glycidoxypropyl-trimethoxysilane
GPS	γ-glycidoxypropyl-trimethoxysilane
IR	Infrared
LDPE	Low density polyethylene
LN	Lewis-Nielsen model

Abbreviation	Description
MC	Microcomposite
MesC	Mesocomposite
MgO	Magnesium oxide
$Mg(OH)_2$	Magnesium hydroxide
MTPHA	Methyltetrahydrophthalic acid anhydride
MWCNT	Multiwalled carbon nanotubes
$Na_4P_2O_7$	Sodium-diphosphate
NC	Nanocomposite
NMC	Nano-micro-composite
NMR	Nuclear magnetic resonance
OM	Optical microscope
OMLS	Organically modified layered silicates
PA	Polyamide
PC	Polycarbonate
PE	Polyethylene
PI	Polyimide
PMC	Polymer microcomposite
PMesC	Polymer mesocomposite
PMMA	Polymethyl methacrylate
PNC	Polymer nanocomposite
PP	Polypropylene
PVC	Polyvinyl chloride
prm	Revolutions per minute
SC	Silicon carbide
SCA	Silane coupling agent
SF_6	Sulfur hexafluoride gas
SEM	Scanning electron microscope
Si_3N_4	Silicon nitride
SiO_2	Silicon dioxide
$SrTiO_3$	Strontium titanate
US	Ultrasonic
SWCNT	Single-walled carbon nanotubes
TEM	Transmission electron microscope
TGA	Thermogravimetric analysis
THASYS	Thin heater apparatus system
TiO_2	Titanium dioxide
UV	Ultraviolet
XRD	X-ray diffraction
ZnO	Zinc oxide

List of symbols

Symbol	Unit	Description
A	J	Hamakar constant
C	$J \cdot kg^{-1} \cdot K^{-1}$	Specific heat per unit volume
C_p	$J \cdot m^{-3} \cdot K^{-1}$	Heat capacity
d	nm	Particle size
D	$m^2 s^{-1}$	Thermal diffusivity
H_{eff}	mm	Effective sample thickness
M	$g \cdot mol^{-1}$	Molar mass
N_A	mol^{-1}	Avogadro's number
q	J	Heat flow
R_K	$m^2 \cdot K \cdot W^{-1}$	Kapitza's resistance
T_g	K	Glass transition temperature
r	nm	Average radius of nanoparticles
W		Weight fraction of the filler additives
ε_0	$C^2 \cdot s^2 \cdot kg^{-1} \cdot m^{-3}$	Permittivity of vacuum
ε^*		Complex permittivity
ε'		Real part of the complex permittivity
ε''		Imaginary part of the complex permittivity
ε_c		Real part of the complex permittivity of the composite
ε_m		Real part of the complex permittivity of the polymer matrix
ε_p		Real part of the complex permittivity of the particles
ε_r		Relative permittivity

Symbol	Unit	Description
Θ_D	K	Debye temperature
v_f	nm^3	Volume of a particle
v_l	nm^3	Volume of an interface layer
φ	$W \cdot m^2$	Heat flux
ξ		Shape factor
λ	$W \cdot m^{-1} \cdot K^{-1}$	Thermal conductivity
λ_c	$W \cdot m^{-1} \cdot K^{-1}$	Thermal conductivity of a composite
λ_f	$W \cdot m^{-1} \cdot K^{-1}$	Thermal conductivity of a filler
λ_m	$W \cdot m^{-1} \cdot K^{-1}$	Thermal conductivity of a polymer matrix
ρ	$kg \cdot m^{-3}$	Density of a material
ρ_f	$kg \cdot m^{-3}$	Density of a filler material
ρ_m	$kg \cdot m^{-3}$	Density of a polymer matrix
ρ_{GPS}	$kg \cdot m^{-3}$	Density of GPS
υ	$m \cdot s^{-1}$	Average sound velocity
σ	$S \cdot m^{-1}$	Electrical conductivity
ϕ		Volume fraction of a filler
ϕ_M		Maximum packing fraction of the dispersed particles
ψ		Sphericity
ζ	mV	Zeta potential
ϖ		Grüneisen's constant

List of figures

List of tables

References

[1] R.P. Feynman, "There's plenty of room at the bottom", *American Physical Society Meeting, Pasadena, CA, USA*, December 1959.
[2] M.S.P. Shaffer, J.K.W. Sandler, "Carbon nanotube/nanofibers polymer nanocomposites", *Processing and properties of nanocomposites,* Edited by S.G. Advani, Chapter 1, 1-59*,* World scientific, 2007.
[3] "Nanotechnology. Big things from a tiny world", www.nano.gov.
[4] H. Tait, *Five thousand years of glass*, British Museum Press, 1991.
[5] C. Green, A.S. Vaughan, "Nanodielectrics - how much do we really understand?", *IEEE Electrical Insulation Magazine, Vol. 24, Nº4*, 6-16, 2008.
[6] A.S. Vaughan, "Raman nanotechnology – the Lycurgus cup", *IEEE Electrical Insulation Magazine, Vol. 24, Nº6*, 4, 2008.
[7] M. Reibold, P. Paufler, A.A. Levin, W. Kochmann, N. Pätzke, D.C. Meyer, "Discovery of nanotubes in ancient Damascus steel", *Springer Proceedings in Physics; Physics and Engineering of New Materials, Vol. 127*, 305-310, 2009.
[8] T. Andritsch, *Epoxy based nanocomposites for high voltage DC applications. Synthesis, dielectric properties and space charge dynamics*, PhD thesis, Delft University of Technology, 2010.
[9] R.K. Gupta, E.B. Kennel, K-J. Kim, "Overview of challenges and opportunities", *Polymer nanocomposites. Handbook*, Edited by R.K. Gupta, E.B. Kennel, K-J. Kim, CRC Press, Taylor & Francis Group, Chapter 1, 1-6, 2010.
[10] I. Capek, *Nanocomposite structures and dispersions. Science and nanotechnology – fundamental principles and colloidal particles*, Elsevier, 2006.
[11] J.H. Koo, *Polymer nanocomposites. Processing, characterization, and applications*, McGraw-Hill, 2006.
[12] R. Roy, S. Komarneni, "Nanophase and nanocomposite materials", *Materials Research Society*, 241, 1984.
[13] J.E. Mark, J. Wen, "Inorganic-organic composites containing mixed-oxide phases", *Macromolecular Symposia, Vol. 93, Nº1*, 89-96, 1995.
[14] Y-W. Mai, Z-Z. Yu, *Polymer nanocomposites*, Woodhead publishing Ltd., 2006.
[15] L.W. Carter, J.G. Hendricks, D.S. Bolley, *U.S. Patent 2.531.396, November 28, 1950*, submitted March 29, 1947.
[16] A. Okada, Y. Fukushima, M. Kawasumi, S. Inagaki, A. Usuki, S. Sugiyama, T. Kurauchi, O. Kamigaito, "Composite materials and process for manufacturing same", *U.S. Patent 4.739.007*, April 19, 1988.
[17] A. Okada, A. Usuki, "The chemistry of polymer-clay hybrids", *Materials Science and Engineering: C, Vol. 3, Nº2*, 109-115, 1995.
[18] A. Okada, A. Usuki, "Twenty years of polymer-clay nanocomposites", *Macromolecular Materials and Engineering, Vol. 291, Nº12*, 1449-1476, 2006.
[19] S. Iijima, "Helical microtubes of graphic carbon", *Nature, Vol. 354, Nº6348*, 56-58, 1991.
[20] M. Bockrath, D.H. Cobden, P.L. McEuen, N.G. Chopra, A. Zettl, A. Thess, R.E. Smalley, "Single-electron transport in ropes of carbon nanotubes", *Science, Vol. 275, Nº5308*, 1922-1925, 1997.
[21] S.J. Tans, M.H. Devoret, H. Dai, A. Thess, R.E. Smalley, L.J. Geerligs, C. Dekker, "Individual single-wall carbon nanotubes as quantum wires", *Nature, Vol. 386, Nº6624*, 474-477, 1997.
[22] T.E. Twardowski, *Introduction to nanocomposite materials. Properties, processing, characterization*, DEStech publications, Inc., 2007.
[23] M.J. Schulz, A.D. Kelkar, M.J. Sundaresan, *Nanoengineering of structural, functional, and smart materials*, CRC press, Taylor & Francis group, 2006.

[24] C. Eger, M. Heuer, "Surface scratching. New ideas for scratch and abrasion resistant coatings", *Nanomaterials*, 36-39, Wiley-VCH Verlag GmbH & Co. KGaA, Weinheim, Germany, 2008.
[25] Y. Ju-Nam, J.R. Lead, "Manufactured nanoparticles: an overview of their chemistry, interactions and potential environmental implications", *Science of the Total Environment, Vol. 400, Nº1-3*, 396-414, 2008.
[26] M. Köhler, W. Fritzsche, *Nanotechnology: an introduction to nanostructuring techniques*, Wiley-VCH, 2nd edition, 2007.
[27] C.N.R. Rao, *Nanomaterials chemistry, recent developments and new directions*, Wiley-VCH, 2007.
[28] A.B. Morgan, C.A. Wilkie, *Flame retardant polymer nanocomposites*, Wiley-Interscience, 2007.
[29] P. Pissis, "Molecular dynamics of thermoset nanocomposites", *Thermoset nanocomposites for engineering applications*, edited by R. Kotsilkova, Chapter 5, 143-206, Smithers Rapta Technology, 2007.
[30] M. Wouters, "Improving thermal-electrical behaviour of insulating materials by diamond-epoxy nanocomposites to clarify physical and chemical interactions between nanoparticles with polymeric matrices", *TNO report*, 2009.
[31] J.K. Nelson, *Dielectric polymer nanocomposites*, Springer, 2010.
[32] S. Rätzke, J. Kindersberger, "Erosion behaviour of nano filled silicone elastomers", *XIVth International Symposium on High Voltage Engineering, Beijing, China*, 2005.
[33] K-J. Kim, J.L. White, "Nanoparticle dispersion and reinforcement by surface modification with additives for rubber compounds", *Polymer nanocomposites. Handbook*, Edited by R.K. Gupta, E.B. Kennel, K-J. Kim, CRC Press, Taylor & Francis Group, Chapter 4, 45-76, 2010.
[34] S. Singha, M.J. Thomas, "Polymer composite/nanocomposite processing and its effect on the electrical properties", *IEEE Conference on Electrical Insulation and Dielectric Phenomena, Kansas City, MO, USA*, 557-560, 2006.
[35] M. Kurimoto, H. Watanabe, K. Kato, M. Hanai, Y. Hoshina, M. Takei, H. Okubo, "Dielectric properties of epoxy/alumina nanocomposite influenced by particle dispersibility", *IEEE Conference on Electrical Insulation Dielectric Phenomena*, *Québec City, Canada*, 706-709, 2008.
[36] M. Roy, J.K. Nelson, R.K. MacCrone, L.S. Schadler, C.W. Reed, R. Keefe, W. Zenger, "Polymer nanocomposite dielectrics – the role of the interface", *IEEE Transactions on Dielectrics and Electrical Insulation, Vol. 12, Nº4,* 629-643, 2005.
[37] R.C. Smith, C. Liang, M. Landry, J.K. Nelson, L.S. Schadler, "The mechanisms leading to the useful electrical properties of polymer nanodielectrics", *IEEE Transactions on Dielectrics and Electrical Insulation, Vol. 15, Nº1,* 187-196, 2008.
[38] R. Krishnamoorti, R.A. Vaia, *Polymer nanocomposites: synthesis, characterization, and modelling*, Washington: American Chemical Society, 2002.
[39] C. Sun, *Controlling the rheology of polymers/silica nanocomposites*, PhD thesis, Eindhoven University of Technology, 2010.
[40] R. Kotsilkova, *Thermoset nanocomposites for engineering applications*, Smithers Rapta Technology, 2007.
[41] T.J. Lewis, "Nanometric dielectrics", *IEEE Transactions on Dielectrics and Electrical Insulation, Vol. 1, Nº5*, 812-825, 1994.
[42] M.F. Fréchette, M.L. Trudeau, H.D. Alamdari, S. Boily, "Introductory remarks on nanodielectrics", *IEEE Transactions on Dielectrics and Electrical Insulation, Vol. 11, Nº5*, 808-818, 2004.
[43] L.A. Dissado, J.C. Fothergill, "Dielectrics and nanotechnology", *IEEE Transactions on Dielectrics and Electrical Insulation, Vol. 11, Nº5*, 737-738, 2004.
[44] M.F. Fréchette, A. Vijn, L. Utracki, M.L. Trudeau, A. Sami, C. Laurent, P.H.F. Morshuis, T. Andritsch, R. Kochetov, A.S. Vaughan, E. David, J. Castellon, D. Fabiani, S. Gubanski, J. Kindersberger, C. Reed, A. Krivda, J.C. Fothergill, S. Dodd, F. Guastavino, H. Alamdari, "Nanodielectrics – a universal panacea for solving all electrical insulation problems?", *10th IEEE International Conference on Solid Dielectrics, Potsdam, Germany*, 2010.

[45] J.K. Nelson, J.C. Fothergill, L.A. Dissado, W. Peasgood, "Towards an understanding of nanometric dielectrics", *IEEE Conference on Electrical Insulation and Dielectric Phenomena, Cancun, Quintana Roo, Mexico*, *295*-298, 2002.
[46] T. Tanaka, G.C. Montanari, R. Mülhaupt, "Polymer nanocomposites as dielectrics and electrical insulation – perspectives for processing technologies, material characterization and future applications", *IEEE Transactions on Dielectrics and Electrical Insulation, Vol. 11, Nº5*, 763-784, 2004.
[47] M. Kozako, N. Fuse, K. Shibata, N. Hirai, Y. Ohki, T. Okamoto, T. Tanaka, "Surface charge of polyamide nanocomposites caused by partial discharges", *IEEE Conference on Electrical Insulation and Dielectric Phenomena*, Albuquerque, NM, USA, 75-78, 2003.
[48] J.I. Hong, L.S. Schadler, R.W. Siegel, E. Mårtensson, "Rescaled electrical properties of ZnO/low density polyethylene nanocomposites", *Applied Physics Letters, Vol. 82, Nº12*, 1956-1958, 2003.
[49] G.C. Montanari, D. Fabiani, F. Palmieri, D. Kaempfer, R. Thomann, R. Mülhaupt, "Modification of electrical properties and performance of EVA and PP insulation through nanostructure by organophilic silicates", *IEEE Transactions on Dielectrics and Electrical Insulation, Vol. 11, Nº5,* 754-762, 2004.
[50] J. Jordan, K.I. Jacob, R. Tannenbaum, M.A. Sharaf, I. Jasiuk, "Experimental trends in polymer nanocomposites – a review", *Materials Science and Engineering A, Vol. 393, Nº1-2,* 1-11, 2005.
[51] S.S. Bamji, M. Abou-Dakka, A.T. Bulinski, L. Utracki, K. Cole, "Dielectric properties of propylene containing nano-particles", *IEEE Conference on Electrical Insulation and Dielectric Phenomena, Nashville, TN, USA*, 166-170, 2005.
[52] S.C. Tjong, G.D. Liang, "Electrical properties of low-density polyethylene / ZnO nanocomposites", *Materials Chemistry and Physics, Vol. 100, Nº1*, 1-5, 2006.
[53] A.S. Vaughan, S.G. Swingler, Y. Zhang, "Polyethylene nanodielectrics: the influence of nanoclays on structure formation and dielectric breakdown", *IEEJ Transactions on Fundamentals and Materials, Vol. 126, Nº11*, 1057-1063, 2006.
[54] D. Kumlutas, I.H. Tavman, "A numerical and experimental study on thermal conductivity of particle filled polymer composites", *Journal of Thermoplastic Composite Materials, Vol. 19*, *Nº4*, 441-455, 2006.
[55] M. Moniruzzaman, K.I. Winey, "Review: polymer nanocomposites containing carbon nanotubes", *Macromolecules, Vol. 39*, *Nº16*, 5194-5205, 2006.
[56] S.S. Bamji, A. Bulinski, M. Abou-Dakka, D. McIntyre, "Space charge in polypropylene containing synthetic nanoparticles", *IEEE Conference on Electrical Insulation and Dielectric Phenomena, Virginia Beach, VA, USA*, 662-665, 2009.
[57] M. Takala, H. Ranta, J. Pelto, S. Virtanen, V. Koivu, M. Pettersson, K. Kannus, "Dielectric properties of polypropylene – silica nanocomposites", *Nordic Insulation Symposium, Gothenburg, Sweden*, 31-35, 2009.
[58] E. Tuncer, I. Sauers, D.R. James, A.R. Ellis, M. Pace, K.I. More, S. Sathyamurthy, J. Woodward, A.J. Rondinone, "Nanodielectrics for cryogenic applications", *IEEE Transactions on Applied Superconductivity, Vol. 19, Nº3,* 2354-2358, 2009.
[59] S. Rätzke, J. Kindersberger, "The role of the interphase on the resistance to high-voltage arcing and to tracking and erosion of silicon/SiO_2 nanocomposites", *IEEE Transactions on Dielectrics and Electrical Insulation, Vol. 17, Nº2*, 607-614, 2010.
[60] P. Irwin, W. Zhang, Y. Cao, X. Fang, D.Q. Tan, "Mechanical and thermal properties", *Dielectric polymer nanocomposites*, edited by J.K. Nelson, Chapter 6, 163-196, Springer, 2010.
[61] M. Kozako, S. Yamano, R. Kido, Y. Ohki, M. Kohtoh, S. Okabe, T. Tanaka, "Preparation and preliminary characteristic evaluation of epoxy / alumina nanocomposites", *International Symposium on Electrical Insulating Materials, Kitakyushu, Japan,* 231-234*,* 2005.
[62] P.O. Henk, T.W. Korsten, T. Kvarts, "Increasing the electrical discharge endurance of acid anhydride cured DGEBA epoxy resin by dispersion of nanoparticle silica", *High Performance Polymers, Vol. 11, Nº3*, 281-296, 1999.

[63] P.O. Henk, T.W. Korsten, T. Kvarts, A. Saeidi, "Increasing the PD-endurance of epoxy and XLPE insulation by nanoparticles silica dispersion in the polymer", *Nordic Insulation Symposium, Stockholm, Sweden,* 2001.
[64] T. Imai, F. Sawa, T. Ozaki, T. Shimuzu, R. Kido, M. Kozako, T. Tanaka, "Evaluation of insulation properties of epoxy resin with nano-scale silica particles", *International Symposium on Electrical Insulating Materials, Kitakyushu, Japan*, 239-242, 2005.
[65] T. Imai, F. Sawa, T. Ozaki, T. Shimizu, R. Kido, M. Kozako, T. Tanaka, "Influence of temperature on mechanical and insulation properties of epoxy-layered silicate nanocomposite", *IEEE Transactions on Dielectrics and Electrical Insulation, Vol. 13, Nº1*, 445-452, 2006.
[66] M. Kozako, S. Kuge, T. Imai, T. Ozaki, T. Shimizu, T. Tanaka, "Surface erosion due to partial discharges on several kinds of epoxy nanocomposites", *IEEE Conference on Electrical Insulation and Dielectric Phenomena,* Nashville, TN, USA, 162-165, 2005.
[67] T. Tanaka, T. Yazagawa, Y. Ohki, M. Ochi, M. Harada, T. Imai, "Frequency accelerated partial discharge resistance of epoxy/ clay nanocomposite prepared by newly developed organic modification and solubilization methods", *IEEE International Conference on Solid Dielectrics, Winchester, UK,* 337-340, 2007.
[68] T. Tanaka, Y. Matsuo, K. Uchida, "Partial discharge endurance of epoxy/SiC nanocomposite", *IEEE Conference on Electrical Insulation and Dielectric Phenomena*, Québec City, QC, Canada, 13-16, 2008.
[69] D. Fabiani, A. Cavallini, G.C. Montanari, L. Testa, "Extraction of aging markers for nanostructured epoxy resin under surface discharges", *29th IEEE Electrical Insulation Conference, Montréal, Québec, Canada*, 2009.
[70] Y. Chen, T. Imai, Y. Ohki, T. Tanaka, "Tree initiation phenomena in nanostructured epoxy composites", *IEEE Transactions on Dielectrics and Electrical Insulation, Vol. 17, Nº5,* 1509-1515, 2010.
[71] S. Li, G. Yin, G. Chen, J. Li, S. Bai, L. Zhong, Y. Zhang, Q. Lei, "Short-term breakdown and long-term failure in nanodielectrics: a review", *IEEE Transactions on Dielectrics and Electrical Insulation, Vol. 17, Nº5,* 1523-1535, 2010.
[72] R. Sarathi, R.K. Sahu, P. Rajeshkumar, "Understanding the thermal, mechanical and electrical properties of epoxy nanocomposites", *Materials Science and Engineering A, Vol. 445-446*, 567-578, 2007.
[73] F. Guastavino, G. Coletti, A. Dardano, A. Fina, A.S. Thelakkadan, "Thermo-mechanical and electrical characterization of epoxy/nanoclay composites", *IEEE Conference on Electrical Insulation and Dielectric Phenomena, Virginia Beach, VA, USA*, 549-552, 2010.
[74] S. Singha, M.J. Thomas, "Dielectric properties of epoxy nanocomposites", *IEEE Transactions on Dielectrics and Electrical Insulation, Vol. 15, Nº1*, 12-23, 2008.
[75] Q. Wang, P. Curtis, G. Chen, "Effect of nano-fillers on electrical breakdown behavior of epoxy resin", *IEEE Conference on Electrical Insulation and Dielectric Phenomena*, *West Lafayette, IN, USA*, 393-396, 2010.
[76] T. Imai, F. Sawa, T. Nakano, T. Ozaki, T. Shimizu, M. Kozako, T. Tanaka, "Effects of nano- and micro-filler mixture on electrical insulation properties of epoxy based composites", *IEEE Transactions on Dielectrics and Electrical Insulation, Vol. 13, Nº1*, 319-326, 2006.
[77] T. Andritsch, R. Kochetov, Y.T. Gebrekiros, U. Lafont, P.H.F. Morshuis, J.J. Smit, "Synthesis and dielectric properties of epoxy based nanocomposites", *IEEE Conference on Electrical Insulation and Dielectric Phenomena, Virginia Beach, VA, USA*, 523-526, 2009.
[78] T. Andritsch, R. Kochetov, Y.T. Gebrekiros, P.H.F. Morshuis, J.J. Smit, "Short term DC breakdown strength in epoxy based BN nano- and microcomposites", *IEEE International Conference on Solid Dielectrics, Potsdam, Germany*, 179-182, 2010.
[79] T. Andritsch, R. Kochetov, P.H.F. Morshuis, J.J. Smit, "Short term DC breakdown and complex permittivity of Al_2O_3- and MgO-epoxy nanocomposites", *IEEE Conference on Electrical Insulation and Dielectric Phenomena, West Lafayette, IN, USA*, 530-533, 2010.
[80] Y. Murata, Y. Murakami, M. Nemoto, Y. Sekiguchi, Y. Inoue, M. Kanaoka, N. Hozumi, M. Nagano, "Effects of nano-sized MgO-filler on electrical phenomena under DC voltage

application in LDPE", *IEEE Conference on Electrical Insulation and Dielectric Phenomena, Nashville, TN, USA*, 158-161, 2005.
[81] R. Kurnianto, Y. Murakami, N. Hozumi, M. Nagao, Y. Murata, "Some fundamentals on Treeing breakdown in inorganic-filler/LDPE nano-composite material", *IEEE Conference on Electrical Insulation and Dielectric Phenomena, Kansas City, MO, USA,* 373-376, 2006.
[82] T. Tanaka, D. Ueno, T. Iizuka, Y. Ohki, Y. Sekiguchi, Y. Murata, "Tree initiation and growth in LDPE/MgO nanocomposites and roles of nano fillers", *IEEE Conference on Electrical Insulation and Dielectric Phenomena, Virginia Beach, VA, USA*, 646-649, 2009.
[83] C.C. Reddy, T.S. Ramu, "Polymer nanocomposites as insulation for HV DC cables – investigations on the thermal breakdown", *IEEE Transactions on Dielectrics and Electrical Insulation, Vol. 15, Nº1*, 221-227, 2008.
[84] H-Z. Ding, B.R. Varlow, "Effect of nano-fillers on electrical treeing in epoxy resin subjected to AC voltage", *IEEE Conference on Electrical Insulation and Dielectric Phenomena, Boulder, CO, USA*, 332-335, 2004.
[85] S. Alapati, M.J. Thomas, "Electrical tree growth in high voltage insulation containing inorganic nanofillers", *16th International Symposium on High Voltage Engineering, Cape Town, South Africa,* 145-150, 2009.
[86] M.G. Danikas, T. Tanaka, "Nanocomposites – a review of electrical treeing and breakdown", *IEEE Electrical Insulation Magazine, Vol. 25, Nº4*, 19-25, 2009.
[87] J.K. Nelson, J.C. Fothergill, "Internal charge behaviour of nanocomposites", *Nanotechnology, Vol. 15, Nº5*, 586-595, 2004.
[88] J.C. Fothergill, J.K. Nelson, M. Fu, "Dielectric properties of epoxy nanocomposites containing TiO_2, Al_2O_3 and ZnO fillers", *IEEE Conference on Electrical Insulation and Dielectric Phenomena, Boulder, CO, USA*, 406-409, 2004.
[89] A. Hajiyiannis, G. Chen, C. Zhang, G. Stevens, "Space charge formation in epoxy resin including various nanofillers", *IEEE Conference on Electrical Insulation and Dielectric Phenomena, Québec City, QC, Canada*, 741-717, 2008.
[90] T. Andritsch, R. Kochetov, P.H.F. Morshuis, J.J. Smit, "Dielectric properties and space charge behavior of MgO-epoxy nanocomposites", *IEEE International Conference on Solid Dielectrics, Potsdam, Germany*, 344-347, 2010.
[91] C. Zhang, R. Mason, G.C. Stevens, "Dielectric properties of epoxy and polyethylene nanocomposites", *International Symposium on Electrical Insulating Materials, Kitakyushu, Japan*, 393-396, 2005.
[92] S. Singha, M.J. Thomas, "Reduction of permittivity in epoxy nanocomposites at low nano-filler loadings", *IEEE Conference on Electrical Insulation and Dielectric Phenomena, Québec City, QC, Canada*, 726-729, 2008.
[93] S. Singha, M.J. Thomas, "Permittivity and tan delta characteristics of epoxy nanocomposites in the frequency range of 1 MHz-1GHz", *IEEE Transactions on Dielectrics and Electrical Insulation, Vol. 15, Nº1*, 2-11, 2008.
[94] T. Andritsch, R. Kochetov, P.H.F. Morshuis, J.J. Smit, "Comparison of the dielectric response of alumina-epoxy composites with nano- and conventional sized filler", *16th International Symposium on High Voltage Engineering, Cape Town, South Africa*, A-28, 2009.
[95] R. Kochetov, T. Andritsch, P.H.F. Morshuis, J.J. Smit, "Anomalous behaviour of the dielectric spectroscopy response of nanocomposites", *IEEE Transactions on Dielectrics and Electrical Insulation, IEEE Transactions on Dielectrics and Electrical Insulation, Vol. 19, Nº1*, 107-117, 2012.
[96] L. Ekstrand, H. Kristiansen, J. Liu, "Characterization of thermally conductive epoxy nano composites", *IEEE 28th International Spring Seminar on Electronics Technology: Meeting the Challenges of Electronics Technology Progress, Wiener Neustadt, Austria*, 19-23, 2005.
[97] Z. Han, J.W. Wood, H. Herman, C. Zhang, G.C. Stevens, "Thermal properties of composites filled with different fillers", *IEEE International Symposium on Electrical Insulation, Vancouver, Canada,* 497-501, 2008.

[98] G.C. Stevens, H. Herman, J. Han, J.W. Wood, A. Mitchell, J. Thomas, "The role of nano and micro fillers in high thermal conductivity electrical insulation systems", *11th Insucon Conference, Birmingham, UK,* 286-291, 2009.
[99] R. Kochetov, T. Andritsch, U. Lafont, P.H.F. Morshuis, J.J. Smit, "Thermal conductivity of nanofilled Epoxy systems", *IEEE Conference on Electrical Insulation and Dielectric Phenomena, Virginia Beach, VA, USA*, 658-661, 2009.
[100] R. Kochetov, A.V. Korobko, T. Andritsch, P.H.F. Morshuis, S.J. Picken, J.J. Smit, "Modelling of the thermal conductivity in polymer nanocomposites and the impact of the interface between filler and matrix", *Journal of Physics D: Applied Physics, Vol. 44, 395401*, 2011.
[101] Y. Shimazaki, Y. Miyazaki, Y. Takezawa, M. Nogi, K. Abe, S. Ifuku, H. Yano, "Excellent thermal conductivity of transparent cellulose nanofiber/epoxy resin nanocomposites", *Biomacromolecules, Vol. 8*, *№9*, 2976-2978, 2007.
[102] P.C. Ma, J-K. Kim, B.Z. Tang, "Effects of silane functionalization on the properties of carbon nanotubes/epoxy nanocomposites", *Composite Science and Technology, Vol. 67*, *№14*, 2965-2972, 2007.
[103] Y. Geng, M.Y. Liu, J. Li, X.M. Shi, J.K. Kim, "Effects of surfactant treatment on mechanical and electrical properties of CNT/epoxy nanocomposites", *Composites: Part A, Vol. 39*, *№12*, 1876-1883, 2008.
[104] H. Miyagawa, A.K. Mahanty, L.T. Drzal, M. Misra, "Nanocomposites form bio-based epoxy and single-wall carbon nanotubes: synthesis, and mechanical and thermophysical properties evaluation", *Nanotechnology, Vol. 16, №1*, 118-124, 2005.
[105] H. Li, Z. Zhang, X. Ma, M. Hu, X. Wang, P. Fan, "Synthesis and characterization of epoxy resin modified with nano-SiO_2 and γ-glycidoxypropyltrimethoxy silane", *Surface & Coating Technology, Vol. 201, №9-10*, 5269-5272, 2007.
[106] C-F. Ou, M-C. Shiu, "Epoxy composites reinforced by different size silica nanoparticles", *Journal of Applied Polymer Science, Vol. 115, №5*, 2648-2653, 2010.
[107] C-C. Wu, S.L-C. Hsu, "Preparation of epoxy/silica and epoxy/titania hybrid resist via a sol-gel process for nanoimprint lithography", *The Journal of Physical Chemistry C, Vol. 114, №5*, 2179-2183, 2010.
[108] S. Zhao, L.S. Schadler, H. Hillborg, T. Auletta, "Effect of interfacial strength on mechanical properties of Al_2O_3/epoxy nanocomposites", *Nordic Insulation Symposium, Gothenburg, Sweden*, 41-44, 2009.
[109] E. Tuncer, I. Sauers, D.R. James, G. Polizos, A.R. Ellis, K.I. More, C. Cantoni, "Properties of a nanodielectrics cryogenic resin", *ASME Conference on Smart Materials, Adaptive Structures and Intelligent Systems, Philadelphia, PA, USA,* 2010.
[110] G. Polizos, E. Tuncer, I. Sauers, K.I. More, "Physical properties of epoxy resin/titanium dioxide nanocomposites", *Polymer Engineering and Science, Vol. 51, №1*, 87-93, 2011.
[111] T. Andritsch, R. Kochetov, P.H.F. Morshuis, J.J. Smit, "The complex permittivity of epoxy based nanocomposites with alumina and magnesium oxide fillers at very low temperatures", *IEEE Conference on Electrical Insulation and Dielectric Phenomena, Cancun, Mexico*, 306-309, 2011.
[112] C.A. Harper, *Handbook of plastics, elastomers, and composites*, McGraw-Hill, 2002.
[113] C.A. May, *Epoxy resins. Chemistry and technology*, 2nd ed., Marcel Dekker, Inc., New York and Basel, 1988.
[114] N. Prilezhaev, *Berichte der Deutschen Chemischen Gessellschaft 42*, 4811-4815, 1910.
[115] H. Lee, K. Neville, *Epoxy resins. Their applications and technology*, McGraw-Hill, 1957.
[116] C. Zhang, R. Mason, G.C. Stevens, "Dielectric properties of alumina-polymer nanocomposites", *IEEE Conference on Electrical Insulation and Dielectric Phenomena, Nashville, TN, USA,* 721-724, 2005.
[117] C. Zou, J.C. Fothergill, S.W. Rowe, "The effect of water absorption on the dielectric properties of epoxy nanocomposites", *IEEE Transactions on Dielectrics and Electrical Insulation, Vol.15, №1*, 106-117, 2008.

[118] D.B. Miracle, S.L. Donaldson, "Introduction to composites", *ASM Handbook: Composites*, Vol. 21, ASM International, Materials Park, Ohio, 3-17, 2001.
[119] S-H. Xie, B-K. Zhu, J-B Li, X-Z. Wei, Z-K. Xu, "Preparation and properties of polyimide / aluminum nitride composites", *Polymer Testing, Vol. 23, Nº7*, 797-804, 2004.
[120] J. Wang, X.-S. Yi, "Preparation and the properties of PMR – type polyimide composites with aluminum nitride", *Journal of Applied Polymer Science, Vol. 89*, *Nº14*, 3913-3917, 2003.
[121] C.P. Wong, R.S. Bollampally, "Comparative study of thermally conductive fillers for use in liquid encapsulants for electronic packaging", *IEEE Transactions on Advanced Packaging, Vol. 22, Nº1*, 54-59, 1999.
[122] K.C. Yung, H. Liem, "Enhanced thermal conductivity of boron nitride epoxy-matrix composite through multi-modal particle size mixing", *Journal of Applied Polymer Science, Vol. 106*, *Nº6*, 3587-3591, 2007.
[123] L.S. Schadler, L.C. Brinson, W.G. Sawyer, "Polymer nanocomposites: a small part of the story", *JOM, Nanocomposite materials,* 53-60, 2007.
[124] K. Sill, S. Yoo, T. Emrick, "Polymer-nanoparticle composites", *Dekker Encyclopedia of Nanoscience and Nanotechnology*, 2004.
[125] M. Xanthos, "Polymers and polymer composites", *Functional fillers for plastics*, 2nd ed., edited by M. Xanthos, Chapter 1, Wiley VCH Verlag GmbH&Co. KGaA, Weinheim, 2010.
[126] M.R. Wiesner, J-Y. Bottero, *Environmental nanotechnology*, McGraw-Hill, 2007.
[127] X. Chen, K.E. Gonsalves, G.-M. Chow, T.D. Xiao, "Homogeneous dispersion of nanostructured aluminum nitride in a polyimide matrix", *Advanced Materials, Vol. 6, Nº6*, 481-484, 1994.
[128] E. Allen, J. Henshaw, P. Smith, "A review of particle agglomeration", *AEA Technology Engineering Services, Inc.*, 2001.
[129] K. Friedrich, A.K. Schlarb, *Tribology of polymeric nanocomposites. Friction and wear of bulk materials and coatings*, Elsevier, 2008.
[130] N. Chisholm, H. Mahfuz, V.K. Rangari, A. Ashfaq, S. Jeelani, "Fabrication and mechanical characterization of carbon/SiC nanocomposites", *Composite Structures, Vol. 67, Nº1*, 115-124, 2005.
[131] C.K. Lam, K.T. Lau, "Localized elastic modulus distribution of nanoclay / epoxy composites by using nanoindentation", *Composite Structures, Vol. 75, Nº1-4*, 553-558, 2006.
[132] L. Matějka, O. Dukh, J. Kolařík, "Reinforcement of crosslinked rubbery epoxies by in situ formed silica", Polymer, Vol. 41, *Nº4*, 1449-1459, 2000.
[133] M-I. Baraton, *Synthesis, functionalization and surface treatment of nanoparticles*, American scientific publishers, 2003.
[134] C.J. Brinker, G.W. Scherer, *Sol-gel science: the physics and chemistry of sol-gel processing*, Academic press, San Diego, 1990.
[135] B. Wetzel, F. Haupert, M.Q. Zhang, "Epoxy nanocomposites with high mechanical and tribological performance", *Composites Science and Technology, Vol. 63, Nº14*, 2055-2067, 2003.
[136] Y. Sun, Z. Zhang, C.P. Wong, "Fundamental research on surface modification of nano-size silica for underfill applications", *IEEE 9th Symposium on Advanced Packaging Materials*, 132-138, 2004.
[137] Y.W. Zhu, X.Q. Shen, B.C. Wang, X.Y. Xu, Z.J. Feng, "Chemical mechanical modification of nanodiamond in an aqueous system", *Physics of the Solid State, Vol. 46, Nº4*, 681-684, 2004.
[138] C. Özdilek, *Colloidal liquid crystalline reinforced nanocomposites*, PhD thesis, Delft University of Technology, 2006.
[139] K.C. Yung, J. Wang, T.M. Yue, "Thermal management for boron nitride filled metal core printed circuit board", *Journal of Composite Materials, Vol. 42, Nº24*, 2615-2627, 2008.
[140] A.W. Levering, *Interphases in zirconium silicate filled high density polyethylene and polypropylene*, PhD thesis, Delft University of Technology, 1995.

[141] C.W. Reed, "Functionalization of nanocomposite dielectrics", *IEEE International Symposium on Electrical Insulation, San Diego, CA, USA*, 353-356, 2010.
[142] E.P. Plueddemann, *Silane coupling agents*, Plenum Press, 1982.
[143] B. Arkles, *Silane coupling agents: connecting across boundaries*, Gelest Inc., 2004.
[144] S. Shokoohi, A. Arezafar, R. Khosrokhavar, "Silane coupling agents in polymer-based reinforced composites: a review", *Journal of Reinforced Plastics and Composites, Vol. 27, Nº5*, 473-485, 2008.
[145] Y. Xu, D.D.L. Chung, "Increasing the thermal conductivity of boron nitride and aluminum nitride particle epoxy-matrix composites by particle surface treatments", *Composite Interfaces, Vol. 7, Nº4*, 243-256, 2000.
[146] H. Hubner, E. Dorre, *Alumina: processing, properties and applications*, Springer-Verlag, Berlin, 1984.
[147] R. Sun, M.A. White, "Ceramics and glasses", *Thermal conductivity. Theory, properties and applications*, edited by T.M. Tritt, Chapter 3.1, Kluwer Academic / Plenum Publishers, New York, 2004.
[148] W. Werdecker, F.A. Aldinger, "Aluminum nitride – an alternative ceramic substrate for high power applications in microcircuits", *IEEE Transactions on Components, Hybrids, and Manufacturing Technology, Vol. 7, Nº4*, 399-404, 1984.
[149] C.J. Cremers, H.A. Fine, *Thermal conductivity*, New York and London, 1990.
[150] K. Ishimoto, T. Tanaka, Y. Ohki, Y. Sekiguchi, Y. Murata, M. Gosyowaki, "Comparison of dielectric properties of low-density polyethylene/MgO composites with different size fillers", *IEEE Conference on Electrical Insulation Dielectric Phenomena*, *Québec City, Canada*, 208-211, 2008.
[151] W. Zhou, S. Qi, Q. An, H. Zhao, N. Liu, "Thermal conductivity of boron nitride reinforced polyethylene composites", *Materials Research Bulletin, Vol. 42*, *Nº10*, 1863-1873, 2007.
[152] H. Ishida, S. Rimdusit, "Very high thermal conductivity obtained by boron nitride-filled polybenzoxazine", *Thermochimica Acta, Vol. 320, Nº1-2*, 177-186, 1998.
[153] T.H. Chiang, T-E. Hsieh, "A study of encapsulation resin containing hexagonal boron nitride (hBN) as inorganic filler", *Journal of Inorganic and Organometallic Polymers and Materials, Vol. 16, Nº2*, 175-183, 2006.
[154] R. Brütsch, A. Lutz, G. Lupták, R. Schuler, "New high voltage insulation with increased thermal conductivity", *Electrical Electronics Insulation Conference and Electrical Manufacturing & Coil Winding Conference, Chicago, IL, USA*, 1993.
[155] P.H.F. Morshuis, T. Andritsch, R. Kochetov, M.F. Fréchette, H.D. Martinez, S. Savoie, A. Krivda, L.E. Smith, D. Zegaraz, "Dielectric Frequency Response of Epoxy-based Composites with Various Silica Filler Sizes", *IEEE International Conference on Solid Dielectrics, Potsdam, Germany*, 200-203, 2010.
[156] T. Imai, F. Sawa, T. Nakano, T. Ozaki, T. Shimizu, S. Kuge, M. Kozako, T. Tanaka, "Insulation properties of nano- and micro-filler mixture composite", *IEEE Conference on Electrical Insulation and Dielectric Phenomena, Nashville, TN, USA*, 171-174, 2005.
[157] P. Preetha, S. Alapati, S. Singha, B. Venkatesulu, M.J. Thomas, "Electrical discharge resistance characteristics of epoxy nanocomposites", *IEEE Conference on Electrical Insulation and Dielectric Phenomena, Québec City, Canada*, 718-721, 2008.
[158] S.M. Olhero, S. Novak, M. Oliveira, K. Krnel, T. Kosmac, J.M.F. Ferreira, "A thermo-chemical surface treatment of AlN powder for the aqueous processing of AlN ceramics", *Journal of Materials Research, Vol. 19, Nº3*, 746-751, 2004.
[159] X-J. Luo, B-L. Zhang, W-L. Li, H-R. Zhuang, "Preparation of aluminum nitride green sheets by aqueous tape casting", *Ceramics International, Vol. 30*, *Nº8*, 2099-2103, 2004.
[160] J. Xu, C.P. Wong, "High-K nanocomposites with core-shell structured nanoparticles for decoupling applications", *Electronic Components and Technology Conference*, *Lake Buena Vista, FL, USA*, 1234-1240, 2005.
[161] F. Li, D. Zhang, "Nickel coating on hexagonal boron nitride particles by chemical plating", *Metallurgical and Materials Transactions B*, Vol. 38, *Nº2*, 149-157, 2007.
[162] www.ika.de

[163] B.A. Waldman, "Silane coupling agents improve performance", *Modern Paint and Coatings, Vol. 86, Nº2*, 34-38, 1996.
[164] E.M. Petrie, *Handbook of adhesives and sealants*, 2nd ed., McGraw-Hill, New York, 2006.
[165] P. Bowen, J.G. Highfield, A. Mocellin, T.A. Ring, "Degradation of aluminum nitride powder in aqueous environment", *Journal of the American Ceramics Society, Vol. 73, Nº3,* 724-728, 1990.
[166] S.N. Bhattacharya, R.K. Gupta, M.R. Kamal, *Polymeric nanocomposites. Theory and practice*, Hancer, 2007.
[167] P. Maity, S.V. Kasisomayajula, V. Parameswaran, S. Basu, N. Gupta, "Improvement of surface degradation composites due to pre-processed nanometric alumina fillers", *IEEE Transactions on Dielectrics and Electrical Insulation, Vol. 15, Nº1*, 63-72, 2008.
[168] Z. Guo, T. Pereira, O. Choi, Y. Wang, T.H. Hahn, "Surface functionalized alumina nanoparticle filled polymeric nanocomposites with enhanced mechanical properties", *Journal of Materials Chemistry, Vol. 16*, 2800-2808, 2006.
[169] R. Kochetov, T. Andritsch, U. Lafont, P.H.F. Morshuis, J.J. Smit, "Effects of inorganic nanofillers and combinations of them on the complex permittivity of epoxy-based composites", *IEEE International Symposium on Electrical Insulation, San Diego, CA, USA,* 340-344, 2010.
[170] R. Kochetov, T. Andritsch, U. Lafont, P.H.F. Morshuis, J.J. Smit, "The thermal conductivity in epoxy – aluminum nitride and epoxy – aluminum oxide nanocomposite systems", *Nordic Insulation Symposium, Gothenburg, Sweden*, 27-30, 2009.
[171] R. Kochetov, T. Andritsch, P.H.F. Morshuis, J.J. Smit, "Impact of postcuring and water absorption on the dielectric response of the epoxy-based composites filled with MgO nanoparticles", *IEEE Conference on Electrical Insulation and Dielectric Phenomena, Cancun, Mexico*, 342-345, 2011.
[172] M.M.S. Shirazi, H. Borsi, E. Gockenbach, "Evaluation of the influence of nano fillers on the electrical and dielectric properties of epoxy resin", *IEEE Electrical Insulation Conference, Annapolis, MD, USA*, 497-500, 2011.
[173] W.H. Gitzen, *Alumina as a ceramic material*, The American ceramic society, Ohio, USA, 1970.
[174] C.J-P. Steiner, D.P.H. Hasselman, R.M. Springgs, "Kinetics of the gamma-to-alpha alumina phase transformation", *Journal of the American Ceramic Society, Vol. 54, Nº8*, 412-413, 1971.
[175] E. Kostić, Š. Kiss, S. Boškovic, S. Zec, "Mechanical activation of the gamma to alpha transition in Al_2O_3", *Powder Technology, Vol. 91, Nº1*, 49-54, 1997.
[176] A.J. Moulson, J.M. Herbert, *Electroceramics: materials, properties, applications,* Chapman & Hall, London, UK, 1990.
[177] C. Ruberto, *Bulk and surface structure of k alumina*, Licentiate thesis, Chalmers University of Technology and Göteborg University, 1998.
[178] N.W. Ashcroft, N.D. Mermin, *Solid state physics*, Holt-Saunders, Philadelphia, 1976.
[179] B.D. Cullity, *Elements of X-ray diffraction*, Addison-Wesley, Reading, 1978.
[180] J.W. Niemantsverdriet, *Spectroscopy in catalysis*, 3rd ed., Wiley-VCH Verlag GmbH&Co. KGaA, Weinheim, 2007.
[181] H & M Analytical Services, Inc., "Particle size and strain analysis by X-ray diffraction", 2002.
[182] D.D.L. Chung, *Materials for electronic packaging*, Butterworth-Heinemann, 1995.
[183] T. Araki, Q. Tran-Cong, M. Shibayama, *Structure and properties of multiphase polymeric materials*, Marcel Dekker Inc., 1998.
[184] R. Berman, *Thermal conduction in solids*, Clarendon press, Oxford, 1976.
[185] E.H. Weber, *Development and modeling of thermally conductive polymer/carbon composites*, PhD thesis, Michigan Technological University, 1999.
[186] J.E. Parrott, A.D. Stuckes, *Thermal conductivity of solids*, Pion Ltd., 1975.
[187] S.L. Shindé, J.S. Goela, *High thermal conductivity materials*, Springer, 2006.
[188] Y. Yang, "Thermal conductivity", *Physical properties of polymers. Handbook*, edited by J.E. Mark, Chapter 10, 2nd ed., Springer, 2007.

[189] Y.K. Godovsky, *Thermophysical properties of polymers*, Springer-Verlag, 1992.
[190] H.S. Tekce, D. Kumlutas, I.H. Tavman, "Effect of particle shape on thermal conductivity of copper reinforced polymer composites", *Journal of Reinforced Plastics and Composites, Vol. 26*, 113-121, 2007.
[191] D. Hansen, G.A. Bernier, "Thermal conductivity of polyethylene: the effect of crystal size, density and orientation on the thermal conductivity", *Polymer Engineering and Science, Vol. 12, Nº3*, 204-208, 1972.
[192] K. Kurabayashi, "Anisotropic thermal properties of solid polymers", *International Journal of Thermophysics, Vol. 22, Nº1*, 277-288, 2001.
[193] K. Fukushima, H. Takahashi, Y. Takezawa, M. Hattori, M. Itoh, M. Yonekura, "High thermal conductive epoxy resins with controlled high-order structure", *IEEE Conference on Electrical Insulation and Dielectric Phenomena, Boulder, CO, USA*, 340-343, 2004.
[194] W. Kim, J-W. Bae, I-D. Choi, Y-S. Kim, "Thermally conductive EMC (Epoxy Molding Compound) for microelectronic encapsulation", *Polymer Engineering and Science, Vol. 39, Nº4*, 756-766, 1999.
[195] C-Y. Hsieh, S-L. Chung, "High thermal conductivity epoxy molding compound filled with a combustion synthesized AlN powder". *Journal of Applied Polymer Science, Vol. 102*, 4734-4740, 2006.
[196] P.A. Tipler, G. Mosca, *Physics for scientists and engineers*, W.H. Freeman and Company, New York, 6th ed., 2008.
[197] P. Kim, L. Shi, A. Majumdar, P.L. McEuen, "Thermal transport measurements of individual multiwalled nanotubes", *Physical Review Letters, Vol. 87, Nº21*, 215502, 2001.
[198] Z. Han, A. Fina, "Thermal conductivity of carbon nanotubes and their polymer nanocomposites: a review", *Progress in Polymer Science, Vol. 36, Nº7*, 914-944, 2011.
[199] G. Leibfried, E. Schlömann, "Wärmeleitung in elektrisch isolierenden Kristallen", *Nach. Akad. Wiss. Göttingen, Math. Phys. Klasse 4*, 1954.
[200] C.L. Julian, "Theory of heat conduction in rare-gas crystals", *Physical Review, Vol. 137, Nº1A*, 128-137, 1965.
[201] G.P. Strivastava, "Lattice thermal conduction mechanism in solids", *High thermal conductivity materials*, Edited by S.L. Shindé and J.S. Goela, Springer, 2006.
[202] R.B. Dinwiddie, A.J. Whittaker, D.G. Onn, "Thermal conductivity, heat capacity, and thermal diffusivity of selected commercial AlN substrates", *International Journal of Thermophysics, Vol. 10, Nº5*, 1075-1084, 1989.
[203] G.A. Slack, "Nonmetallic crystals with high thermal conductivity", *Journal of Physics and Chemistry of Solids, Vol. 34*, 321-335, 1973.
[204] R.L. McCullough, "Generalized combining rules for predicting transport properties of composite materials", *Composites Science and Technology, Vol. 22*, 3-21, 1985.
[205] R.C. Progelhof, J.L. Throne, R.R. Ruetsch, "Methods for predicting the thermal conductivity of composite systems: a review", *Polymer Engineering and Science, Vol. 16, Nº9*, 615-625, 1976.
[206] I.H. Tavman, "Effective thermal conductivity of isotropic polymer composites", *International Communications in Heat and Mass Transfer, Vol. 25, Nº5*, 723-732, 1998.
[207] S. Agarwal, M.M.K. Khan, R.K. Gupta, "Thermal conductivity of polymer nanocomposites made with carbon nanofibers", *Polymer Engineering and Science*, *Vol. 48, Nº12*, 2474-2481, 2008.
[208] J.C. Maxwell, *A treatise on electricity and magnetism*, 3rd edition, Dover Inc., New York, NY, 1954.
[209] R. Pal, "On the Lewis-Nielsen model for the thermal / electrical conductivity of composites", *Composites: Part A, Vol. 39*, *Nº5*, 718-726, 2008.
[210] H. Fricke, "Mathematical treatment of the electric conductivity and capacity of the dispersed systems", Physical Review, Vol. 24, Nº5, 575–587, 1924.
[211] D.A.G. Bruggeman, "Berechnung verschiedener physikalischer Konstanten von heterogenen Substanzen. I. Dielektrizitätskonstanten und Leitfähigkeiten der Mischkörper aus isotropen Substanzen", *Annalen der Physik, Vol. 24*, 636-679, 1935.
[212] R.F. Hill, P.H. Supancic, ''Thermal Conductivity of Platelet-Filled Polymer Composites,'' *Journal of the American Ceramic Society, Vol. 85, Nº4*, 851–857, 2002.

[213] E-S. Lee, S-M. Lee, D.J. Shanefield, W.R. Cannon, "Enhanced thermal conductivity of polymer matrix composite via high solids loading of aluminum nitride in epoxy resin", *Journal of the American Ceramic Society Vol. 91, Nº4*, 1169-1174, 2008.
[214] G.T-N. Tsao, "Thermal conductivity of two-phase materials", *Industrial & Engineering Chemistry, Vol. 53, Nº5*, 395-397, 1961.
[215] S.C. Cheng, R.I. Vachon, "The prediction of the thermal conductivity of two and three phase solid heterogeneous mixtures", *International Journal of Heat and Mass Transfer, Vol. 12,* 249-264, 1969.
[216] D.W. Sundstrom, Y-D. Lee, "Thermal conductivity of polymer filled with particulate solids", *Journal of Applied Polymer Science, Vol. 16*, 3159-3167, 1972.
[217] R.L. Hamilton, O.K. Crosser, "Thermal conductivity of homogeneous two-component systems", *Industrial and Engineering Chemistry Fundamentals, Vol. 1, Nº3*, 187-191, 1962.
[218] R.L. Hamilton, *Thermal conductivity of two-phase materials*, Dissertation, University of Oklahoma, 1960.
[219] H. Hatta, M. Taya, "Equivalent inclusion method for steady state heat conduction in composites", *International Journal of Engineering Science, Vol. 24, Nº7*, 1159-1170, 1986.
[220] R.E. Meredith, C.W. Tobias, ''Conduction in Heterogeneous Systems'', *Advances in Electrochemistry and Electrochemical Engineering*, Edited by C.W. Tobias, Vol. 2, Wiley, New York, 1962.
[221] T.B. Lewis, L.E. Nielsen, "Dynamic mechanical properties of particulate-filled composites", *Journal of Applied Polymer Science, Vol. 14, Nº6*, 1449-1471, 1970.
[222] L.E. Nielsen, "Thermal conductivity of particulate filled polymers", *Journal of Applied Polymer Science, Vol. 17*, *Nº12*, 3819-3820, 1973.
[223] L.E. Nielsen, R.F. Landel, *Mechanical properties of polymers and composites*, 2nd ed., Marcel Dekker, New York, 1994.
[224] J.C. Halpin, "Stiffness and expansion estimates for oriented short fiber composites", *Journal of Composite Materials, Vol. 3, Nº1*, 732–734, 1969.
[225] L.E. Nielsen, "The thermal and electrical conductivity of two-phase systems", *Industrial and Engineering Chemistry Fundamentals, Vol. 13, Nº1*, 17–20, 1974.
[226] Y. Agari, T. Uno, "Thermal conductivity of polymer filled with carbon materials: effect of conductive particle chains on thermal conductivity", *Journal of Applied Polymer Science, Vol. 30, Nº5*, 2225-2235, 1985.
[227] Y. Agari, T. Uno, "Estimation on thermal conductivities of filled polymers", *Journal of Applied Polymer Science, Vol. 32, Nº7*, 5705-5712, 1986.
[228] Y. Agari, A. Ueda, S. Nagai, "Thermal conductivity of a polymer composite", *Journal of Applied Polymer Science, Vol. 49, Nº9*, 1625-1634, 1993.
[229] W. Zhou, S. Qi, H. Li, S. Shao, "Study on insulating thermal conductive BN/HDPE composites", *Thermochimica Acta, Vol. 452, Nº1*, 36-42, 2006.
[230] R. Kochetov, T. Andritsch, U. Lafont, P.H.F. Morshuis, S.J. Picken, J.J. Smit, "Thermal behaviour of epoxy resin filled with high thermal conductivity nanopowders", *IEEE Electrical Insulation Conference, Montreal, QC, Canada*, 524-528, 2009.
[231] H.W. Russell, "Principles of heat flow in porous insulators", *Journal of the American Ceramic Society, Vol. 18*, 1-5, 1935.
[232] L. Topper, "Analysis of porous thermal insulating materials", *Industrial & Engineering Chemistry, Vol. 47, Nº7*, 1377-1379, 1955.
[233] J.B. Jefferson, O.W. Witzell, W.L. Sibitt, "Thermal conductivity of graphite-silicon oil and graphite-water suspensions", *Industrial & Engineering Chemistry, Vol. 50, Nº10*, 1589-1592, 1958.
[234] G.S. Springer, S.W. Tsai, "Thermal conductivities of unidirectional materials", *Journal of Composite Materials, Vol. 1, Nº2*, 166-173, 1967.
[235] B. Budiansky, "Thermal and thermoelastic properties of isotropic composites", *Journal of Composite Materials, Vol. 4, Nº3*, 286-295, 1970.
[236] A.B. Baschirow, J.W. Selenew, "Thermal conductivity of composites", *Plaste Kaut, Vol. 23*, 656, 1976.

[237] S. McGee, R.L. McCullough, "Combining rules for predicting the thermoelastic properties of particulate filled polymers, polyblends, and foam", *Polymer Composites, Vol. 2, Nº4,* 149-161, 1981.
[238] V.P. Privalko, V.V. Novikov, "Model treatments of the heat conductivity of heterogeneous polymers", *Thermal and electrical conductivity of polymer materials, Advances in Polymer Science, Vol. 119,* Springer-Verlag, Berlin Heidelberg, 31-77, 1995.
[239] G.N. Dulnev, V.V. Novikov, *Transport processes in heterogeneous systems*, in Russian, Energoatomizdat, Leningrad, 1991.
[240] I.H. Tavman, "Thermal conductivity of particle reinforced polymer composites", *International Communications in Heat and Mass Transfer, Vol. 27, Nº2*, 253-261, 2000.
[241] P.L. Kapitza, "The study of heat transfer in helium II", *Journal of Physics (USSR), Vol. 4*, 177-181, 1941.
[242] E.T. Swartz, R.O. Pohl, "Thermal boundary resistance", *Reviews of Modern Physics, Vol. 61, Nº3*, 1989.
[243] W. Evans, R. Prasher, J. Fish, P. Meakin, P. Phelan, P. Keblinski, "Effect of aggregation and interfacial thermal resistance on thermal conductivity of nanocomposites and colloidal nanofluids", *International Journal of Heat and Mass Transfer, Vol. 51, Nº5-6*, 1431-1438, 2008.
[244] P.C. Irwin, Y. Cao, A. Bansal, L.S. Schadler, "Thermal and mechanical properties of polyimide nanocomposites", *IEEE Conference on Electrical Insulation and Dielectric Phenomena, Albuquerque, NM, USA*, 120-123, 2003.
[245] S. Rätzke, Zur Wirkungsweise von nanoskalingen Füllstoffpartikeln in polymeren Isolier-werkstoffen der Hochspannungstechnik, PhD thesis, Technischen Universität München, 2009.
[246] X-Q. Wang, A.S. Mujumdar, "Heat transfer characteristics of nanofluids: a review", *International Journal of Thermal Sciences*, *Vol. 46, Nº1*, 1-19, 2007.
[247] M. Chandrasekar, S. Suresh, "A review on the mechanisms of heat transfer in nanofluids", *Heat Transfer Engineering*, *Vol. 30, Nº14*, 1136−1150, 2009.
[248] P. Keblinski, S.R. Phillpot, S.U.S. Choi, J.A. Eastman, "Mechanisms of heat flow in suspensions of nano-sized particles (nanofluids)", *International Journal of Heat and Mass Transfer, Vol. 45, Nº4*, 855 -863, 2002.
[249] W. Yu, S.U.S. Choi, "The role of interfacial layers in the enhanced thermal conductivity of nanofluids: a renovated Maxwell model", *Journal of Nanoparticle Research*, *Vol. 5, Nº1-2*, 167 -171, 2003.
[250] Q. Xue, W-M. Xu, "A model of thermal conductivity of nanofluids with interfacial shells", *Materials Chemistry and Physics, Vol. 90, Nº2-3*, 298-301, 2005.
[251] C-W. Nan, R. Birringer, D.R. Clarke, H. Gleiter, "Effective thermal conductivity of particulate composites with interfacial thermal resistance," *Journal of Applied Physics, Vol. 81, Nº10*, 6692–6699, 1997.
[252] S.V. Kidalov, F.M. Shakhov, "Thermal conductivity of diamond composites", *Materials, Vol. 2*, 2467-2495, 2009.
[253] Y.K. Godovsky, *Thermophysical methods of polymers characterization*, in Russian, Khimija, Moscow, 1976.
[254] A.F. Chudnovsky, *Thermophysical characteristics of dispersion materials*, in Russian, Fizmatgiz, Moscow, 1962.
[255] G.M. Kondratyev, *Thermal measurements*, in Russian, Mashgiz, Moscow, 1957.
[256] K.D. Maglic, A. Gazairliyan, V.E. Peletsky, *Thermal conductivity measurement methods*, in: *Compendium of thermophysical property measurement methods*, Vol. 1, Part I, Plenum New York, 1984.
[257] Hukseflux Thermal Sensors, *Thin Heater Apparatus Measurement System Manual*, v0811, Delft, 2008.
[258] S. Konzelmann, C. Hoffmann, R. Metre, D. Peier, "Thermal and electrical properties of aluminum nitride filled epoxy-resin compound", *IEEE Transactions on Dielectrics and Electrical Insulation, Vol. 15, Nº2*, 327-333, 2008.

[259] H.Y. Ng, X. Lu, S.K. Lau, "Thermal conductivity of boron nitride – filled thermoplastics: effect of filler characteristics and composite processing conditions", *Polymer Composites*, Vol. 26, *Nº6*, 778-790, 2005.
[260] W. Jiajun, Y. Xiao-Su, "Effects of interfacial thermal barrier resistance and particle shape and size on the thermal conductivity of AlN/PI composites", *Composites Science and Technology, Vol. 64*, 1623-1628, 2004.
[261] Y. Miyazaki, T. Nishiyama, H. Takahashi, J. Katagiri, Y. Takezawa, "Development of highly thermoconductive epoxy composites", *IEEE Conference on Electrical Insulation and Dielectric Phenomena, Virginia Beach, VA, USA*, 638-641, 2009.
[262] Y. Shimazaki, F. Hojo, Y. Takezawa, "Preparation and characterization of thermoconductive polymer nanocomposite with branched alumina nanofibers", *Applied Physics Letters, Vol. 92, 133309*, 2008.
[263] M.A. van Es, *Polymer-clay nanocomposites, the importance of particle dimensions*, PhD thesis, Delft University of Technology, 2001.
[264] Y. Miwa, A.R. Drews, S. Schlick, "Detection of the direct effect of clay on polymer dynamics: the case of spin-labeled poly(methyl acrylate)/clay nanocomposites studied by ESR, XRD, and DSC", *Macromolecules, Vol. 39. Nº9*, 3304-3311, 2006.
[265] L. Chen, K. Zheng, X. Tian, K. Hu, R. Wang, C. Liu, Y. Li, P. Cui, "Double glass transitions and interfacial immobilized layer in in-situ-synthesized poly(vinyl alcohol)/silica nanocomposites", *Macromolecules, Vol. 43, Nº2,* 1076-1082, 2010.
[266] M. Hu, S. Shenogin, P. Keblinski, "Molecular dynamics simulations of interfacial thermal conductance between silicon and amorphous polyethylene", *Applied Physics Letters, Vol. 91*, *Nº24*, 241910, 2007.
[267] K. Jiang, L. Cheng, L. Zheng, Z. Yao, G. Li, Q. Yin, "The unique dielectric behaviour of nanosilica epoxy composites", *7th IEEE International Conference on Nanotechnology, Hong Kong,* 1101-1106, 2007.
[268] R. Kochetov, T. Andritsch, P.H.F. Morshuis, J.J. Smit, "Effect of filler size on complex permittivity and thermal conductivity of epoxy-based composites filled with BN particles", *IEEE Conference on Electrical Insulation and Dielectric Phenomena, West Lafayette, IN, USA*, 534-537, 2010.
[269] I. Levin, D. Brandon, "Metastable alumina polymorphs: crystal structures and transition sequences", *Journal of the American Ceramic Society, Vol. 81, Nº8*, 1995-2012, 1998.
[270] Y. Hu, D.D.L. Chung, C. Mroz, "Thermally conducting aluminum nitride polymer-matrix composites", *Composites Part A: Applied Science and Manufacturing, Vol. 32, Nº12*, 1749-1757, 2001.
[271] R. Kochetov, T. Andritsch, P.H.F. Morshuis, J.J. Smit, "Dielectric response and thermal conductivity of epoxy resin filled with nanoalumina particles of different size in α, γ and δ phase", *IEEE Conference on Electrical Insulation and Dielectric Phenomena, West Lafayette, IN, USA*, 538-541, 2010.
[272] F. Kremer, A. Schönhals, *Broadband dielectric spectroscopy*, Springer, 2003.
[273] A.J. Jonscher, "Dielectric relaxation in solids", *Journal of Physics D: Applied Physics, Vol. 32, Nº14*, 57-70, 1999.
[274] J.I. Hong, P. Winberg, L.S. Schadler, R.W. Siegel, "Dielectric properties of zinc oxide / low density polyethylene nanocomposites", *Materials Letters, Vol. 59, Nº4*, 474-476, 2005.
[275] X.Y. Huang, P.K. Jiang, C.U. Kim, "Electrical properties of polyethylene / aluminum nanocomposites", *Journal of Applied Physics, Vol. 102, 124103,* 2007.
[276] F. Ciuprina, I. Plesa, P.V. Notingher, T. Tudorache, D. Panaitescu, "Dielectric properties of nanodielectrics with inorganic fillers", *IEEE Conference on Electrical Insulation Dielectric Phenomena*, *Québec City, Canada*, 682-685, 2008.
[277] T. Tanaka, J. Kindersberger, M. Fréchette, S. Gubanski, A.S. Vaughan, S. Sutton, P.H.F. Morshuis, J-P. Mattmann, G.C. Montanari, C. Reed, A. Krivda, J. Castellon, T. Shimizu, P. Pélissou, M. Nagao, "Polymer nanocomposites – fundamentals and possible applications to power sectors", *Cigré Group D1.24 Brochure*, February 2011.

[278] G. Schaumburg, "New broadband dielectric spectrometers", *Dielectric Newsletter,* 8-12, 1994.
[279] G. Schaumburg, "New integrated dielectric analyzer extends accuracy and impedance range for material measurements", *Dielectric Newsletter, Issue 11*, 4-6, 1999.
[280] G. Schaumburg, "Novocontrol cryo system for dielectric applications improved by the new QUATRO 4.0 controllers", *Dielectric Newsletter, Issue 4*, 7-10, 1995.
[281] G. Schaumburg, "On the accuracy of dielectric measurements", *Dielectric Newsletter, Issue 8*, 5-10, 1997.
[282] B. Alijagić-Jonuz, *Dielectric properties and space charge dynamics of polymeric high voltage DC insulating materials*, PhD thesis, Delft University of Technology, 2007.
[283] C.J.F. Böttcher, P. Borderwijk, *Theory of electric polarization – Volume II – Dielectrics in time-dependent fields*, University of Leiden, the Netherlands, Elsevier Scientific Publishing Company, 1978.
[284] M. Wübbenhorst, J. van Turnhout, "Conduction free dielectric loss de/dln(f) – a powerful tool for the analysis of strong (ion) conduction materials", *Dielectric Newsletter, Issue 14*, 1-3, 2000.
[285] http://www.psrc.usm.edu/mauritz/dilect.html
[286] S. Havriliak, S. Negami, "A complex plane representation of dielectric and mechanical relaxation processes in some polymers", *Polymer, Vol. 8*, 161-210, 1967.
[287] G.G. Raju, *Dielectrics in electric fields*, Marcel Dekker, New York, 2003.
[288] J.P. Eloundou, "Dipolar relaxations in an epoxy-amine system", *European Polymer Journal, Vol. 38, Nº3*, 431-438, 2002.
[289] S. Singha, M.J. Thomas, A. Kulkarni, "Complex permittivity characteristics of epoxy nanocomposites at low frequencies", *IEEE Transactions on Dielectrics and Electrical Insulation, Vol. 17, Nº4*, 1249-1258, 2010.
[290] A. Vioux, "Nonhydrolytic sol-gel routes to oxides", *Chemistry of Materials, Vol. 9*, 2292-2299, 1997.
[291] N. McN. Alford, J. Breeze, X. Aupi, "Dielectric loss of oxide single crystals and polycrystalline analogous from 10 to 320 K", *Journal of the European Ceramic Society, Vol. 21,* 2605-2611, 2001.
[292] T.J. Lewis, "Interfaces: nanometric dielectrics", *Journal of Physics D: Applied Physics, Vol. 38, Nº2*, 202-212, 2005.
[293] T. Tanaka, M. Kozako, N. Fuse, Y. Ohki, "Proposal of a multi-core model for polymer nanocomposite dielectrics", *IEEE Transactions on Dielectrics and Electrical Insulation, Vol. 12, Nº4*, 669-681, 2005.
[294] M.G. Todd, F.G. Shi, "Complex permittivity of composite systems: a comprehensive interphase approach", *IEEE Transactions on Dielectrics and Electrical Insulation, Vol. 12, Nº3*, 601-611, 2005.
[295] T. Andritsch, R. Kochetov, P.H.F. Morshuis, J.J. Smit, "Comparison of the dielectric behavior of epoxy based Al_2O_3- and SiO_2- nanocomposites", *Nordic Insulation Symposium, Gothenburg, Sweden*, 137-140, 2009.
[296] H. Looyenga, "Dielectric constants of heterogeneous mixtures", *Physica 31*, 401-406, 1965.
[297] A.S. Vaughan, "On the dielectric response of nanofilled materials", unpublished.
[298] T. Tanaka, "Multi-core model for nanodielectrics as fine structures of interaction zones", *IEEE Conference on Electrical Insulation and Dielectric Phenomena,* Nashville, TN, USA, 713-716, 2005.
[299] J.R. Birchak, C.G. Gardner, J.E. Hipp, J.M. Victor, "High dielectric constant microwave probes for sensing soil moisture", *Proceedings of the IEEE, Vol. 62, Nº1*, 93-98, 1974.
[300] K. Lichtenecker, K. Rother, "Die Herleitung des logarithmischen Mischungsgesetzes als allgemeinen Prinzipien der stationären Strömung", *Physikalische Zeitschrift, Vol. 32*, 255-260, 1931.
[301] X. Lu, G. Xu, P.G. Hofstra, R.C. Bajcar, "Moisture-absorption, dielectric relaxation, and thermal conductivity studies of polymer composites", *Journal of Polymer Science Part B: Polymer Physics, Vol. 36, Nº13*, 2259-2265, 1998.

[302] Y. Sun, Z. Zhang, C.P. Wong, "Influence of interphase and moisture on the dielectric spectroscopy of epoxy/silica composites", *Polymer, Vol. 46*, 2297-2305, 2005.
[303] C. Zhang, G.C. Stevens, "The dielectric response of polar and non-polar nanodielectrics", *IEEE Transactions on Dielectrics and Electrical Insulation, Vol. 15, Nº2*, 606-617, 2008.
[304] M.F. Fréchette, E. David, H.D. Martinez, S. Savoie, "Post-heat treatment effect on the dielectric response of epoxy samples", *IEEE Conference on Electrical Insulation and Dielectric Phenomena, Virginia Beach, VA, USA*, 705-708, 2009.
[305] C. Zou, M. Fu, J.C. Fothergill, S.W. Rowe, "Influence of absorbed water on the dielectric properties and glass-transition temperature of silica-filled epoxy nanocomposites", *IEEE Conference on Electrical Insulation and Dielectric Phenomena, Kansas City, MO, USA*, 321-324, 2006.
[306] *The National Nanotechnology Initiative Strategic Plan*, Nanoscale Science, Engineering and Technology Subcommittee, Committee on Technology, National Science and Technology Council, Arlington, VA, December 2004.
[307] Y. Li, H. Ishida, "Solution intercalation of polystyrene and comparison with poly(ethylmethacrylate)", *Polymer, Vol. 44, Nº21*, 6571-6577, 2003.
[308] J-W. Shen, X-M. Chen, W-Y. Huang, "Structure and electrical properties of grafted polypropylene/graphite nanocomposites prepared by solution intercalation", *Journal of Applied Polymer Science, Vol. 88, Nº7*, 1864-1869, 2003.
[309] L. Liu, Z. Qi, X. Zhu, "Studies on nylon 6/clay nanocomposites by melt-intercalation process", *Journal of Applied Polymer Science, Vol. 71, Nº7*, 1133-1138, 1999.
[310] X. Liu, Q. Wu, "PP/clay nanocomposites prepared by grafting-melt intercalation", *Polymer, Vol. 42, Nº25*, 10013-10019, 2001.
[311] C.L. Wu, M.Q. Zhang, M.Z. Rong, K. Friedrich, "Tensile performance improvement of low nanoparticles filled-polypropylene composites," Composite Science and Technology, Vol. 62, *Nº10-11*, 1327-1340, 2002.
[312] I.D. Rosca, S.V. Hoa, "Highly conductive multiwall carbon nanotubes and epoxy composites produced by three-roll milling", *Carbon, Vol. 47, Nº8*, 1958-1968, 2009.
[313] J.H. Koo, L.A. Pilato, G.E. Wissler, A. Lee, A. Abusafieh, J. Weispfenning, "Epoxy nanocomposites for carbon reinforced polymer matrix composites", *SAMPE Symposium, CA, USA*, 2005.
[314] C. Park, Z. Ounaies, K.A. Watson, R.E. Crocks, J. Smith, S.E. Lowther, J.W. Connell, E.J. Siochi, J.S. Harrison, T.L.St. Clair, "Dispersion of single wall carbon nanotubes by in situ polymerization under sonication", *Chemical Physics Letters, Vol. 364, Nº3-4*, 303-308, 2002.
[315] Y. Chen, S. Zhou, H. Yang, L. Wu, "Structure and properties of polyurethane/nanosilica composites", *Journal of Applied Polymer Science, Vol. 95, Nº5*, 1032-1039, 2005.
[316] F. Yang, Y. Ou, Z. Yu, "Polyamide 6/silica nanocomposites prepared by in situ polymerization", *Journal of Applied Polymer Science, Vol. 69, Nº2*, 355-361, 1998.
[317] S. Bian, S.H. Jayaram, E.A. Cherney, "Use of electrospinning to disperse nanosilica into silicone rubber", *IEEE Annual Report Conference on Electrical Insulation and Dielectric Phenomena*, *West Lafayette, IN, USA*, 230-233, 2010.
[318] X. Huang, W.J. Brittain, "Synthesis and characterization of PMMA nanocomposites by suspension and emulsion polymerization", *Macromolecules, Vol. 34, Nº10*, 6255-3260, 2001.
[319] R. Arshady, "Suspension, emulsion, and dispersion polymerization: a methodological survey", *Colloid & Polymer Science, Vol. 270, Nº8*, 717-732, 1992.
[320] C. Zhang, G.C. Stevens, "Dielectric properties of boron nitride filled epoxy composites", *IEEE Annual Report Conference on Electrical Insulation and Dielectric Phenomena, Kansas City, MO, USA*, 19-22, 2006.
[321] J.H. Koo, L.A. Pilato, G.E. Wissler, "Polymer nanostructured materials for propulsion systems", *Journal of Spacecraft and Rockets, Vol. 44, Nº6*, 1250-1262, 2007.

[322] F. Hussain, M. Hojjati, M. Okamoto, R.E. Gorga, "Review article: polymer-matrix nanocomposites, processing, manufacturing, and application: an overview", *Journal of Composite Materials, Vol. 40, Nº17,* 1511-1575, 2006.
[323] A. Vale, "Methanol", *Medicine, Vol. 35, Nº12*, 633-634, 2007.
[324] S.C. Jana, S. Jain, "Dispersion of nanofillers in high performance polymers using reactive solvents as processing aids", *Polymer, Vol. 42, Nº16*, 6897-6905, 2001.
[325] T. Imai, F. Sawa, T. Ozaki, Y. Inoue, T. Shimizu, T. Tanaka, "Roles of fillers on properties of nano-TiO_2 and micro-SiO_2 filler mixed composites", *IEEE, International Conference on Solid Dielectrics, Winchester, UK,* 407-410, 2007.
[326] www.nanocor.com
[327] www.nanoresins.com
[328] www.jpowers.co.jp
[329] Y. Maekawa, T. Yamanaka, T. Kimura, Y. Murata, S. Katakai, O. Mitsunaga, "DC 500 kV submarine XLPE cable", *Hitachi Densen, Nº21*, 65-72, 2002.
[330] T. Imai, T. Ozaki, F. Sawa, T. Shimizu, M. Harada, M. Ochi, N. Tagami, Y. Ohki, T. Tanaka, "Nanocomposite insulating materials for environmental-conscious heavy electric apparatuses", *International Symposium on Electrical Insulating Materials, Yokkaichi, Mie, Japan*, 2008.
[331] T. Ozaki, G. Komiya, K. Murayama, T. Imai, F. Sawa, T. Shimizu, M. Harada, M. Ochi, Y. Ohki, T. Tanaka, "Nano-clay and micro-silica mixed composites for insulating materials for environmentally-conscious switchgear", *9th International Conference on Properties and Applications of Dielectric Materials, Harbin, China*, 864-867, 2009.
[332] T. Imai, G. Komiya, K. Murayama, T. Ozaki, F. Sawa, T. Shimizu, M. Harada, M. Ochi, Y. Ohki, T. Tanaka, "Improving epoxy-based insulating materials with nano-fillers towards practical application", *IEEE International Symposium on Electrical Insulation, Vancouver, BC, Canada*, 201-204, 2008.
[333] B. Zhang, C. Xie, J. Hu, H. Wang, Y.H. Gui, "Novel 1-3 metal nanoparticle/polymer composites induced by hybrid external fields", *Composites Science and Technology, Vol. 66, Nº11-12*, 1558-1563, 2006.
[334] M.A. Correa-Duarte, M. Grzelczak, V. Salgueirino-Maceira, M. Giersig, L.M. Liz-Marzan, M. Farle, K. Sierazdki, R. Diaz, "Alignment of carbon nanotubes under low magnetic fields through attachment of magnetic nanoparticles", *Journal of Physical Chemistry B, Vol. 109, Nº41*, 19060-19063, 2005.
[335] V. Tomer, C.A. Randall, G. Polizos, J. Kostelnick, E. Manias, "High- and low-field dielectric characteristics of dielectrophoretically aligned ceramic/polymer nanocomposites", *Journal of Applied Physics, Vol. 103, 034115*, 2008.
[336] J.E. Martin, C.P. Tiggers, R.A. Anderson, J. Odinek, "Enhanced dielectric standoff and mechanical failure in field-structured composites", *Physical Review B, Vol. 60, Nº10*, 7127-7139, 1999.
[337] V. Tomer, C.A. Randall, "High field dielectric properties of anisotropic polymer-ceramic nanocomposites", *Journal of Applied Physics, Vol. 104,* 074106, 2008.
[338] D. Khastgir, K. Adachi, "Piezoelectric and dielectric properties of siloxane elastomers filled with bariumtitanate", *Journal of Polymer Science: Part B: Polymer Physics, Vol. 37*, 3065-3070, 1999.
[339] Y. Ding, H. Chen, L. Wang, C-Y. Yang, Y. He, W. Yang, W.P. Lee, L. Zhang, R. Huo, "Heat transfer intensification using nanofluids", *KONA, Vol. 25, Nº25*, 23-38, 2007.
[340] J. Wensel, B. Wright, D. Thomas, W. Douglas, B. Mannhalter, W. Cross, H. Hong, J. Kellar, "Enhanced thermal conductivity by aggregation in heat transfer nanofluids containing metal oxide nanoparticles and carbon nanotubes", *Applied Physics Letters, Vol. 92, 023110*, 2008.
[341] J.G. Hwang, M. Zahn, F.M. O'Sullivan, L.A.A. Pettersson, O. Hjortstam, R. Liu, "Electron scavenging by conductive nanoparticles in oil insulated power transformers", *Electronics Joint Conference, Boston, MA, USA*, 2009.
[342] DU Yue-fan, L.V. Yu-zhen, Z. Jian-quan, LI Xiao-xin, LI Cheng-rong, "Breakdown properties of transformer oil-based TiO_2 nanofluid", *IEEE Annual Report Conference on Electrical Insulation and Dielectric Phenomena*, *West Lafayette, IN, USA*, 604-607, 2010.

[343] A.S. Cherkasova, *Thermal conductivity enhancement in micro- and nano-particle suspensions*, PhD thesis, State University of New Jersey, 2009.
[344] A.A. Shvedova, E.R. Kison, R. Mercer, A.R. Murray, V.J. Johnson, A.I. Potapovich, Y.Y. Tyurina, O. Gorelik, S. Arepalli, D. Schwegler-Berry, A.F. Hubbs, J. Antonini, D.E. Evans, B.-K. Ku, D. Ramsey, A. Maynard, V.E. Kagan, V. Castranova, P. Baron, "Unusual inflammatory and fibrogenic pulmonary responses to single walled carbon nanotube in mice", *American Journal of Physiology: Lung Cellular and Molecular Physiology, Vol. 289, Nº5*, 698-708, 2005.
[345] S.K. Smart, A.I. Cassady, G.Q. Lu, D.J. Martin, "The biocompatibility of carbon nanotubes", *Carbon, Vol. 44, Nº6*, 1034-1047, 2006.
[346] A. Afshari, U. Matson, L. Ekberg, "Characterization of indoor sources of fine and ultrafine particles: a study conducted in a full-scale chamber", *Indoor Air, vol. 15, Nº2*, 141-150, 2005.
[347] A. Krivda, T. Tanaka, M. Fréchette, J. Castellon, D. Fabiani, G.C. Montanari, R. Gorur, P.H.F. Morshuis, S. Gubanski, J. Kindersberger, A.S. Vaughan, S. Pelissou, Y. Tanaka, L.E. Schmidt, G. Iyer, T. Andritsch, J. Seiler, M. Anglhuber, "Characterization of epoxy micro and nano composite materials for power engineering applications", Electrical Insulation Magazine, *Vol. 28, Nº2*, 38-51, 2012.
[348] U.S. Environmental Protection Agency (EPA). Nanotechnology white paper.
[349] O. Preining, "The physical nature of very, very small particles and its impact on their behaviour", *Journal of Aerosol Science, Vol. 29, Nº*5-6, 481-495, 1998.
[350] K.R. Spurny, "On the physics, chemistry and toxicology of ultrafine anthropogenic, atmospheric aerosols (UAAA): new advances", *Toxicology Letters, Vol. 96-97*, 253-261, 1998.
[351] R. Atkinson, "Atmospheric oxidation", *Handbook of Property Estimation Methods for Chemicals, Environmental and Health Sciences*, Edited by R.S. Boethling and D. Mackay, Chapter 14, Lewis Publishers, CRC Press, Boca Raton, FL, USA, 2000.
[352] K.L. Dreher, "Toxicological highlight – health and environmental impact of nanotechnology: toxicological assessment of manufactured nanoparticles", *Toxicological Sciences, Vol. 73*, 3-5, 2004.
[353] G. Oberdörster, Z. Sharp, V. Atudorei, A. Elder, R. Gelein, W. Kreyling, C. Cox, "Translocation of inhaled ultrafine particles to the brain*", Inhalation Toxicology, Vol. 16, Nº6-7*, 437-445, 2004.
[354] A. Nemmar, P.H.M. Hoet, B. Vanquickenborne, D. Dinsdale, M. Thomeer, M.F. Hoylaerts, H. Vanbilloen, L. Mortelmans, B. Nemery, "Passage on inhaled particles into the blood circulation in humans", *Circulation, Vol. 105*, 411-414, 2002.
[355] M. Geiser, B. Rothen-Rutishauser, N. Kapp, S. Schürch, W. Kreyling, H. Schulz, M. Semmler, V. Im Hof, J. Heyder, P. Gehr, "Ultrafine particles cross cellular membranes by nonphagocytic mechanisms in lungs and in cultured cells", *Environmental Health Perspectives, Vol. 113, Nº11*, 1555-1560, 2005.
[356] P.U. Jani, D.E. McCarthy, A.T. Florence, "Titanium dioxide (rutile) particle uptake from the rat GI tract and translocation to systemic organs after oral administration", *International Journal of Pharmaceutics, Vol. 105, Nº2*, 157-168, 1994.
[357] B. Baroli, M.G. Ennas, F. Loffredo, M. Isola, R. Pinna, M.A. Lopez-Quintela, "Penetration of metallic nanoparticles in human full-thickness skin", *Journal of Investigative Dermatology, Vol. 127*, 1701-1712, 2007.
[358] G.J. Nohynek, E. Antignac, T. Re, H. Toutain, "Safety assessment of personal care products/cosmetics and their ingredients", *Toxicology and Applied Pharmacology, Vol. 243, Nº2*, 239-259, 2010.
[359] A.A. Shvedova, V. Castranova, E. Kisin, D. Schwegler-Berry, A.R. Murray, V.Z. Gandelsman, A. Maynard, P. Baron, "Exposure to carbon nanotubes material: assessment of nanotube cytotoxicity using human keratinocyte cells", *Journal of Toxicology and Environmental Health, Part A, Vol. 66*, *Nº20*, 1909-1926, 2003.
[360] P.J.A. Borm, "Particle toxicology: from coal to nanotechnology", *Inhalation Toxicology, Vol. 14, Nº3*, 311-324, 2002.

[361] C. Lam, J.T. James, R. McCluskey, S. Arepally, R.L. Hunter, "A review of carbon nanotube toxicity and assessment of potential occupational and environmental health risks", *Critical Reviews in Toxicology, Vol. 36, Nº3*, 189-217, 2006.
[362] J. Muller, F. Huaux, D. Lison, "Respiratory toxicity of carbon nanotubes: how worried should we be?", *Carbon, Vol. 44, Nº6*, 1048-1056, 2006.
[363] D.B. Warheit, "What is currently known about the health risks related to carbon nanotube exposures?", *Carbon, Vol. 44, Nº6*, 1064-1069, 2006.
[364] C.A. Poland, R. Duffin, I. Kinloch, A. Maynard, W.A.H. Wallace, A. Seaton, V. Stone, S. Brown, W. MacNee, K. Donaldson, "Carbon nanotubes introduced into the abdominal cavity of mice show asbestos-like pathogenicity in a pilot study", *Nature Nanotechnology, Vol. 3*, 423-428, 2008.
[365] J. Muller, F. Huaux, N. Moreau, P. Misson, J.-F. Heilier, M. Delos, M. Arras, A. Fonseca, J.B. Nagy, D. Lison, "Respiratory toxicity of multi-wall carbon nanotubes", *Toxicology and Applied Pharmacology, Vol. 207, Nº3*, 221-231, 2005.
[366] Nanoscience and nanotechnologies, *The Royal Society & the Royal Academy of Engineering*, 2004.
[367] K. Donaldson, V. Stone, C.L. Tran, W. Kreyling, P.J.A. Borm, "Nanotoxicology", *Occupational & Environmental Medicine, Vol. 61, Nº9*, 727-728, 2004.
[368] D.B. Warheit, "Nanoparticles: health impact?", *Materials Today, Vol. 7, Nº2*, 32-35, 2004.
[369] D.B. Warheit, T.R. Webb, C.M. Sayes, V.L. Colvin, K.L. Reed, "Pulmonary instillation studies with nanoscale TiO_2 rods and dots in rats: toxicity is not dependent upon particle size and surface area", *Toxicological Sciences, Vol. 91, Nº1*, 227-236, 2006.
[370] C.M. Sayes, R. Wahi, P.A. Kurian, Y. Liu, J.L. West, K.D. Ausman, D.B. Warheit, V.L. Colvin, "Correlating nanoscale titania structure with toxicity: a cytotoxicity and inflammatory response study with human dermal fibroblasts and human lung epithelial cells", *Toxicological Sciences, Vol. 92, Nº1*, 174-185, 2006.
[371] R. Dunford, A. Salinaro, L. Cai, N. Serpone, S. Horikoshi, H. Hidaka, J. Knowland, "Chemical oxidation and DNA damage catalyzed by inorganic sunscreen ingredients", *FEBS Letters, Vol. 418, Nº1-2*, 87-90, 1997.
[372] J. Nijenhuis, V.C.L. Butselaar-Orthlieb, *TNW nanosafety guidelines*, Delft University of Technology, Faculty of Applied Sciences, SHE Committee of DelftChemTech, 2008.
[373] P.A. Schulte, F. Salamanca-Buentello, "Ethical and scientific issues of nanotechnology in the workplace", *Environmental Health Perspectives, Vol. 115, Nº1*, 5-12, 2007.
[374] S. Agarwal, E. Tatli, N.N. Clark, R. Gupta, "Potential health effects of manufactured nanomaterials: nanoparticle emission arising from incineration of polymer nanocomposites", *International Symposium on Polymer Nanocomposites Science and Technology*, Boucherville, Canada, 2005.
[375] G. Oberdörster, A. Maynard, K. Donaldson, V. Castranova, J. Fitzpatrick, K. Ausman, J. Carter, B. Karn, W. Kreyling, D. Lai, S. Olin, N. Monteiro-Riviere, D. Warheit, H. Yang, "Principles for characterizing the potential human health effects from exposure to nanomaterials: elements of a screening strategy", *Particle and Fibre Toxicology, Vol. 2, Nº8*, 1-35, 2005.
[376] K. Thomas, P. Sayre, "Research strategies for safety evaluation of nanomaterials, Part I: Evaluating he human health implications of exposure to nanoscale materials", *Toxicological Sciences, Vol. 87, Nº2*, 316-321, 2005.
[377] R.H. Hurt, M. Monthioux, A. Kane, "Toxicology of carbon nanomaterials: status, trends, and perspectives on the special issue", *Carbon, Vol. 44, Nº6*, 1028-1033, 2006.
[378] R. von Schomberg, "Introduction: understanding public debate on nanotechnologies options for framing public policy", *Understanding public debate on nanotechnologies options for framing public policy. A report from the European Commission Services*, Edited by R. von Schomberg and S. Davies, 2010.
[379] Huntsman Advanced Materials, *Araldite CY225/Aradur HY925/Silica*, Product data sheet, 2004.

[380] S.A. Wilson, G.M. Maistros, R.W. Whatmore, "Structure modification of 0–3 piezoelectric ceramic/polymer composites through dielectrophoresis", *Journal of Physics D: Applied Physics, Vol. 38*, 175–182, 2005.
[381] C.P. Bowen, T.R. Shrout, R.E. Newnham, C.A. Randall, "Tunable Electric Field Processing of Composite Materials", *Journal of Intelligent Material Systems and Structures, Vol. 6*, 159-168, 1995.
[382] S.A. Wilson, Electric-field structuring of piezoelectric composite materials, PhD thesis, Cranfield University, 1999.
[383] J.S. Reed, *Introduction to the principals of ceramic processing*, John Wiles & Sons, New York, Chichester, Brisbane, Toronto and Singapore, 1988.
[384] W.F. Schmidt, "Conduction mechanisms in liquids", *Electrical insulating liquids*, Edited by R. Bartnikas, Chapter 2, Vol. 3, ASTM, Philadelphia, PA, USA, 1994.
[385] T.C. Halsey, "Electrorpheological fluids", *Science, Vol. 258*, 761-764, 1992.
[386] W.M. Winslow, Induced fibration of suspensions, *Journal of Applied Physics, Vol. 20, Nº12*, 1137-1140, 1949.
[387] C.A. Randall, D.V. Miller, J.H. Adair, A.S. Bhalla, "Processing of electroceramic-polymer composites using the electrorheological effect", *Journal of Materials Research, Vol. 8, Nº4*, 899-904, 1993.
[388] C.P. Bowen, R.E. Newnham, C.A. Randall, "Dielectric properties of dielectrophoretically assembled particulate-polymer composites", *Journal of Materials Research, Vol. 13, Nº1*, 205-210, 1998.
[389] C.P. Bowen, T.R. Shrout, R.E. Newnham, C.A. Randall, "A study of the frequency dependence of the dielectrophoretic effect in thermoset polymers", *Journal of Materials Research, Vol. 12, Nº9*, 2345-2356, 1997.
[390] R.S. Carmichael, *Handbook of physical properties of rocks*, CRC, Boca Raton, FL., USA, 1982.

List of publications

1. R. Kochetov, "Investigations of GaAs based heterostructures for spintronics", Master's Thesis, Lappeenranta University of Technology, 2007.
2. R. Kochetov, T. Andritsch, U. Lafont, P.H.F. Morshuis, S.J. Picken, J.J. Smit, "Preparation and dielectric properties of epoxy–BN and epoxy-AlN nanocomposites", *IEEE Electrical Insulation Conference (EIC), Montreal, QC, Canada*, pp. 397-400, 31 May-3 June, 2009.
3. R. Kochetov, T. Andritsch, U. Lafont, P.H.F. Morshuis, S.J. Picken, J.J. Smit, "Thermal behaviour of epoxy resin filled with high thermal conductivity nanopowders", *IEEE Electrical Insulation Conference (EIC), Montreal, QC, Canada*, pp. 524-528, 31 May-3 June, 2009.
4. R. Kochetov, T. Andritsch, U. Lafont, P.H.F. Morshuis, J.J. Smit, "The thermal conductivity in epoxy – aluminum nitride and epoxy – aluminum oxide nanocomposite systems", *Nordic Insulation Symposium (Nord-IS 09), Gothenburg, Sweden*, pp. 27-30, June 15-17, 2009.
5. R. Kochetov, T. Andritsch, U. Lafont, P.H.F. Morshuis, J.J. Smit, "Thermal conductivity of nano-filled epoxy systems", *IEEE Conference on Electrical Insulation and Dielectric Phenomena (CEIDP), Virginia Beach, Virginia, USA*, pp. 658-661, October 18-21, 2009.
6. R. Kochetov, T. Andritsch, U. Lafont, P.H.F. Morshuis, J.J. Smit, "Effects of inorganic nanofillers and combinations of them on the complex permittivity of epoxy-based composites", *IEEE International Symposium on Electrical Insulation (ISEI), San Diego, California, USA*, pp. 340-344, June 6-9, 2010.
7. R. Kochetov, T. Andritsch, P.H.F. Morshuis, J.J. Smit, "Thermal and electrical behaviour of epoxy based microcomposites filled with Al_2O_3 and SiO_2 particles", *IEEE International Symposium on Electrical Insulation (ISEI), San Diego, California, USA*, pp. 509-513, June 6-9, 2010.
8. R. Kochetov, T. Andritsch, P.H.F. Morshuis, J.J. Smit, "Effect of filler size on complex permittivity and thermal conductivity of epoxy-based composites filled with BN particles", *IEEE Conference on Electrical Insulation and Dielectric Phenomena (CEIDP), West Lafayette, Indiana, USA*, pp. 534-537, October 17-20, 2010.
9. R. Kochetov, T. Andritsch, P.H.F. Morshuis, J.J. Smit, "Dielectric response and thermal conductivity of epoxy resin filled with nanoalumina particles of different size in α, γ and δ phase", *IEEE Conference on Electrical Insulation and Dielectric Phenomena (CEIDP), West Lafayette, Indiana, USA*, pp. 538-541, October 17-20, 2010.
10. R. Kochetov, T. Andritsch, P.H.F. Morshuis, J.J. Smit, "Evaluation of the influence of various nanofillers on the AC breakdown strength of epoxy-based nanocomposites", *IEEE International Symposium on Electrical Insulation Materials, Kyoto, Japan*, pp. 383-386, September 6-10, 2011.
11. R. Kochetov, A.V. Korobko, T. Andritsch, P.H.F. Morshuis, S.J. Picken, J.J. Smit, "Modelling of the thermal conductivity in polymer nanocomposites

and the impact of the interface between filler and matrix", *Journal of Physics D: Applied Physics, Vol. 44*, № 395401, 2011.

12. R. Kochetov, A.V. Korobko, T. Andritsch, P.H.F. Morshuis, , S.J. Picken, J.J. Smit, "Three-phase Lewis-Nielsen model for the thermal conductivity of polymer nanocomposites", *IEEE Conference on Electrical Insulation and Dielectric Phenomena (CEIDP), Cancun, Mexico*, pp. 338-341, October 16-19, 2011.
13. R. Kochetov, T. Andritsch, P.H.F. Morshuis, J.J. Smit, "Impact of postcuring and water absorption on the dielectric response of epoxy-based composites filled with MgO nanoparticles", *IEEE Conference on Electrical Insulation and Dielectric Phenomena (CEIDP), Cancun, Mexico*, pp. 342-345, October 16-19, 2011.
14. R. Kochetov, T. Andritsch, P.H.F. Morshuis, J.J. Smit, "Anomalous behaviour of the dielectric spectroscopy response of nanocomposites", *IEEE Transactions on Dielectrics and Electrical Insulation, IEEE Transactions on Dielectrics and Electrical Insulation, Vol. 19, №1*, 107-117, 2012.
15. T. Andritsch, R. Kochetov, P.H.F. Morshuis, J.J. Smit, "Comparison of the dielectric behavior of epoxy based Al_2O_3 - and SiO_2 - nanocomposites", *Nordic Insulation Symposium (Nord-IS 09), Gothenburg, Sweden*, pp. 137-140, June 15-17, 2009.
16. T. Andritsch, R. Kochetov, Y.T. Gebrekiros, U. Lafont, P.H.F. Morshuis, J.J. Smit, "Space charge behavior of epoxy based nanocomposites with Al_2O_3 and AlN filler", *Nordic Insulation Symposium (Nord-IS 09), Gothenburg, Sweden*, pp. 141-144, June 15-17, 2009.
17. T. Andritsch, R. Kochetov, P.H.F. Morshuis, J.J. Smit, "Comparison of the dielectric response of alumina-epoxy composites with nano- and conventional sized filler", *International Symposium on High Voltage Engineering (ISH), Cape Town, South Africa*, A-28, August 24-28, 2009.
18. T. Andritsch, R. Kochetov, Y.T. Gebrekiros, U. Lafont, P.H.F. Morshuis, J.J. Smit, "Space charge accumulation in epoxy based magnesium oxide and boron nitride nanocomposites", *International Symposium on High Voltage Engineering (ISH), Cape Town, South Africa*, F-6, August 24-28, 2009.
19. T. Andritsch, R. Kochetov, Y.T. Gebrekiros, U. Lafont, P.H.F. Morshuis, J.J. Smit, "Synthesis and dielectric properties of epoxy based nanocomposites", *IEEE Conference on Electrical Insulation and Dielectric Phenomena (CEIDP), Virginia Beach, Virginia, USA*, October 18-21, pp. 523-526, 2009.
20. M.F. Fréchette, A. Vijn, M.L. Trudeau, L. Utracki, A. Sami, E. David, C. Laurent, P.H. Morshuis, T. Andritsch, R. Kochetov, A. Vaughan, J. Castellon, D. Fabiani, S. Gubanski, J. Kindersberger, C. Reed, A. Krivda, J. Fothergill, S. Dodd, F. Guastavino, H. Alamdari, "Nanodielectrics. A "universal" panacea for solving all electrical insulation problems?", *IEEE International Conference on Solid Dielectrics (ICSD), Potsdam, Germany*, pp. 127-158, July 4-9, 2010.
21. T. Andritsch, R. Kochetov, Y.T. Gebrekiros, P.H.F. Morshuis, J.J. Smit, "Short term DC breakdown strength in epoxy based BN nano- and microcomposites", *IEEE International Conference on Solid Dielectrics (ICSD), Potsdam, Germany*, pp. 179-182, July 4-9, 2010.
22. P.H.F. Morshuis, T. Andritsch, R. Kochetov, M.F. Fréchette, H.D. Martinez, S. Savoie, A. Krivda, L.E. Smith, D. Zegaraz, "Dielectric frequency

response of epoxy-based composites with various silica filler sizes*", IEEE International Conference on Solid Dielectrics (ICSD), Potsdam, Germany*, pp. 200-203, July 4-9, 2010.

23. T. Andritsch, R. Kochetov, P.H.F. Morshuis, J.J. Smit, "Dielectric properties and space charge behavior of MgO-epoxy nanocomposites", *IEEE International Conference on Solid Dielectrics (ICSD), Potsdam*, Germany, pp. 344-347, July 4-9, 2010.
24. T. Andritsch, R. Kochetov, P.H.F. Morshuis, J.J. Smit, "Short term DC breakdown and complex permittivity of Al_2O_3 - and MgO - epoxy nanocomposites", *IEEE Conference on Electrical Insulation and Dielectric Phenomena (CEIDP), West Lafayette, Indiana, USA*, pp. 530-533, October 17-20, 2010.
25. T. Andritsch, R. Kochetov, P.H.F. Morshuis, J.J. Smit, "DC conduction in epoxy based nano- and mesocomposites", *IEEE Conference on Electrical Insulation and Dielectric Phenomena (CEIDP), West Lafayette, Indiana, USA*, pp. 542-545, October 17-20, 2010.
26. T. Andritsch, R. Kochetov, B. Lennon, P.H.F. Morshuis, J.J. Smit, "Space charge behavior of magnesium oxide filled epoxy nanocomposites at different temperatures and electric field strengths", *IEEE Electrical Insulation Conference (EIC), Annapolis, Maryland, USA*, pp. 136-140, June 5-8, 2011.
27. T.L. Koltunowicz, R. Kochetov, G. Bajracharya, D. Djairam, J.J. Smit, "Repetitive transient aging, the influence of rise time", *IEEE Electrical Insulation Conference (EIC), Annapolis, Maryland, USA*, pp. 151-155, June 5-8, 2011.
28. T.L. Koltunowicz, R. Kochetov, G. Bajracharya, D. Djairam, J.J. Smit, "Repetitive transient aging, the influence of repetition frequency", *IEEE Electrical Insulation Conference (EIC), Annapolis, Maryland, USA*, pp. 443-448, June 5-8, 2011.
29. T. Andritsch, R. Kochetov, P.H.F. Morshuis, J.J. Smit, "The complex permittivity of epoxy based nanocomposites with alumina and magnesium oxide fillers at very low temperatures", *IEEE Conference on Electrical Insulation and Dielectric Phenomena (CEIDP), Cancun, Mexico*, pp. 306-309, October 16-19, 2011.
30. T. Andritsch, R. Kochetov, P.H.F. Morshuis, J.J. Smit, "Proposal of the polymer chain alignment model", *IEEE Conference on Electrical Insulation and Dielectric Phenomena (CEIDP), Cancun, Mexico*, pp. 624-627, October 16-19, 2011.

Acknowledgements

Many people have made a contribution to this thesis, directly or indirectly.
First of all, I would like to thank my promoter prof. dr. Johan Smit for providing me the opportunity to join and work at the High Voltage Technology and Management group.
I am grateful to my supervisor dr. ir. Peter Morshuis for guiding me all these years, for constant and insightful feedback, for encouragement and helpful discussions, for all the time and effort. I appreciate the freedom I was given in making my own choices along the way.
I am also thankful to prof. dr. Stephen Picken from ChemE for his valuable advices and inspiring conversations.
Without any doubt my roommate Thomas Andritsch is the person who contributed most to the creation of this work. Thank you very much for all the time we spent together, the discussions, ideas, help in improving my English and proofreading all my publications and this dissertation. Thank you for being my nano-twin brother.
I am also in debt of Paul van Nes, Aad van der Graaf, Bertus Naagen and Wim Termorshuizen from HV laboratory for indispensible technical help and efficient solutions, especially in design and construction of all the molds I needed for my research.
I would like to thank our former secretary Maria, who helped me a lot in avoiding problems, when I came to the Netherlands more than 4 years ago. I would like to thank our current secretary Iris for printing out all the posters for the conferences and meetings.
I acknowledge Ugo Lafont for the TEM micrographs, Ben Norder, Piet Droppert and Marcel Bus from ChemE for their help and characterization of my samples. Many thanks to Sasha for the helpful and productive collaboration.
I am grateful to SenterNovem and all the industrial partners (Prysmian Cables and Systems, Mekufa, Hapam, Eaton Electric, TNO Industrie en Techniek) for the financial support of my project.
Thanks to my fellow PhD students Pantelis, Jur, Rogier, Gautam, Mo, Xiaolin, Qikai, Roy, Barry, Piotr, Lukasz, Ravish and Dennis who were and are the part of the team. Thank you for being great colleagues and providing a friendly atmosphere in the group.
Special thank to Huifei for being indifferent to the music that was played by me or Thomas in the office.
I would like to express many thanks to Dhiradj, my former roommate for his help and tips about Dutch language and Dutch culture. I still remember my first working day, when you showed me everything

around. Hope to see you at our next Thanksgiving day celebration. I believe one day you will be married.
Tom thanks for being a good looser during our beer drinking competitions and all trips we made together with Thomas in the old days. Fortunately my social life did not end at the university. I met a lot of interesting people. Thank you Misha, Alex, Katya, Daniela, Kostas, Juan, Aris, Alfonso, Augusto, Felipe, Zdenek for being around with a positive attitude.
One important part of my life is sport. Thanks to my gym-buddies Wouter & Wouter, Michael & Michiel, Nan & Raghu, Diomidis & Andrei, Christos & Foek.
I appreciate the support and warm friendship of the guys who are living in Russia, who are always willing to meet me when I am in Saint-Petersburg, Moscow or Kadui. Maxim, Zhenya & Olya, Timur, Egor, Dasha, Alisa, Tolstaya, Xenia and Vika, thank you for your priceless friendship.
I would also like to express gratitude to my co-pilots Mohsen, Soto and Miguel, who became like brothers for me. Even though you are far away from me, your spirits are always around me! Thanks for your shared wisdom!
Many thanks to my best friend Dima for always being able to cheer me up and encouraged me to continue my PhD. We are in far away places, but always close in our hearts.
Juliana and Svetlana, I appreciate your contribution in designing the cover of this thesis.
Kira, many thanks for the graphical work you have done for this thesis, but not only for that.
I address my gratitude to my parents, grandparents and sister for their love, support and confidence in me during all the time I am living far away from them.
My final thanks are for the woman who makes me a better man. Thanks to you, Sveta!

Curriculum Vitae

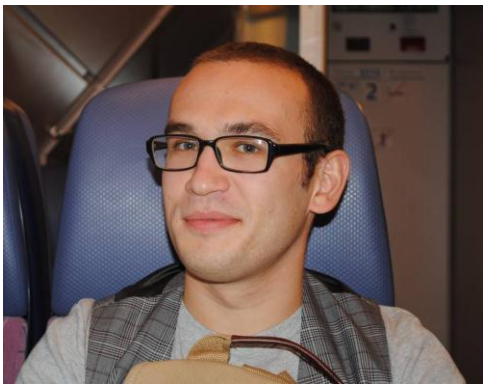

Roman Kochetov was born in 1984 in Kazakhstan (USSR). He received his B.Sc. and M.Sc. in Technique and Technology (Microelectronics and Semiconductors) from Saint-Petersburg Electrotechnical University with distinction in 2005 and 2007, respectively. He participated in an exchange program and received his second M.Sc. degree in Electrical Engineering (Technical Physics) from Lappeenranta University of Technology in 2007. His thesis project '*Investigations of GaAs based heterostructures for spintronics*' discusses investigations of structural, magnetic and electronic properties of quantum wells, which are having a manganese monolayer.

He joined the High Voltage Technology and Management group in October 2007 and started on the PhD research project nanoPOWER. His main research interests are focused on nanostructured systems, thermal conductivity of polymer composites and dielectric spectroscopy of electrical insulation materials.